NTNU – Trondheim
Norwegian University of
Science and Technology

Numerical Simulation of Extended Leak-Off Tests

Vegard Veiteberg Eide

Petroleum Geoscience and Engineering
Submission date: June 2014
Supervisor: Andreas Bauer, IPT

Norwegian University of Science and Technology
Department of Petroleum Engineering and Applied Geophysics

Preface

This report is the final product of "TPG4910 Petroleum Engineering - Drilling Engineering, Master's Thesis" at the Norwegian University of Science and Technology (NTNU), Department of Petroleum Engineering and Applied Geophysics.

First of all I would like to thank my supervisor Prof. Andreas Bauer (NTNU) for guidance, support and helpful feedback throughout this work. I would also like to thank Idar Larsen and Alexandre Lavrov at SINTEF Petroleum Research.

A special thanks to my family and friends, and to my student colleagues at NTNU who have made the last five years truly an amazing experience. Without all of you these years would have been far less rewarding.

I hereby declare that this thesis is written by me, Vegard Eide, and that I have been working in accordance with regulations passed down by NTNU. All sources used are stated under References.

Trondheim, 2014-06-10

Vegard Eide

Abstract

In-situ stresses are key information for well and formation integrity assessments, especially in difficult drilling operations such as high pressure high temperature wells, extended reach wells and in-fill drilling. During drilling, the minimum horizontal stress is best obtained by dedicated tests. In particular the extended leak-off test. Challenges associated with such tests are the quality of stress data obtained in complex stress regimes, difficult formations (plasticity, ductility, thermal effects) and difficult geometries. These conditions present the need for more reliable determination of in-situ stresses during drilling.

This thesis was part of the full development of an extended leak-off test simulator for deep wells based on a modified discrete element method (MDEM) at SINTEF Petroleum. The overlying objective of MDEM as a fracturing simulator is modelling of dynamic fracture initiation and propagation in 3D. XLOT in deviated wells may be evaluated for information, and phenomena such as fracture twisting may be captured.

The process of refining MDEM to become an XLOT simulator in low-permeable rock in 2D is described with results and discussion.

In low permeability formations, the only volume available for the well fluid to flow into is the induced fracture volume. With single phase water as fracturing fluid in an open hole segment of unit length (modelled by MDEM, in 2D), this corresponds to a highly stiff and non-linear system, where fracture mechanics and fluid flow are intimately coupled. Change in flow rate immediately translates to fracturing rate. A full well volume attached to the fracturing simulator implies that decompressed volume will flow at high rates into the fracture at formation break-down, inducing a large fracture. A sequentially coupled geomechanical and fluid flow model requires limited fracture extension per simulation timestep to ensure a stable hydromechanical coupling, which makes coupling of third model, the well, a non-trivial problem.

Two schemes to couple a deep petroleum well to the MDEM fracturing simulator were developed in MATLAB, and applied to simulate XLOT in a 2000 mTVD well. Simulation results are presented. Flow-back through a fixed choke was implemented in the coupling algorithms in MATLAB.

Samandrag

In-situ spenningar i undergrunnen er nøkkelinformasjon for vurdering av brønn- og formasjonsintegritet, spesielt i vanskelege boreoperasjonar som høgtrykk-høgtemperaturbrønnar, horisontalbrønnar og seinfase produksjonsboring. Under boring er det lettast å fastsette minimum horisontalspenning ved hjelp av spesifikk testing – spesielt utvida formasjonsintegritets- og barrieretrykktestar (XLOT), som allereie er ein obligatorisk del av operasjonen når foringsrøyr har blitt senka og sementert i brønnen. Utfordringar knytta til slike testar er kvaliteten på spenningsinformasjonen innsamla i vanskelege spenningsområde i stein, vanskelege formasjonar (plastisk, duktil og temperaturavhengig oppførsel i stein) og vanskelige geometriar. Desse tilhøva viser behovet for meir påliteleg fastsetjing av spenningar under boring.

Denne oppgåva var ein del av den fullstendige utviklinga av ein testsimulator for brønnar basert på ein modifisert diskretiseringsmodell (MDEM) ved SINTEF Petroleum. Hovudmålet med MDEM som fraktursimulator er modellering av dynamisk sprekkedanning i 3D. XLOT i avvikande brønnar kan evaluerast for informasjon, og fenomen som sprekkevridning kan fangast opp.

Prosessen med å utvikle MDEM til å bli ein XLOT-simulator i berggrunn med lav permeabilitet i 2D er skildra med resultat og diskusjon.

I formasjonar med låg permeabilitet er det induserte sprekkevolumet det einaste tilgjengelege holrom som injeksjonsvæske kan flyte inn i. Med einfase vatn som injeksjonsvæsle injisert i eit rottehol av lengde på ei eining (i 2D), stemmer dette overeins med eit svært stivt og ulineært system der sprekkemekanikk og væskeflyt er nært knytta til kvarandre. Endringar i strømningsrate vert umiddelbart oversett til rate av sprekkedanning. Med ein brønn kopla til rotteholet, som blir modellert av sprekkesimulatoren, vil dekomprimert væske strøyme med stor rate inn i sprekker når boreholsveggen går i strekkbrot. Då vil ei sprekke av stort volum vekse ut frå brønnen. Ei sekvenskopling av den geomekaniske modellen og strømningsmodellen krever at mengda nytt sprekkevolum er under eit visst nivå for kvart tidssteg i simuleringa. Dette er for å kunne gripe dei nært knytta hydromekaniske prosessane som er tilstade når ei sprekk blir hydraulisk indusert og veks i lavpermeabilitetsstein.

To system for å kople ein brønn til sprekkesimulatoren MDEM vart utvikla i MATLAB, og nytta til å simulere XLOT i ein 2000 mTVD brønn. Resultata av simuleringa er presenterte. Tilbakestrøyming gjennom ein fast choke vart implementert i koplingsalgoritma i MATLAB.

List of Figures

List of Tables

Contents

Chapter 1

Introduction

The Modified Discrete Element Method (MDEM) for geomechanical modelling was developed originally by Alassi [2] in 2008 during his PHD thesis at NTNU. Its main advantage over discrete element methods is that it behaves like a finite element method before failure and like a discrete element method after failure. In MDEM, macroscopic elastic properties (the constitutive matrix) are inverted directly to the particle interaction parameters used in the microscopic stiffness matrix. Tensile and shear failure are captured between discrete elements, and the model can be assigned heterogeneous rock strength. There is no need for an empirical leak-off law, as the geomechanical model MDEM is coupled to the reservoir simulator TOUGH2. Another strength of MDEM is that the physics remain the same in 2D and 3D. These abilities enable it to describe dynamic hydraulic fracture initiation and propagation in 2D (and 3D).

Simulation of XLOT using MDEM is part of a joint research project by the Drilling and Well Centre for Improved Recovery (DrillWell). The main goal of the project is to "Improve precision in stress determination from XLOT, in challenging formations and complex stress regimes". The author of this master's thesis was part of the SINTEF Petroleum team that develops MDEM throughout the course of the thesis work.

As an XLOT simulator, MDEM had to be refined to be able to describe fracture initiation and propagation in low-permeability rock such as shale, where most XLOTs are performed. The modifications included poroelasticity, fracture permeability model and implementation of mass conservation. The team at SINTEF Petroleum consists of Idar Larsen, Alexandre Lavrov and Andreas Bauer. The structure of this work was such that Idar did most of the implementation of code in MDEM (C++), Alexandre and Andreas were focusing on theoretical aspects of the model and the physics of hydraulic fracturing, while the undersigned continuously ran the numerical simulator on computers as it was developed and fed back results and issues.

In addition the undersigned developed and implemented some code in MATLAB, specifically the parts that regard how to couple the fracturing simulator to a well, with constant surface injection, well shut-in, and flow-back through a fixed surface choke. The well will act as a

fluid-storage container, which implies that large volumes of decompressed fluid will flow from the well upon fracture initiation and propagation, resulting in more unstable fracture growth and a longer and wider fracture. In MDEM the borehole and formation are given a height of unit length in 2D, which corresponds to a very stiff system, sensitive to changes in volume. In reality, the well is very compliant.

Chapter 2 presents an overview of different methods applied for numerical simulation of rock behaviour, and their ability to describe geomechanical phenomena, along with some theoretical framework. In particular the Modified Discrete Element Method, and how it is coupled to a reservoir flow simulator. Chapter 3 introduces XLOT and XLOT interpretation. In Chapter 4, the process of refining MDEM to become an XLOT simulator in low-permeable rock, and in deep wells, is described, along with simulation results and discussion. Appendix A contains plots, Appendix B contains MATLAB scripts, and Appendix C a literature review on the use of pressure integrity tests as methods for sub-surface stress determination.

Chapter 2

Numerical Modeling in Geomechanics

Numerical methods have become an essential tool for geomechanical simulations as they allow modeling of non-linear behavior of rocks and soils. Before the advancements in computing power during the late 20th century, analytical solutions were preferred due to their efficiency and their ability to show results where impact of different parameters included in the solution easily can be identified. The application of analytical methods are however limited to the specific sets of assumptions to which they are derived. Assumptions may be e.g. that the medium is homogeneous (zero heterogeneities within the rock mass), isotropic, that it behaves within limits of linear elasticity and that it is independent of time (e.g. loading rate, loading response). Cases where available theory fails to predict or even explain behaviour observed in the field are often seen. Numerical models may then be the only way to achieve some understanding of the results, especially in complex stress regimes, complex geometries and difficult formations (anisotropy, ductility, plasticity).

In the offshore wells of the Norwegian continental shelf, most XLOTs are conducted in Shale overburden to assess drilling gradients and to obtain stress information for field planning purposes. Conditions are often far from what conventional analytical methods are able to describe, which is manifested by how observed field results deviate from the ideal case. In addition to natural properties specific to the formation drilled (e.g. as mentioned complex stress regimes and geometries), several complicating factors are introduced during an extended leak-off test (XLOT), such as varying impacts of injection rate, plastic rock deformation, poroelastic and thermal effects, presence of faults, natural fractures, loading history, well direction, as well as all of these effects' impact on fracture orientation and growth. To evaluate these, and how they interact relatively, they must be included in a more advanced numerical simulation.

It is important to recognize that no numerical analysis tools solve the actual physical problem of the field, but rather a problem designed to optimally mimic the real field case. Proper knowledge and understanding of the system as well as of the desired analysis are thus crucial to achieve cost-saving results. The simulation software will uncritically produce results from

whatever input specified, and it may be dangerous to blindly manipulate parameters until a desired output is seen, instead of the intended more systematic analysis. It is the engineer's task to define an initial-boundary problem that is in agreement with the field case, define the type of analysis to be conducted, and to predict and define relevant features of the formation. Such features include properties, parameters and dominant processes expected during the simulation. Subsequent to the initial problem set-up, the model needs to be properly calibrated, for which a sensitivity analysis is necessary. Then, planning of the systematic analysis/modelling procedure and verification of results follow. This is all part of the planning phase of a numerical simulation, and it is thus clear that most of the work done to produce successful results is in fact prior to operating the actual numerical tool.

2.1 Numerical Modelling Methods

Numerical methods can be divided into two main groups, continuum and discontinuum methods [12]. Within these two groups there are many different numerical methods available. Which method to choose is largely dependent on factors specific to the case that needs to be simulated. The continuum approach is best used if only a negligible number of fractures are present and if fracture opening and block detachment are insignificant factors, while the discontinuum approach is suitable where the number of fractures is too large for the continuum approach to be used, where fractures are expected to be induced, or where large-scale displacements of individual blocks are possible. For finite element models inducement of fractures necessitates to re-mesh the problem model. Fracture system geometry and the size of the discontinuities relative to size of the problem can be said to be the two main factors to look at when deciding whether a continuum or a discontinuum method is most suited

A wide range of different methods are available, each with its advantages and disadvantages for different applications. As XLOT simulation is the focus of this thesis, it will be explained why any pure continuum approach, as well as conventional discrete element methods fail as XLOT simulation tools.

On a reservoir scale it has up until recently been impossible to realistically model loading response of fractured rock mass, as well as realistic modeling of fracture growth. Later in this chapter, available discontinuum methods will be reviewed as methods to simulate field scale problems, and it is argued why the Modified Discrete Element Method is a promising tool for simulating XLOT.

2.1.1 Finite Element Method and Finite Difference method

Two continuum methods that are largely used in the industry for geomechanical reservoir modeling are the Finite Element Method (FEM) and The Finite Difference Method (FDM). Both approximate solutions of a set of partial differential equations (PDEs). The disadvantage of FEM and other continuum methods in solving geomechanical problems is that discontinuities have to be defined beforehand. This implies that neither fracture development nor fault reactivation can be modeled dynamically, but require continous remeshing [2]. Fracture systems, if not too complex, can be modeled when included in a domain, and time dependent strains can be implemented as well as material properties such as heterogeneity and anisotropy.

Using FEM, the formation or problem is divided into many elements with specific shapes defined by shape functions, resulting in either triangular or rectangular elements. FEM then approximates the solution of a set of PDEs, by use of these shape functions. The approximation is done for each element by a trial function, that calculates nodal displacement of elements due to applied load, from which stress and strain is calculated. The type of trial function will decide accuracy and duration. If rough approximations are provided by the trial function, then the number of elements can be increased to improve accuracy.

FDM does on the other hand not apply shape functions. Instead, FDM approximates the PDEs with a local[1] Taylor expansion. FDM is in general simpler and more efficient in solving PDEs, of domains where boundaries can be sufficiently approximated with rectangular grids, such as for fluid flow modeling in reservoirs. An advantage of FEM as compared to FDM is the ease of having non-uniform grid size in the model, whereas FDM requires a structured mesh, most often consisting of rectangular grids, to cover the formation domain. This limits its use when fractures or heterogeneity within the domain are present, and in general FDM is considered not ideal if the formation to be modeled is given a domain of complex surfaces [2]. FEM is then preferred.

There are two types of FDM, the Eularian based, which is the oldest and usually what referred to as the FDM, and the Lagragian based [2]. The Eularian fixes the grids, while the approximations can change within, and as a result deformation cannot be modelled. The Lagragian allows modelling of rock deformation as it uses non-uniform grids without a fixed structure. This is done by dividing the grids into zones, each surrounded by nodes (four nodes for rectangles in 2D), and constitutive equations are applied to update stresses and strains within the domain. Constitutive relations that include relations for elastic to plastic strain can be implemented, i.e. non-linear stress-strain laws. Although the grid is allowed to move with the solution, faulting and fracturing is still not possible without remeshing the problem. This FDM is more applicable for petroleum reservoir simulations where non-linearity is expected. FLAC^{2D}

[1] Local approximation of a function: Use value and derivative at single point, to approximate neighboring points.

and FLAC^{3D} by Itasca Consulting Group Inc. [4] are examples of software tools using FDM that model plastic flow, and are known to have reasonable computation times as compared to distinct element method tools such as the Itasca DEM software PFC.

Numerical tools are classified based on their solution scheme, as either explicit or implicit methods. Itasca FLAC thus uses an explicit solution scheme, which means that the data used to approximate a solution for a subsequent simulation timestep is expressed explicitly in terms of data from the present timestep, and an approximation is directly calculated. As will be described in Chapter 2.1.2, explicit methods are only conditionally stable as they suffer a time limit constraint to maintain numerical stability, but they are simpler and use less computing power than implicit methods [2, 17]. Implicit methods require iterations because the input data for the approximation are given implicitly in the approximation outcome. As a result of this complexity implicit methods generally require more computing power than explicit methods [17].

Conventional continuum methods alone are not optimal XLOT simulation tools, due to their limited ability in describing discontinuities, and as continuum models cannot capture the different failure modes in fractured rock mass or complex stress distributions of even simple fracture configurations [13]. The above tasks are highly relevant for simulation of XLOT or hydraulic fracturing treatments in natural fractured reservoirs.

2.1.2 Discrete Element Method

Geomechanical simulation addressing problems at large scale for field development has conventionally been done by FEM methods, which as mentioned in Chapter 2.1.1 allows for plastic strain modelling, but not faulting and fracturing. To be able to model the latter, discrete element methods must be used [2].

A discrete element medium differs from a continuous medium by the existence of contacts or interfaces between the discrete elements that the domain consists of [4].

☞ A software is called discrete element method only if it allows finite displacements and rotations of discrete bodies as well as complete detachment, and that it recognizes new contacts automatically during calculation [4]. The former is essential be able to reproduce mechanism in a discontinuous medium, and the latter is a condition for interactions to take place, that are not known beforehand [4]. Discontinuities are treated as boundary conditions between distinct elements, meaning that joints are represented by interfaces.

Distinct element method

Distinct element method (DEM) is a particular discrete element method introduced by P. A. Cundall in 1971 [5], and was applied for soils on a grain scale by Cundall and Strack [6] in 1979. In this explicit scheme equilibrium forces and displacements in a stressed assembly of discs (in 2-D) or spheres (in 3-D) are found. Particles interact only at contacts points, contacts are allowed to deform, complying a contact law, and all particle dynamic interaction is monitored. Tensile strength is given to a model by a threshold force to be overcome at each contact, called bonds (see Chapter 2.1.2). Element motion is following Newton's 2^{nd} law.

The solution procedure involves that for each explicit time step and for each particle, a calculation cycle is run, where Newton's 2^{nd} (force displacement) law is *applied to each particle* and updates its position, then relative motion of two particles in contact is handed over to the contact law which is *applied on each contact* to update the contact forces, and the total force on the particles are calculated, before an updated contact force is sent back to Newton's 2^{nd} law. The cycle is run until a state of equilibrium is found. To reach such a state it is necessary to add damping of particle motion, in the form of a viscous force on every contact. Energy can then dissipate during loading, which allows the particle to reach steady state [6].

Implementation of Rock Strength

As rocks are inherent of tensile and shear strength that work as thresholds against fracturing, bonding models are implemented in discontinuum methods. It is done by adding a normal and a shear force on each contact that must be overcome for the contact to break in either tensile or shear failure. At failure, the elements separate, and the forces are set to zero. This is when $U^n \leq 0$ in Fig. 2.2. Another type of strength implementation used in DEM is the parallel bond. The difference from the contact bond, is that the parallel bond is represented by an own piece of material located between particles that is inherent of shear and tensile strength, i.e. its own shear and normal stiffnesses. Essentially, the contact bond is a parallel bond with zero radius. A feature of parallel bonds is in addition that they can feel force from neighbouring particles that can contribute to failure. Cementation of rocks are represented in DEM by bonds. This are the models implemented in the Itasca DEM software PFC^{2D} [2, 5]. The two bonding models mentioned are illustrated in Fig. 2.1, and is also seen on the right on Fig. 2.2.

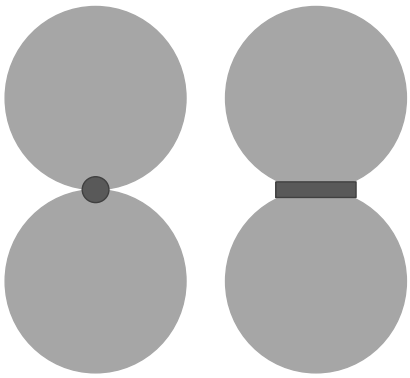

Figure 2.1: Illustration of Contact Bond and Parallel Bond Between Two DEM elements. (Reproduced from Alassi [2])

Relating Contact Force and Particle Position

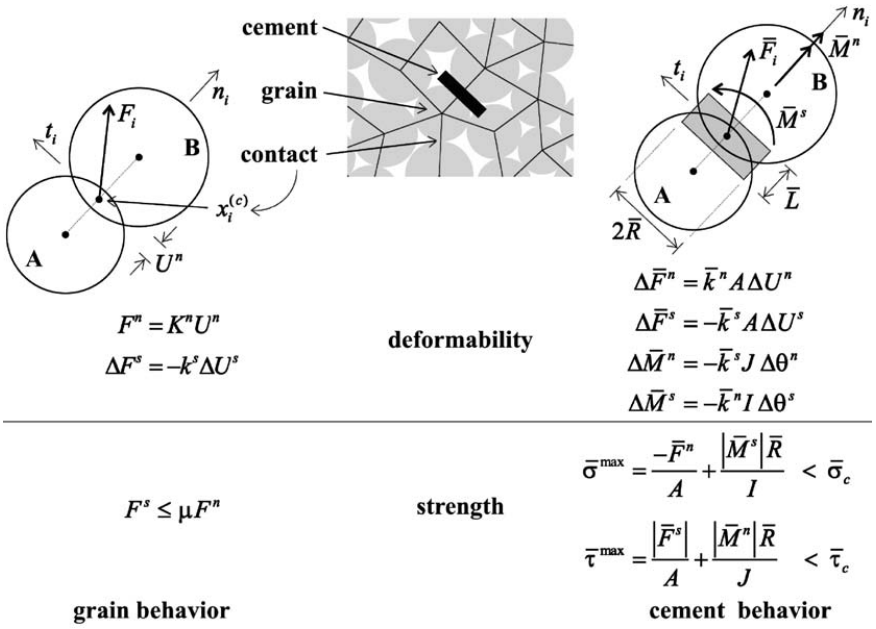

Figure 2.2: Force-displacement behaviour of grain-cement system: Grains bounded by the BPM as implemented in PFC using DEM (from Cundall and Potyond [5]).

In Figure 2.2 the force-displacement behaviour of particles inherent of contact strength is illustrated: F_i is the contact force vector, which represents the action of particle A on particle B. It consists of normal and a shear force components F_n and F_s, in directions n_i and t_i equated as

$$F_i = F_n n_i + F_s t_i \tag{2.1}$$

In Figure 2.2, U^n is the particle overlap displacement, and K^n is the contact normal stiffness, which is a function of normal stiffnesses k_n of particles A and B respectively. Shear force F^s is initially set to zero, but then every shear movement of the two particles relative to each other

will add to shear shear force. The shear movement is emerging when the contact plane rotates, and shear force increment is calculated as the product of incremental shear movements ΔU^s times the contact shear stiffness over the time step (see Fig. 2.2). ΔU^s is a function of particles' relative velocities, timestep and clockwise rotational velocity of the two particles. The contact shear stiffness is a function of particle stiffness k_s, of A and B respectively. After shear force is updated, a slip criterion is applied to check for particles slip, which incorporates the rock internal friction angle in particle to particle interaction. In Chapter 2.1.2 failure and slip criteria for bonds are described.

The contact force F_i will in addition cause a moment M^A and M^B acting on particles A and B respectively.

When F_i has been calculated, then any additional force F_{ex} specified by the user, e.g. due to pore pressure, is added, and damping force F_d is subtracted. Then Newton's 2nd law is directly applied to calculate the acceleration of particle A,

$$a = \frac{F_i + F_{ex} - F_d}{m^A} \tag{2.2}$$

where m is mass of the particle Cundall and Strack [6]. The rotational acceleration α of particle A is given as

$$\alpha = \frac{M^A}{I^A} \tag{2.3}$$

where I^A is the moment of inertia of the particle. Accelerations a and α are subsequently used to update velocity and rotational velocity under the assumption that they are constant over timestep Δt. By appliance of a finite difference scheme, the updated velocity is next used to update position of the particle, while the rotational velocity is used to calculate rotation [6]. For the full set of equations and procedure, the reader is referred to the paper by Cundall and Strack [6].

The Time Limit Constraint

Explicit methods have a time limit constraint that implicit do not have. This a numerical stability condition. Time steps must then be small enough so that disturbance felt by an element will not be transmitted farther than to elements in which it is in contact with [6]. The speed of transmission is decided by the physical properties of the medium. The condition makes it possible to simulate loading response and interaction of a large number of elements in a domain with reasonably low computing power, and few iterations. Implicit methods on the other hand, involve letting more distant elements communicate, thus it becomes more an iterative technique. It is more complex to program, and require more computational effort and computer memory per step in matrices storage. Implicit methods need in addition non-physical algorithms to

model physical instability, while in explicit methods this is avoided as failure processes can be modelled realistically [5]. Implicit is thus less optimal for DEM modeling.

Explicit DEM modeling will be stable as long as the time step is shorter than the critical time step determined in the software as function of the system physical properties. Usually the user specifies a fraction of the critical value to be used in the simulation [6].

DEM Numerical Simulation Software Tools Available

UDEC and 3DEC are DEM tools from Itasca, 2009 and 2008, that recently have been used for geomechanical simulation and analysis of rock, in two and three dimensions respectively. They treat discontinuities as boundary conditions between blocks. UDEC utilize an explicit solution scheme, and can model non-linear behavior of rock that contains multiple and intersecting joint structures. Both rigid and deformable blocks can be included in the model. Deformable blocks are defined by a continuum mesh of FDM zones, where the zones are allowed to behave differently according to constitutive relations as described in Chapter 2.1.1. Discontinuity relative motion in normal and shear directions is decided by stress-displacement relations [4]. Among disadvantages are the constraints of the pre-defined geometry of complete blocks, where non-persistent joints needs to be embedded. Thus it may be tedious to set up dense fracture networks. Block breakage due to growth of non-persistent joints, is possible in UDEC, however not in 3DEC [13]. For 3DEC there is thus a fundamental problem in simulating the mechanical response to loading of blocks that contain such joints, especially if the number of non-persistent joints is large, which should affect the behavior of the block [13].

Particle Flow Code

The approach on particle interaction and bonds as described above (page 7) was the introduction to what in 2004 was presented as the Bonded Particle Model (BPM) by Cundall and Potyond [5]. BPM is implemented in Itasca DEM softwares PFC^{2D} and PFC^{3D}. It was refined to include poromechanical coupling [2]. Notice that BPM, PFC and DEM are weaved together. As Particle Flow Code (PFC) is the code that the Modified Discrete Element Method (MDEM) is based upon, some focus is here set on identifying its advantages and disadvantages as they relate to modelling large-scale reservoir geomechanics and MDEM.

In PFC, BPM relates particles and bonds directly to similar objects observed microscopically in rock. Micromechanisms occurring in rock, are complex and difficult to model within frames of continuum methods. With PFC such mechanisms can be modelled, and hypotheses on how the microstructure of rocks affects their macroscopic behaviour can be tested. Fracture toughness is an example of a rock property that is a function of microproperties such as cement and grains, and which controls the formation of macroscopic fractures [5]. BPM lets micro cracks emerge, interact and coalesce into macroscopic fractures automatically and dynamically

in the model, whereas e.g. UDEC (DEM) and 3DEC (DEM) and continuum methods do not. Another strength of DEM worth noticing, is that mechanisms such as plastic flow is automatically incorporated in the model, due to particle rearrangement and rotation. This reduces the number of parameters to calibrate, whereas plastic models usually have too many parameters [2].

A general disadvantage with PFC is that microproperties has to be chosen through a calibration process to match test results, a procedure described in Cundall and Potyond [5], which may be a tedious and difficult process. The challenges regards how to relate DEM parameters to rock properties, which are needed to feed models with correct contact properties. Strength properties are stress based in real life, and contact based in DEM. Thus there is a need to relate the constitutive DEM parameters for grain-to-grain stiffness, k_s and k_n, to rock parameters, specifically unconfined compressive strength (UCS), Young's modulus (E) and Poisson's ratio (ν), P- and S-wave velocities (V_p, V_s).

Alassi [2] concluded that there are three main hinders of using particle based DEM in modeling of large-scale reservoir geomechanics and for seismic modelling:

1. The first main disadvantage regards the process of calibrating DEM parameters to rock properties: Specifically that for a particle based method such as DEM, the maximum P-wave/S-wave ratio is limited by $\frac{V_p}{V_s} = \sqrt{3}$ [2]. This corresponds to maximum Poisson's ratio (the ratio of lateral strain to longitudinal strain) of 0.25. Alassi [2] found this when calibrating DEM interaction parameters using PFC2D. He derived relations for the interaction parameters k_s and k_n for two categories, dense packing and loose random packing, and performed tests on PFC2D models to compare results from the lab and analytical equations with numerical DEM results. Tests included biaxial test for small scale case, and reservoir geomechanical test for large scale case (static tests), and dynamic tests where P-wave and S-wave velocities where compared to numerical results.

2. The second is the difficulty of deriving failure properties, which cannot be done as in FEM and FDM methods, as a simple initial condition. Numerical tests must be done every time a geomechanical model is built, to extract rock properties and construct a failure envelope. Such a procedure is described in Alassi [2]. This is because the properties shear and tensile strength defined at contacts are not equal to or easily inverted to rock mass properties that are obtained in experiments on rock.

3. Third, using DEM it is more difficult to build geomechanical models and, specifically, to install initial stress conditions which are often complicated for hydrocarbon reservoirs.

The second disadvantage is especially a shortcoming for in-field simulations, because you often have estimates or measurements from logs and cores on the elastic macroscopic rock

properties. The optimal thing in the sense of XLOT or general reservoir modelling would be to be able to directly invert these macroscopic rock properties to the DEM particle interaction parameters.

2.2 Modified Discrete Element Method

A Modified Discrete Element Approach (MDEM) was developed originally by Alassi [2] in 2008 during his PHD study at NTNU. The objective was to eliminate the limitations of the regular DEM while keeping its main advantages. In the following MDEM with its solution scheme is reviewed as it relates to regular DEM. The PHD thesis and papers are used as reference (if not otherwise specified).

MDEM is a tool that can model fracture developments and fault reactivation both inside and outside hydrocarbon reservoirs during fluid production and injection. The method is appropriate for XLOT simulation in stiff formations. Its main advantage over conventional DEM methods is that it behaves like a continuum method before failure and like a DEM after failure. In MDEM, macroscopic elastic properties (the conventional constitutive matrix) can be given as input, and are inverted directly to the microscopic stiffness matrix (particle interaction matrix).

While conventional DEM works with single elements, MDEM instead works with triangular clusters, each reaching to 3 element centers (nodes). Each cluster can then be said to be made of three elements. Recall that the in conventional DEM, solutions are achieved through cycles, where each cycle has two steps: 1. Loop through all contacts. 2. Loop through all elements. In MDEM the first step is modified by looping through all clusters to get contact forces for that specific cluster [2], then node displacement is calculated with total force on that node from the forces calculated in the surrounding clusters (see 2.4). the cluster total force and Newton's 2nd law. The constitutive DEM particle interaction parameters, k_s and k_n, that relate the contact forces to relative displacements, are herein referred to as normal and shear particle stiffness. For a cluster of three elements, each inherent of its own stiffness parameters, the relation of contact force F and relative displacement U is written in matrix form as

$$\begin{pmatrix} F_{n1} \\ F_{n2} \\ F_{n3} \end{pmatrix} = \begin{pmatrix} k_{n1} & 0 & 0 \\ 0 & k_{n2} & 0 \\ 0 & 0 & k_{n3} \end{pmatrix} \begin{pmatrix} U_{n1} \\ U_{n2} \\ U_{n3} \end{pmatrix} \tag{2.4}$$

where the contact shear force is neglected by setting $k_s = 0$. The modification from the original DEM to MDEM is done by adding new stiffness coefficients in the off diagonal matrix positions

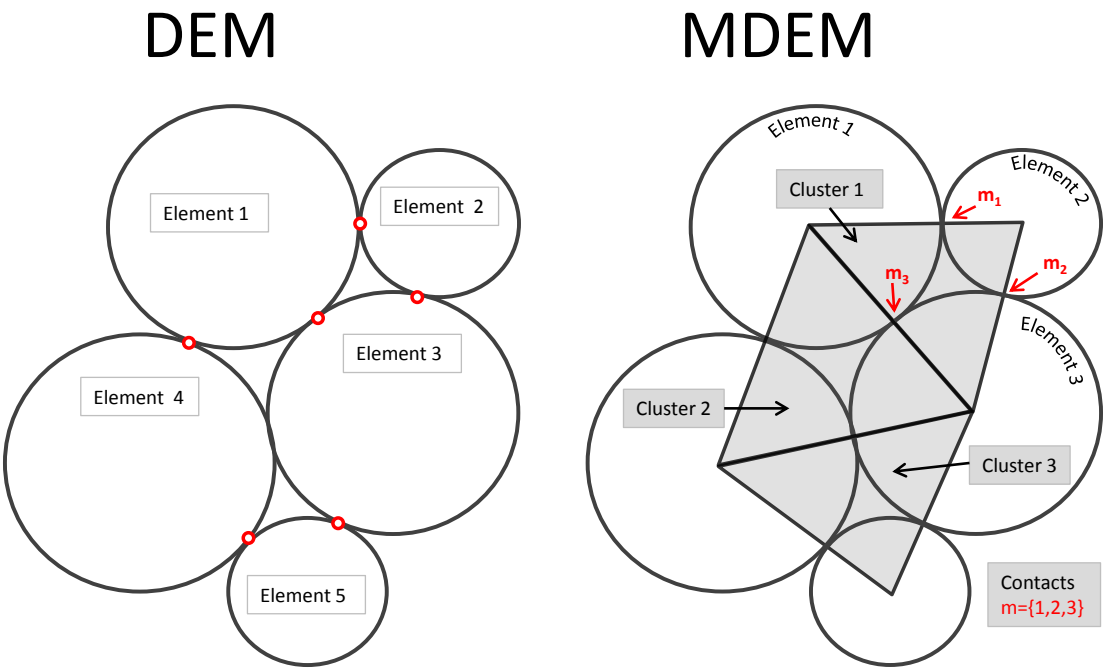

Figure 2.3: Illustration of DEM and MDEM model scheme. Each cycle in the DEM solution scheme consists of a first step that loops through all contacts to updates forces, then a second step that loops through all elements to update displacements. In MDEM, the first step differs by that it loops through all clusters, each consisting of three elements, and then update forces for the contacts in that cluster with a specific procedure that depends on the clusters state and on stress distribution resulting from presence of cracks or displacements. The second step is then similar to regular DEM by that it loops through the model element-wise, and updates element motion.

in the stiffness matrix as

$$\begin{pmatrix} F_{n1} \\ F_{n2} \\ F_{n3} \end{pmatrix} = \begin{pmatrix} k_{n1} & a_{12} & a_{13} \\ a_{21} & k_{n2} & a_{23} \\ a_{31} & a_{32} & k_{n3} \end{pmatrix} \begin{pmatrix} U_{n1} \\ U_{n2} \\ U_{n3} \end{pmatrix} \tag{2.5}$$

The stiffness matrix is equivalent to the one defined in FEM methods with linear elements. An edge of MDEM is that a relation between the stress and the internal forces is obtained. This enables the ability to define initial conditions with ease, as well as to define failure properties just like in continuum methods such as FEM and FDM. The relation between the stress,

$$\sigma = \{\sigma_{xx}\sigma_{yy}\sigma_{xy}\}^{T} \tag{2.6}$$

and the internal forces F_n, is

$$\sigma = \frac{1}{A} M^{T} F_n \tag{2.7}$$

The relation between the strain,

$$\varepsilon = \{\varepsilon_{xx}\varepsilon_{yy}\varepsilon_{xy}\}^{T} \tag{2.8}$$

and the relative displacements u_n is

$$U_n = M\varepsilon \tag{2.9}$$

M is the unit normal vector matrix defined as

$$M = \begin{pmatrix} I^2{}_{11}d_1 & I^2{}_{21}d_2 & I^2{}_{31}d_3 \\ I^2{}_{12}d_1 & I^2{}_{32}d_2 & I^2{}_{32}d_3 \\ I_{11}I_{12}d_1 & I_{21}I_{22}d_2 & I_{31}I_{32}d_3 \end{pmatrix} \tag{2.10}$$

where I_{m1}=cosθ_m and I_{m2}=sinθ_m and θ_m is the normal vector orientation of the contact m inside the cluster. d_m is the distance between the two elements that are in contact, and A is area of the triangle. Note that all area in a model is necessarily covered by triangles. Hence, Eq. 2.7

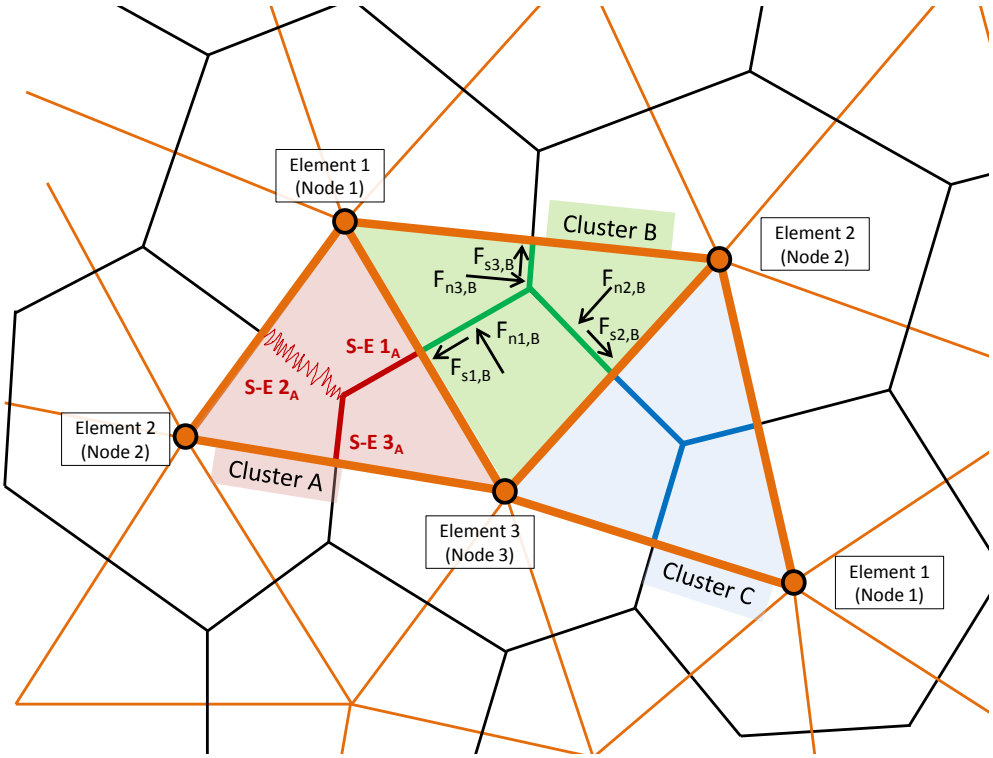

Figure 2.4: Illustration of a triangular element mesh where Voronoi's elements are built from triangles, and where three V. elements comprise a cluster. Each contact between V. elements shares two clusters. All internal forces are updated independently in each cycle, and notice that each sub-edge has its own force vectors. If a cluster fails, its sub-edges will be checked for gaps. Sub-edges with gaps get updated status to be cracks.

is written

$$\begin{pmatrix} \sigma_{xx} \\ \sigma_{yy} \\ \sigma_{xy} \end{pmatrix} = \frac{1}{A} \begin{pmatrix} I^2{}_{11}d_1 & I^2{}_{21}d_2 & I^2{}_{31}d_3 \\ I^2{}_{12}d_1 & I^2{}_{32}d_2 & I^2{}_{32}d_3 \\ I_{11}I_{12}d_1 & I_{21}I_{22}d_2 & I_{31}I_{32}d_3 \end{pmatrix} \begin{pmatrix} F_{n1} \\ F_{n2} \\ F_{n3} \end{pmatrix} \tag{2.11}$$

Remembering the generalized relationship of stress and strain,

$$\sigma = C\varepsilon \tag{2.12}$$

and combining the matrices in Eqs. 2.5, 2.11, 2.9 on matrix form with Eq. 2.12, we get the equation for the macro stiffness matrix,

$$C = \frac{1}{\mathrm{A}} M^T K M \tag{2.13}$$

where K is the micro-stiffness matrix, which is equivalent to the stiffness matrix derived in FEM. Conventional elastic properties are given to a material model based on Equation 2.13 to obtain matrix K. In matrix form, Equation 2.13 is written

$$\begin{pmatrix} C_{11} & C_{12} & C_{13} \\ C_{21} & C_{22} & C_{23} \\ C_{31} & C_{32} & C_{33} \end{pmatrix} = \frac{1}{A} \begin{pmatrix} I^2{}_{11}d_1 & I^2{}_{21}d_2 & I^2{}_{31}d_3 \\ I^2{}_{12}d_1 & I^2{}_{32}d_2 & I^2{}_{32}d_3 \\ I_{11}I_{12}d_1 & I_{21}I_{22}d_2 & I_{31}I_{32}d_3 \end{pmatrix} \begin{pmatrix} k_{n1} & a_{12} & a_{13} \\ a_{21} & k_{n2} & a_{23} \\ a_{31} & a_{32} & k_{n3} \end{pmatrix} \begin{pmatrix} I^2{}_{11}d_1 & I^2{}_{12}d_1 & I_{11}I_{12}d_1 \\ I^2{}_{21}d_2 & I^2{}_{22}d_2 & I_{21}I_{22}d_2 \\ I^2{}_{31}d_3 & I^2{}_{32}d_3 & I_{31}I_{32}d_3 \end{pmatrix} \tag{2.14}$$

On the right in Fig. 2.3 the elements are spherical to illustrate that a cluster spans from element centers (nodes). In MDEM, elements are not spherical but have Voronoi's shapes [2]. This implementation adds to its list of strengths, as it allows use of automatic triangular mesh generation codes, and thus to build complicated models with ease. Another result of triangle meshes is that each cluster has three edges within, and thus that all above equations are applicable. An example of an MDEM model with Voronoi's triangle diagram is shown in Figure 2.4. Each cluster in the model contains three sub edges, denoted S-E 1, S-E 2 and S-E 3 in cluster A in Figure 2.4. Note that these are contained within the cluster triangle. Each contact comprise two sub-edges, i.e. that each contact between the Voronoi's elements shares 2 clusters. All internal forces are updated independently in each cycle, and notice in Figure 2.4, that each sub-edge has its own force vectors.

The failure criteria implemented in MDEM are in addition to the criteria for tensile failure, the Mohr-Coulomb (MC) criterion for shear failure, which incorporates the rock internal angle of friction in MDEM failure criteria. The friction angle is furthermore included in a slip criterion where all failed clusters are checked for slip.

The criteria for cluster tensile failure is that the effective stress exceeds tensile strength of the rock in negative, in addition to for the slip criteria.

$$\sigma - P_f \leq -T_0 \tag{2.15}$$

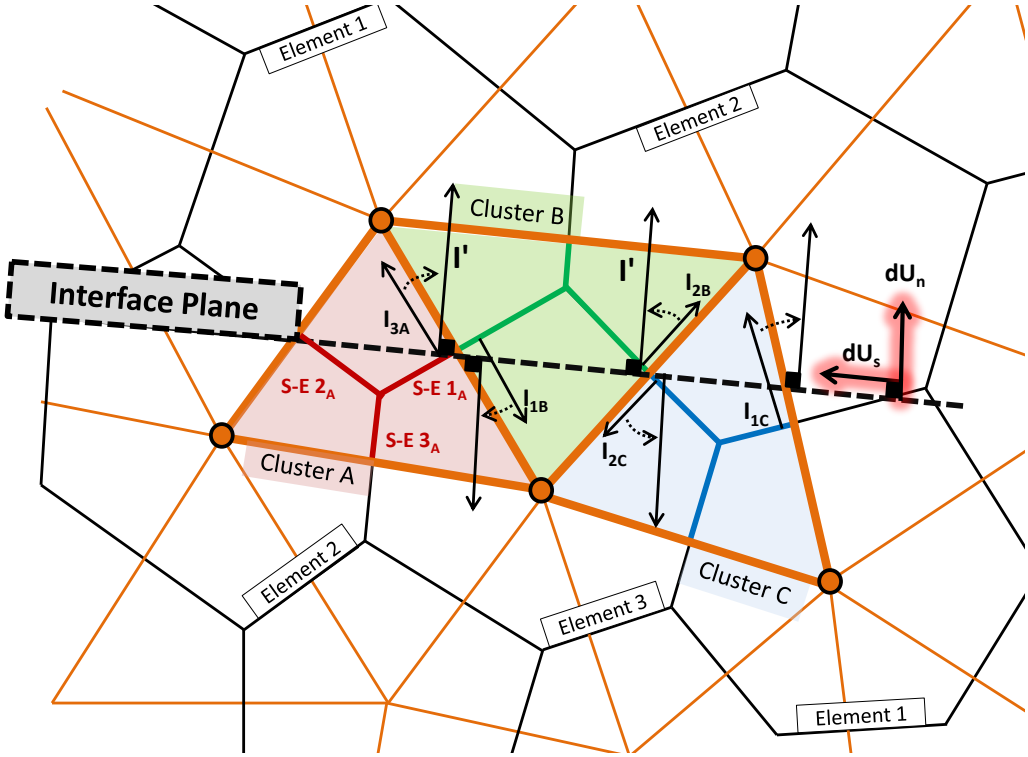

Figure 2.5: Illustration of an interface plane (plane of weakness) in an MDEM model. Three clusters, cluster A, B, and C are intersected by an interface plane, thus these specific clusters are in "interface state", where unit normal vector I on sub-edges (S-E) are replaced by interface plane unit normal vector I' in the relative displacement calculation. dU_s and dU_n are resulting relative displacements in shear and normal direction due to forces applied on each sub-edge in the respective clusters.

where P_f is fluid pressure, and T_0 is the tensile strength which is a property characteristic to the rock. The MC failure criterion is defined for 2D as ([8])

$$|\tau| = S + tan(\phi)N \tag{2.16}$$

where τ is shear stress, S is shear strength, ϕ is the angle of internal friction of the rock and N is the normal stress acting on the failure plane. Stresses are positive in compression. The criterion

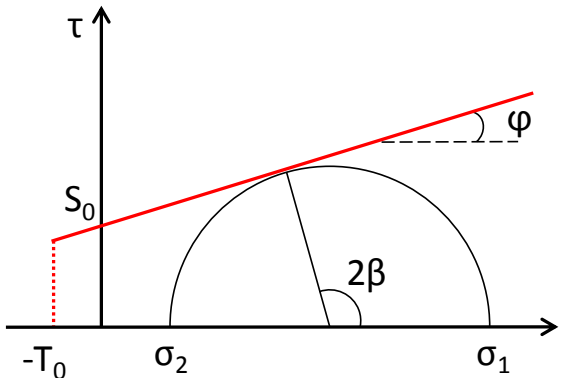

Figure 2.6: Schematic plot of Mohr's stress circle (modified from Fjær et al. [8]).

is drawn in Figure 2.6. In this failure envelope, the shear failure line in red can never intersect the normal stress axis, due to that failure in tensile stress will govern at -T_0 in, compliance with Equation 2.15). From Figure 2.6 the point of failure normal stress acting on the failure plane can be equated

$$N = \frac{1}{2}(\sigma_1 + \sigma_2) + \frac{1}{2}(\sigma_1 - \sigma_2)\cos 2\beta \tag{2.17}$$

and shear stress equated

$$\tau = \frac{1}{2}(\sigma_1 - \sigma_2)\sin 2\beta \tag{2.18}$$

where the angle β at which the failure criterion is fulfilled, i.e. the angle for the failure plane is

$$\beta = \frac{\pi}{4} + \frac{\varphi}{2} \tag{2.19}$$

σ_1 and σ_2 are the principle stresses in 2D found by

$$\sigma_1 = \frac{1}{2}(\sigma_{xx} - \sigma_{yy}) + \frac{1}{2}\sqrt{(\sigma_{xx} - \sigma_{yy})^2 + {\sigma_{xy}}^2} \tag{2.20}$$

$$\sigma_2 = \frac{1}{2}(\sigma_{xx} - \sigma_{yy}) - \frac{1}{2}\sqrt{(\sigma_{xx} - \sigma_{yy})^2 + {\sigma_{xy}}^2} \tag{2.21}$$

The criterion for slip is equated

$$\tau > tan(\phi)N \tag{2.22}$$

The criterion in Equation 2.22 is applied to all failed clusters, including those that have been updated to "failed" based on the previous timestep force calculations. If the criterion is fulfilled, shear force is generated from normal stress, and updated as

$$\tau = tan(\phi)|N|sign(\tau) \tag{2.23}$$

After a simulation timestep where each cluster was looped over, clusters can be in one of three cluster states:

- Intact state, where it behaves similar to FEM or FDM, by material elastic loading.
- Failing state, where it behaves exactly like DEM: DEM as described by Cundall and Strack [6], where contact forces are calculated as function of normal and shear particle stiffness. The off-diagonal elements in the stiffness matrix are then set to zero, and microscopic shear forces are allowed to generate between elements by setting k_s to a finite value. MDEM can then take into account slip as well as shear induced dilatency between crack surfaces (which are never perfectly smooth).
- Interface state, where the cluster is intended to model faults or predefined fractures. In this

state, the normal unit vector I is replaced by the modified I' for all contacts that intersect the interface plane (fault). I' is normal to the interface plane. Thus, relative normal and tangential displacements will now happen with respect to interface plane orientation, regardless of contact orientation. A model with three clusters intersected by an interface plane is shown in Figure 2.5. When looking at Figure 2.5, picture that the plane consists of two surfaces sliding on each other, each with its normal unit vector to be used for the particles associated with the surfaces (only one below and one above at any point along the plane).

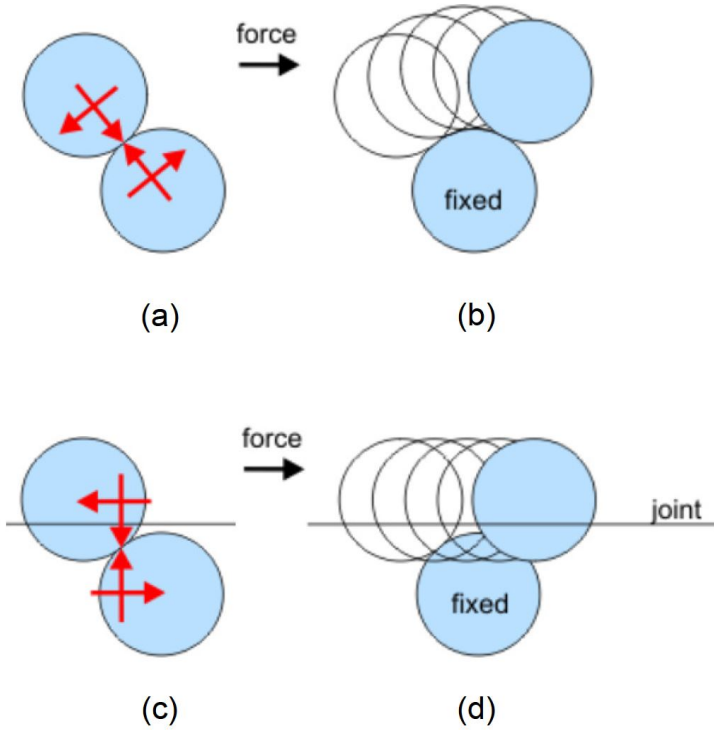

Figure 2.7: Illustration of a particle's response to the same lateral force for BPM with (c and d) and without (a and b) an interface plane as implemented by the smooth-joint contact model. In (c) and (d) the displacement happens regardless of particle contact orientation. "Smooth" denotes that particles joined by an interface plane can overlap and slide past each other, instead of having to go around each other as it is done in the conventional BPM by [5]. (figure from Mas Ivars [13])

This interface plane modification is known as the Smooth-Joint Contact Model, presented by Mas Ivars [13]. See Figure 2.7 for better understanding of the BPM with and without an interface plane as implemented by the smooth-joint contact model.

For each cluster the solution scheme to obtain new contact forces is as follows:

1. Input data are acquired from each cluster, which includes normal and shear force on all three contacts, time increment and elements' velocity, the initial and current positions of elements (nodes in Figure 2.4) the micro-stiffness matrix K obtained from Equation 2.14,

a friction coefficient, ratio of normal to shear particle stiffness, the current cluster state, shear and tensile strength.

2. For failed clusters, gaps are calculated as function of the initial and current elements' positions.

3. Normal and shear relative displacement increment are then calculated for every contact in each cluster as function of the two elements' velocity and relative direction and timestep.

4. If the cluster is intact, then forces are calculated as function of the previously calculated relative displacements by use of Eq. 2.5. For intact clusters the shear force is set to zero, because k_s is zero for intact clusters in the model. Stress is then calculated using Equation 2.11, to check if the intact cluster now has failed.

5. If the cluster is failing, i.e. that it has status as failed and thus needs DEM interaction calculations, or if it has interface status, then k_s is a finite value, and shear force is no longer zero. This is to model the shear force on the crack interface (sub-edge). This is explained physically by that when the bond is broken, shear resistance needs to be allowed to generate at the slip surface in response to the normal stress. The internal force increments applied on each contact, meaning the changes in normal and shear force on sub-edges $F_{ni,B}$ and $F_{si,B}$ for edge $i = 1, 2, 3$ in Fig. 2.4, is then calculated by use of both the normal and shear particle stiffnesses, k_s and k_n. If a cluster is updated as failing, then the sub-edges will be checked for gaps. Sub-edges with gaps get changed status to be cracks, illustrated by a zig-zag sketch in Figure 2.4.

Going from status "intact" to "failed" is done by setting the off-diagonal elements in the stiffness matrix in Eq. 2.5 to zero and setting k_s to a finite value. The assumption is that the k_n are the same for intact and failed clusters.

Fracture propagation has no restriction as it is controlled by the stress distribution in each cluster. When a crack is opening up, it will always open first at the contact where the plane is the closest to perpendicular to the minimum stress. The initiation and direction of propagation of cracks, are thus fully automatic, without the need to know the minimum stress direction as an input to the calculation procedure.

7. After the internal forces on the sub-edges has been calculated for all clusters in the model, each inherent of its respective cluster state, the forces are applied to each element in the model following Newton's second law. The procedure is here just as described by [6] in 1979 on regular DEM (see Chapter 2.1.2), but in this case on Voronoi's elements instead of spheres.

Notice the convenience with being able to define cluster states; fractures or faults can be predefined with ease, by simply predefining clusters states 2 or 3. This allows complex fracture networks to be loaded into a model. Discontinuities

In the following chapter, the coupling of MDEM to a reservoir simulator will be described. This enables MDEM to simulate XLOTs and other injection/production schemes such as hydraulic fracturing treatments. Regarding the latter, another advantage of MDEM should be mentioned. There is great convenience of having DEM physics and FEM behaviour when it comes to dynamic fracture modeling in 3D: A limitation in FEM is the fundamental problem in going from 2-D to 3-D simulations. There are no analytical solutions for FEM in 3-D, while in DEM, e.g. PFC^{3D}, this is not a limitation. The same applies to MDEM. In FEM, discontinuities have to be modelled by re-meshing of the grid in each step, whereas in MDEM there is no fundamental problem, as the physics remain the same in 2D as in 3D, only that the implementation is more complex, and naturally that the computation time will increase.

Hydraulic fracturing simulators used in the industry today (e.g. FracPro) often have very simple fracture models such as the well known 2D models KGD and PKN which both give pre-defined planar fracture geometry. See Figure 2.8.

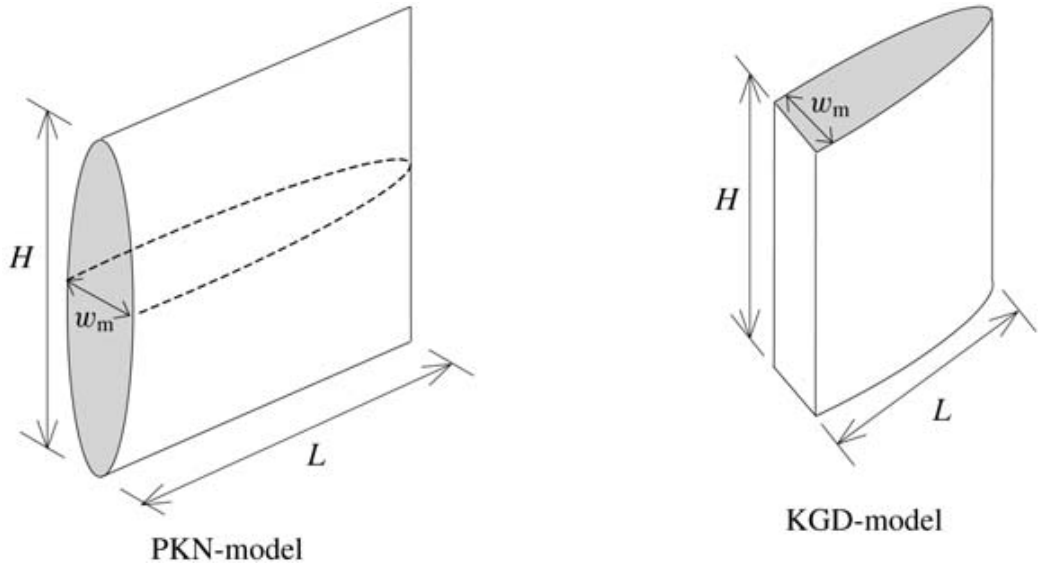

Figure 2.8: Illustration of fracture shapes of PKN and GDK models (from Fjær et al. [8])

Many fracture simulators are specified as 3D, but in most cases this means that in the third dimension the fracture shape is merely an extension of the 2D plane, and in addition they often use empirical leak-off laws. Such simulators cannot capture phenomena such as fracture twisting from a horizontal perforated liner, nor any interaction of fractures extending from multiple stages in a well. In MDEM such phenomena will be captured automatically and dynamically. All equations are readily available, and can be implemented in MDEM, to model true 3D fracture growth.

The most powerful advantage of MDEM over other numerical methods is however still summarized as: MDEM lets you define elastic and failure properties for grid triangles (= clusters) based on macro rock properties. Similar to FEM, only with a more empirical and effective stiffness tensor, where macro properties are inverted directly to the microscopic particle interaction parameters.

2.2.1 MDEM Sequential Coupling to a Reservoir Simulator

Currently, the geomechanical model MDEM is coupled to the fluid flow simulator TOUGH2. TOUGH2 uses integral finite difference method, and can model flow of multiphase, multicomponent fluid, compressible and non-isothermal flow into both intact and fractured porous material [3]. TOUGH2 eliminates the need for simplifying empirical leak-off laws, and facilitates modelling of simultaneous injection into rock at multiple positions and with different fluids. The TOUGH2 version that currently is coupled to MDEM, and used in this thesis, model non-isothermal fluid flow of single phase brine. This is relevant to mention as regard to XLOTs and fracturing jobs, where yield stress fluids such as mud and fracturing fluids usually are used. TOUGH2 works with triangles, which is perfect for MDEM where each cluster comprises a triangle, with the result that the same grid can be used, thus each cluster or triangle may be considered as its a fluid control volume.

The coupling to MDEM is a two-way sequential coupling, with a timestep limitation as described in Chapter 2.1.2. The term "coupling" in this case denotes staggered communication between MDEM and TOUGH2:

1. TOUGH2 hands over to MDEM the current pressure in every cluster triangle after a timestep (of injection, shut-in, or production),

2. MDEM reads these pressure data and applies them as external forces in the model. Then MDEM runs its solution procedure, which includes to check and update every cluster status in the model either to failing or to remain as it was (intact, failed or interface plane). When a cluster is reported as failed, the porosity and permeability in its triangle is scaled up according to a factor called the permeability multiplier.

3. Updated triangles' porosity and permeability are then handed back to TOUGH2, which initiates the next timestep where it again models and updates pressure in all model triangles.

To explain the concept of up-scaled cluster permeability flow can in a simplified view be described by Darcy Law [3]. The flow q between two clusters (triangles) can be described by Darcy's law as

$$q = PM_{\text{mult}} \frac{k}{\mu} \frac{\Delta P}{L} \tag{2.24}$$

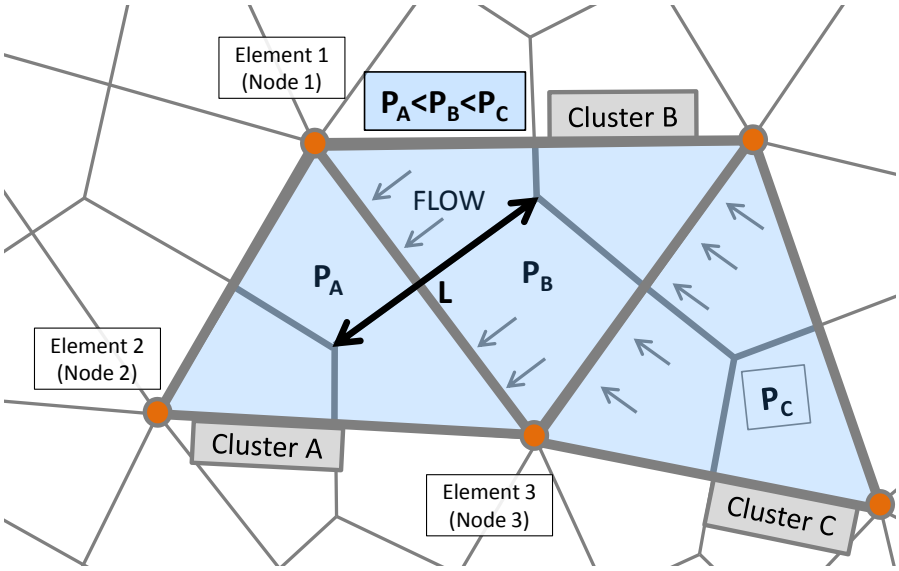

Figure 2.9: Schematic drawing to illustrate coupling between geomechanical and reservoir simulator. Flow between clusters can be described by Darcy's law, where failed clusters are given an upscaled permeability

where PM_{mult} is the permeability multiplier that equals to one if the cluster is intact, and higher than one if it has broken. k is the initial permeability of the rock matrix, μ is the fluid viscosity, ΔP is the pressure difference in clusters, and L is the length of the contact between cluster centers.

In the original MDEM-TOUGH2 coupling code as developed by Alassi et al. [3], the factor PM_{mult} that scales permeability in a cluster (=triangle) when it fails, is set to a constant value for all elements. This means that the permeability is not a function of the fracture aperture, which in fact varies from fracture to fracture. Essentially, the fracture is immediately fully opened in hydraulic sense, to its pre-set permeability, even before any fluid has approached through its opening.

In addition, as will be explained in Chapter 4, this creates a problem for realistic modelling of fracture growth during an XLOT simulation. In such a simulation it is crucial that the fracture permeability multiplier is a function of fracture aperture, which changes from timestep to timestep.

Chapter 4 introduces MDEM as an XLOT simulator. Refinements that needed to be done to the original code to make it a stable hydromechanically coupled fracture simulator are discussed, together with XLOT simulation results.

Chapter 3

Introduction to XLOT and XLOT Interpretation

In-situ stresses are key information for well and formation integrity as they allow accurate evaluation of drilling and completion related risks, especially for narrow drilling windows, in deviated wells and in complex stress regimes [7]. The industry has over the recent decades become aware of how accurate stress data may be used to optimize field development and total recovery. Overburden stress changes due to depletion induced compaction and subsidence may not allow late time production drilling and in-fill drilling. To evaluate and predict such changes, accurate stress data needs to be obtained in the field at an early stage in the field development. As pressure integrity tests to assess and verify formation and cement shoe barrier integrity already have been an integrated part of offshore drilling operations, these tests have been used beyond their original purpose, to determine sub-surface in situ stresses.

In a normal stress regime, where one principal stress is vertical and the other two horizontal, the vertical stress can be determined by density log integration or correlations with reasonable accuracy, while horizontal stress requires dedicated tests [7]. The extended leak-off test (XLOT/ELOT) is considered the most reliable method for estimation of the minimum horizontal stress without the use of down hole packers to isolate the open hole segment [1, 15, 7]. An XLOT optimally approximates results from a hydraulic fracturing stress test, which is the ISRM recommended method for in-situ stress determination (see Haimson et al. [10]). The XLOT's advantage over the latter is simplicity and reduced cost, especially in deep wells, as it by comparison does not necessitate use of packers and uses drilling fluid as pump in fluid [7].

Figure 3.1 shows the characteristic pressure response of an idealized XLOT with two cycles. After casing has been run, and cement shoe set, the cement and a few meters of fresh formation is drilled out. Then annulus is shut, and fluid is pumped into the well at a fixed rate to pressurize the well. In a formation integrity test (FIT), pumping is stopped when a predetermined pressure has been reached, to confirm cement shoe barrier integrity and that the planned mud

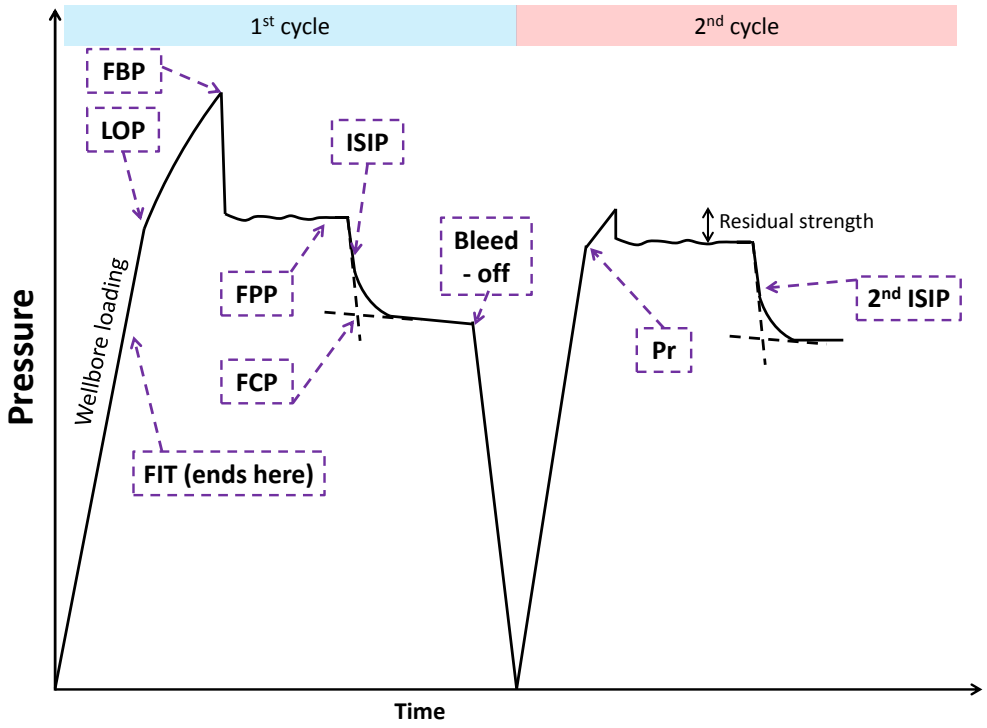

Figure 3.1: Characteristic pressure response of an idealized extended leak off test with two cycles (schematic plot). (from Eide [7])

weight for the subsequent section allows safe drilling without losses. The leak-off test (LOT) is a continuation of the FIT and is essentially a measure of the formation fracture gradient. Pumping is then done until deflection from linearity is seen on the plot of pressure recording versus time, denoted the leak-off point (LOP). The LOP is interpreted as the point where fluid starts to enter permeable parts somewhere in the well system (cement shoe, formation or completion equipment). The LOP has traditionally been interpreted as an indication of the minimum horizontal stress, but recently this interpretation has been strongly challenged [7]. It may at best be interpreted as a highly uncertain upper bound estimate of the minimum horizontal stress. The reader is kindly referred to Appendix C, where it is argued why the LOP and individual LOTs are not suitable for sub-surface stress determination.

In an extended leak-off test the pumping is continued well beyond the formation breakdown pressure (FBP), as illustrated in Fig. 3.1, where clear indication of fracture growth is observed in the pressure versus time plot. Pumping is stopped when the fracture is made sure to have grown beyond influence of near wellbore hoop stresses, i.e. when pressure stabilizes at a stable fracture propagation pressure (FPP) [7]. Then pressure decline is monitored, and the point at which the fracture mechanically closes (FCP) is recorded. This point is the best known indicator of the minor horizontal in-situ stress in tectonically relaxed formations [7]. It is obtained as indicated in Figure 3.1, by intersecting the tangent lines of the instantaneous shut-in pressure (ISIP) and the stabilized shut in pressure decline, see Appendix C section 2.1.1. for a more

detailed explanation of shut-in decline analysis.

In low-permeable formations or in formations were a low-permeable filter cake has formed, the fracture may not entirely close during shut-in pressure decline. In such cases flowing back the injected volume through a fixed choke is recommended. The closure process is then monitored by evaluation of system stiffness during flow-back, and the point of mechanical closure is obtained by different plotting techniques. Statoil ASA has implemented the system stiffness approach as their standard XLOT technique for 15 years [9], to be used in both permeable and impermeable formations.

While the major horizontal stress can not be reliably ascertained from pressure integrity tests in tectonically relaxed formations, there are interpretation techniques to isolate this information in compressive stress settings. In such stress regimes, leak-off may be due to shear induced dilation at lower pressures than tensile failure. This may allow to constrain the maximum horizontal stress (see Appendix C section 2.4). For more information on XLOTs and XLOT interpretation the reader is kindly referred to Appendix C.

Chapter 4

Hydro-Mechanical Coupling During Fracture Propagation in XLOT: Results and Discussion

4.1 Previous Work

Simulation of XLOT using MDEM is part of a joint research project by the Drilling and Well Centre for Improved Recovery (DrillWell). The main goal of the project is to "Improve precision in stress determination from XLOT, in challenging formations and complex stress regimes". As an XLOT simulator, MDEM had to be refined to be able to model fracture initiation and propagation in low-permeability rock such as shale, where most XLOTs are performed. The modifications included poroelasticity and a fracture permeability model.

The status of MDEM-TOUGH2 as an XLOT simulation tool per August 2013 is represented by the 2D simulation result presented in Figure 4.1. The result is seemingly in accordance with a field XLOT result. In this chapter I will identify and explain why this is not the case, and describe the challenges found during test simulations fall 2013 and spring 2014, first listed shortly and later in more detail. Several modifications to MDEM were done in the process of making it a realistic hydro-mechanically coupled XLOT simulator. The simulation result in Figure 4.1 from 2013 suffer the following problems/limitations:

- Mass Balance is not included: This is manifested by initial pressure in a triangle remaining the same during deformation calculated during an MDEM step. Essentially this means that mass is created, as newly "opened" fracture volume at all times already is fluid filled, which results in only negligible volumes of fluid flow into the failed elements. There is still significant pressure drop during breakdown (see Figure 4.1), because of the very low system compliance. Mass balance is less of a problem for permeable formations where the fracturing fluid leaks off into the formation. For low-permeability formations,

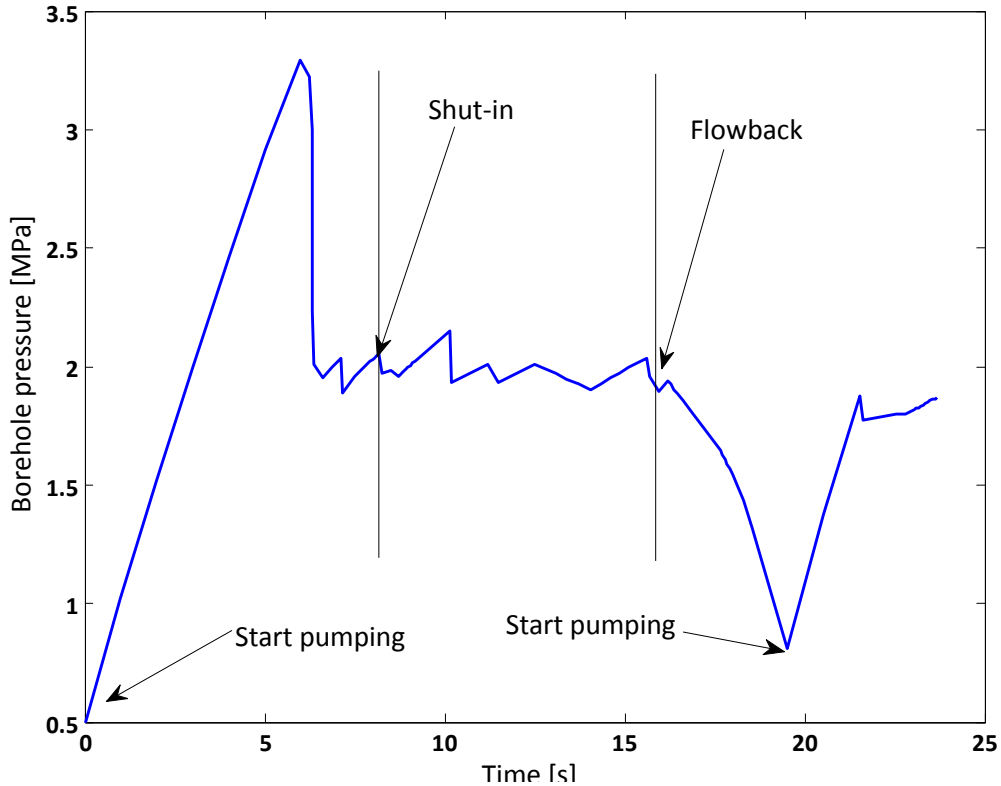

Figure 4.1: XLOT Simulation Result MDEM-TOUGH2 as per August 2013 (with permission from SINTEF Petroleum).

however, the created fracture volume is the only volume the fracturing fluid can flow into.

- The permeability of the boundary between broken clusters (with up-scaled permeability) and their neighbouring intact clusters is calculated by an arithmetic average of the permeability of the two. This induced artefacts such as parallel fractures and borehole instability during XLOT simulations.
- Coupling of the well: The formation model is limited to 2D. This implies that the borehole domain, the thickness of the formation and thus the fracture height is limited to unit length in 2D. This corresponds to a very stiff system. As a result, the well pressure simulated by TOUGH2 is highly sensitive to changes in loading (injection rate, leak off to the formation and into a growing fracture), in a non-linear way. In reality, the well system (well alone, and fracture plus well) is very compliant, and a volume several orders of magnitude larger must be injected into the formation to achieve the same drop in bottom hole pressure (BHP) at formation breakdown.
- Grid dependence: The size of triangles is not taken into account when setting strength properties to the bond models (area in 2D). If strength is not a function of triangle size,

then threshold against failure is a function of triangle size. Variation in triangle size induced numerical artefacts.

In Chapter 4.4 the process of achieving stable numerical simulation of a propagating fracture with mass balance is described. The different approaches, results and challenges are described and shown. In Chapter 4.5 the coupling of a well flow and formation flow is described, with some references to the MATLAB code in Appendix B.

4.2 Boundary Conditions

The numerical simulations presented in this thesis were set up with the following shared boundary conditions

- Grid dimensions: 100 m x 100 m x unit length (1 m, 10 m)
- Initial formation pore pressure: 20 MPa
- Anisotropic in-situ stresses: $\sigma_x = 35$ MPa $\sigma_y = 30$ MPa
- Rollers on left-hand and bottom sides of the grid
- Injection point in the centre [50,50], into a borehole with diameter of 0.3 m
- The fracturing fluid system used is single phase brine, injected into a formation of permeability in the micro darcy range (10^{-19}-10^{-21}).

Additional conditions, specific for the respective simulations are stated in discussions. Note that the in-situ stresses specified above are not exact, but will vary slightly from model to model as MDEM sets up initial stress regimes by looping towards a solution where the model is stable and has the correct strength properties. The minimum formation stress is in the range 29-29.5 MPa in the simulations presented in this thesis.

4.3 Effect of Fracture Aperture on Cluster Porosity and Permeability

For a dynamic fracture propagation model that sees fractures as triangles of up-scaled permeability, it is crucial that the fracture aperture is taken into consideration when permeability and porosity of a failed MDEM cluster/TOUGH2 control volume is calculated. Essentially, such an implementation would for the flow simulator mean that the fracture is only allowed to open gradually after a crack has been induced. From Equation 2.24 we can define the factor PM_{mult} that scales permeability in a failed cluster as

$$PM_{\text{mult}} = \frac{k_{fracture+matrix}}{k_{matrix}} \tag{4.1}$$

In the original MDEM-TOUGH2 coupling code as developed by Alassi et al. [3], PM_{mult}

was set to a constant value for all failed elements. The crack induced at cluster failure would then immediately be fully opened in hydraulic sense, to its pre-set permeability, even before any fluid had approached through its opening. The first step in making MDEM-TOUGH2 an XLOT simulator in tight rocks was to overcome this non-physicality. SINTEF then implemented a fracture permeability model.

The fracture permeability model is based on the work of Ji et al. [11]. Ji et al. [11] presented equations for how to describe the contribution of a fracture to porosity and permeability of a structured (continuum) grid of rectangular elements. For elements in such a grid, the permeability will be increased in either of the directions x or y, depending on which direction the fracture intersects. The fracture permeability, i.e. the permeability contribution due to presence of the fracture, is then given as (e.g. Ji et al. [11])

$$k_f = \frac{\overline{w}^2}{12} \tag{4.2}$$

where $\overline{w}$ is the mechanical aperture of the fracture. If the fracture intersects the element only

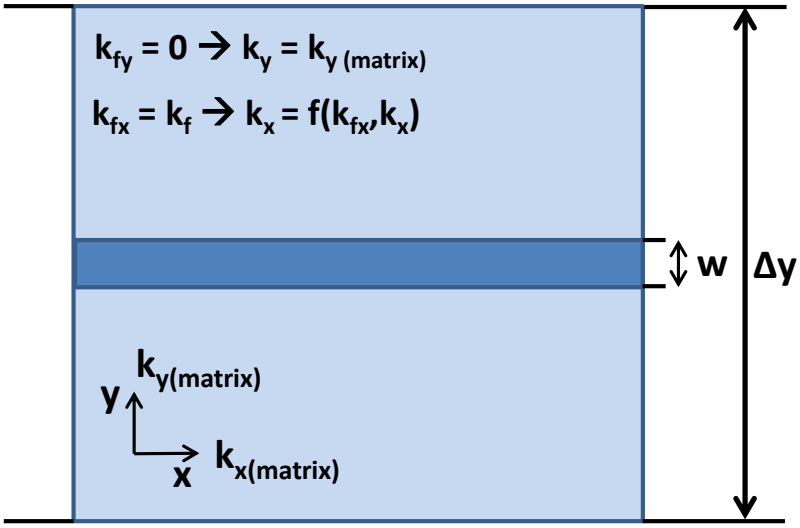

Figure 4.2: llustration of a fracture that intersects an element in the x-direction. The fracture contributes to the element's permeability in the x-direction, while it has zero contributions in the y-direction.

in the x-direction, as in Figure 4.2, it contributes to element permeability to the neighbouring element in the x-direction, and not in the y-direction. Thus in the y-direction the permeability multiplier PMX_{mult} equals 1, while in the direction of the fracture it is equated ([11])

$$PMX_{\text{mult}} = 1 + \frac{k_f \overline{w}}{k_x \Delta y} \tag{4.3}$$

The same logic applies for a fracture in the y-direction. Note that the mechanical aperture of a fracture differs from the hydraulic aperture, as no fracture surface is perfectly smooth. The

approach by Ji et al. [11] for rectangular elements was modified to work with triangular MDEM clusters. In the current MDEM-TOUGH2 implementation, matrix permeability $k_x = k_y$ for a cluster, and the cluster gets a uniform up-scaled permeability regardless of direction. With fracture software such as Extended Finite Element Method (XFEM) a fracture's path through an element could be tracked, and it would be possible to follow the flow, but in the current MDEM-TOUGH2 the permeability anisotropy is ignored. Once a cluster has failed, then from the displacement of the nodes (the corners of the cluster, see Figure 2.4) the fracture openings perpendicular to the sub-edges are calculated for each pair of triangles, and a function of these three is taken as aperture. In the next step, the hydraulic aperture is calculated from the mechanical aperture using a model developed at SINTEF. This model or the modifications cannot be disclosed in this thesis.

The fracture porosity, i.e. the fracture induced porosity in the triangle is given as ([11])

$$\phi_f = \frac{V_f}{V_b} \tag{4.4}$$

where V_f is the fracture volume, and V_b is the bulk cluster volume. Increase in cluster porosity implies an increase in flow capacity in that cluster, and thus the updated porosity is subsequently, and for every step, included in TOUGH2 flow equations. After the fracture permeability model had been implemented focus was set on implementation of mass balance.

4.4 Implementation of Mass Balance

Several options for keeping mass conservation in MDEM-TOUGH2 were considered. Since the undersigned was introduced to the MDEM-TOUGH2 project, there has mainly been three different versions of MDEM-TOUGH2 regarding mass conservation

- No mass balance
- Mass balance staggered coupling
  - Adjustment of pore pressures in failed clusters after completion of each MDEM step
  - For stability reasons, maximum pore-pressure changes per step were introduced and any induced volume mismatches were kept track of
- Mass balance full coupling

4.4.1 Staggered Coupling During Fracture Propagation

The first approach was to reduce pressure in broken clusters in one step. A pressure drop is the way of representing opened space in a failed cluster. A major limitation in the current MDEM-TOUGH2 model is that the fluid system is strictly single phase brine. There is no gas phase that can be taken into account, and as a result we have a very stiff fluid system where

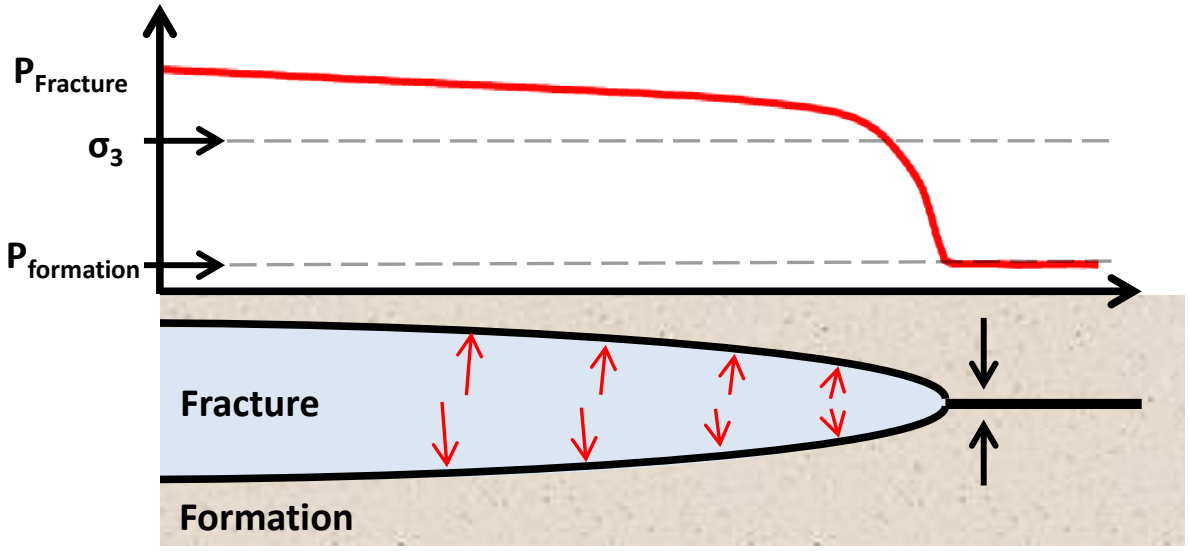

Figure 4.3: Illustration of a crack induced at fracture tip. If the formation fluid system is single phase water, there is a large pull on fracture surfaces preventing the crack from opening until fracturing fluid slowly flows into the fracture and opens it.

enormous pressure drops are needed to represent opened space. If gas was present in the well or formation, mass conservation could be simplified by assuming that when fracture volume is created it is immediately filled by air or vapor. Due to the high compressibility of the gas there would be little pressure change. Simulating multiple phases would on the other hand require a more complex hydromechanical model.

This first approach can be considered more of a numerical "fix" to allow more flow from the well into the cluster matrices, than an implementation to realistically describe a fracturing process. In this approach, the fracture basically was told to open fully at the exact moment the cluster had failed in tensile failure. The opening of space was represented by an immediate and large pressure drop in that step, and this created a tremendous pull on the fracture surfaces. If we consider a real fracturing event, a crack would form in the rock when rock tensile strength is overcome. It is not immediately open, but opens gradually as fluid is allowed to enter, which leaves an increasing pressure gradient leading back to the well.

If the formation fluid system is single phase water, as in our situation, the immediate crack opening would be very small due to the high fluid stiffness. The magnitudes of pressure drop needed to represent opening of small fracture space can be in the giga-pascal range for single phase water. The approach induced large instability to the model and did not describe fracturing physics.

Next, the approach was modified to limit the pressure drop after cluster failure, and then keep track of mass mismatch to keep reducing pressure for every timestep. This way, the fracture get more time to fill. Notice however, that it is still considered an open fracture by TOUGH2 and not a closed crack at failure. The staggered MDEM-TOUGH2 coupling created instabilities

also for this approach: What happens when we reduce pressure in an open fracture just after tensile failure? Recall the criteria for tensile failure defined in Equation 2.15, which says that a crack will be induced if the effective stress exceeds tensile strength T_0 in negative. When a

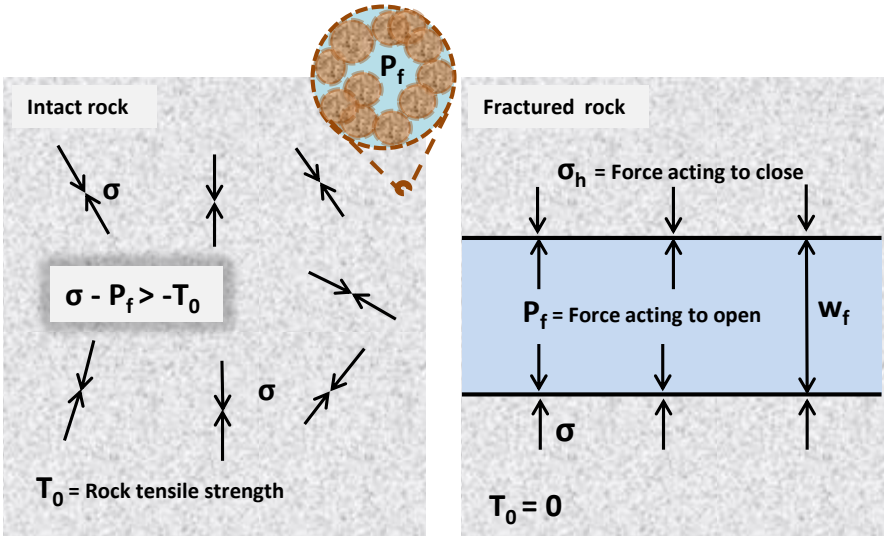

Figure 4.4: Simple sketch of a crack induced in tensile failure. On the left: Intact rock, inherent of tensile strength T_0. On the right: T_0 was overcome, a crack was induced and opened by fluid injection. Fluid pressure is acting on fracture surfaces to maintain opening, while stress is acting to close the fracture.

cluster gets status as failed and a crack is made mechanically by MDEM, the net stress acting on that cluster is zero. At this point the fracture would in reality open very little for a single phase liquid system. MDEM, however, only sees fluid force and opens the fracture. Next TOUGH2 comes in and lowers the pressure by a limited amount, but since the fracture is already open, TOUGH2 pushes fluid into the cluster. The pressure will then have increased in that cluster, all within the same timestep. Thus when MDEM receives the updated high pressure the fracture is opened even further. At the same time the mass balance mismatch will require that pressure is reduced in the failed clusters, which will reduce forces and allow MDEM to reduce the mechanical aperture. In Figure 4.4 an open fracture in force equilibrium is illustrated. Then TOUGH2 receives this pressure drop, but pushes additional flux into the cluster, and as a result the fracture will reopen. As large mass balance mismatch requires pressure to be reduced after each timestep, this results in a mechanically oscillating fracture. The oscillations were consistently observed in simulations by monitoring plots of normal displacement versus radial position during injection. See Figure 4.5 where this is plotted for three different timesteps, only one second (time increment) apart. The approach did not work as expected, but the learning was valuable. The fracture physics during initiation and propagation had to be better implemented. In reality a crack at the tip opens slowly to become a fracture.

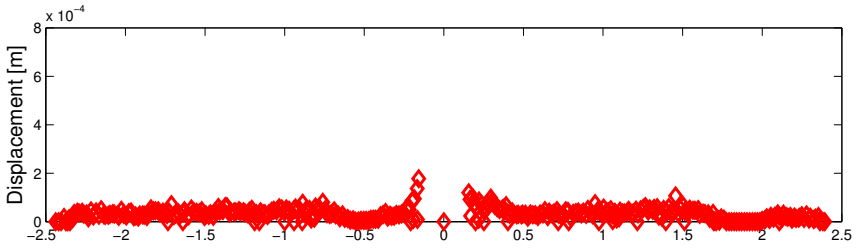

(a) Plot of hydraulic aperture along fracture length at t = 249 seconds

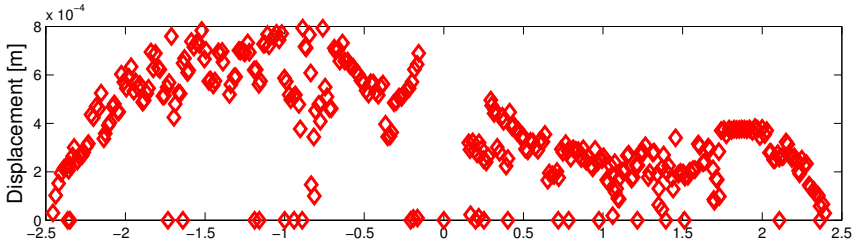

(b) Plot of hydraulic aperture along fracture length at t = 250 seconds.

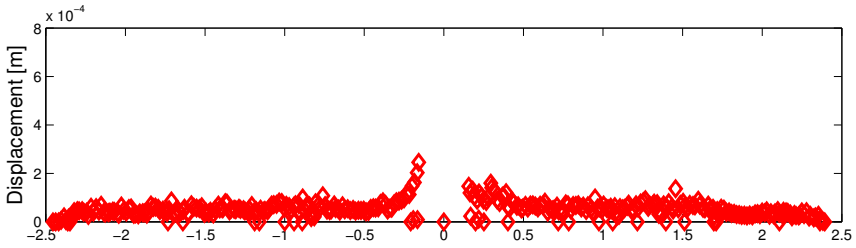

(c) Plot of hydraulic aperture along fracture length at t = 251 seconds

Figure 4.5: Plot of normal displacement (aperture) along the length of a fracture at three different timesteps, one second apart. The plots prove an oscillating fracture that opens and closes for every timestep. The fracture extends from borehole position at x = 0. The test was done with constant TOUGH2 injection rate of 0.00285 l/s in a formation of pemerability k_f=3.16x10^{-21} m2.

4.4.2 Mass Balance: Full Coupling During Fracture Propagation

Staggered coupling had shown to create instability and an oscillating fracture, and an approach on full coupling of hydraulics and mechanics was therefore introduced. In the previous section it was concluded that a crack induced at the tip of a fracture opens as the width of the fracture increases, and the tip crack opens and becomes part of the fracture.

The "saw-tooth" behaviour observed during fracture propagation in Figure 4.1 is interpreted as a numerical artefact attributed filling and failure of large triangles far from the well in the grid, and is not reflective of events in similar field observed behaviour of pressure versus time monitoring. The strength heterogeneity which was set to 25 % may have had minor contributions, but the behaviour is mainly due to discretization. Field observed "saw-tooth" behaviour is by Raaen et al. [15] interpreted as to reflect phases where the fracture widens at constant length, followed by sudden increase in length where fluid flows into the crack, before it again widens at constant length. For more explanation and plots of field test data showing "saw-tooth" behaviour, please see Appendix B 2.2.3.

For a single phase system we can do a simple analysis to show the effect on fluid pressure due to a small crack opening. Consider a crack induced in a quadratic 1 cm long grid element. Displacement is calculated on the nodes, and the crack mechanical aperture ΔW is calculated to be 10^{-5} m. Porosity due to the induced crack aperture can then be calculated with Equation 4.4, which for a quadratic element of unit length can be reformulated and calculated as

$$\begin{aligned} \Delta\phi &= \frac{\Delta w}{L} \\ &= \frac{10^{-5}}{10^{-2}} \\ &= 10^{-3}[-] = 0.1\% \end{aligned} \tag{4.5}$$

If the failed element has a porosity of 50 % and we assume the fluid system to be strictly single

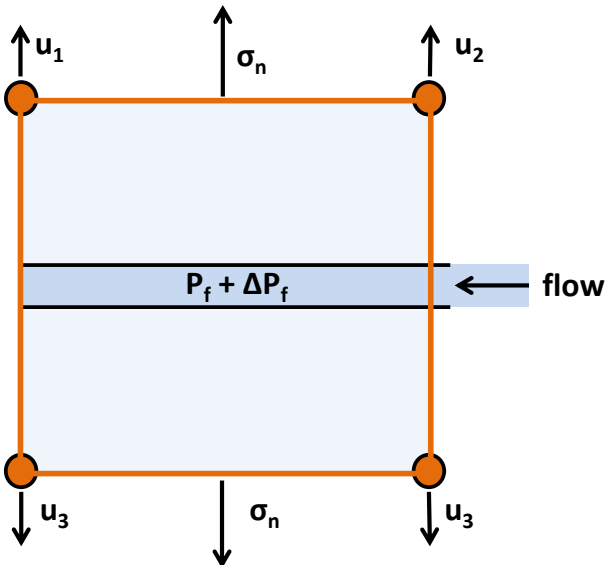

Figure 4.6: Illustration of up-scaled crack in an element. Aperture change is calculated from displacement in each corner, and a corresponding pressure drop in the crack allows fluid to flow into it, to further increase aperture.

phase water with bulk modulus K of $\sim$ 2 GPa, then the change in fluid pressure between the crack surfaces can be calculated as

$$\begin{aligned} \Delta P_f &= K_{\text{fluid}} \frac{\Delta V_p}{V_p} \\ &= K_{\text{fluid}} \frac{\Delta w L}{\phi L^2} \\ &= \frac{2 \text{ GPa}}{0.5} 10^{-3} = 4 \text{ MPa} \end{aligned} \tag{4.6}$$

A pressure drop of 4 MPa is a large drop considering that it is a result of a crack aperture of only 10 μm. With this knowledge there is no reason to have a staggered approach, but rather a dynamic coupling. The mass balance mismatch is known, and a pressure drop is given from

analysis as the fracture opens. Thus full coupling could be implemented. With this approach, the fracture opened gradually as a result of pushing fluid into the crack. As the aperture and corresponding pressure drop are what induce flow into the cluster, the mass balance is enforced as the width increases. In terms of fracture geometry during an injection test, this results in a final fracture geometry that is wider and shorter.

Another important modification made in the MDEM model, that followed the implementation of full coupling, was how the stiffness K of the formation was given. The bulk modulus K is defined as the ratio of hydrostatic stress relative to the volumetric strain [8] defined as

$$K = \frac{\sigma_p}{\varepsilon_{\text{volume}}} \tag{4.7}$$

In MDEM, the formation was previously given a drained stiffness. Drained stiffness, K_{fr}, refers to stiffness of rock measured under conditions where fluid is allowed to escape during loading, whereas an undrained stiffness $K_{undrained}$ refers to stiffness of rock measured while pore fluid is shut in. When an element had failed in MDEM, then full coupling included the fluid stiffness to its calculations on the failed element, i.e. undrained conditions, and as a result the stiffness of the failed elements was actually higher than the stiffness of the formation, which was drained. Young's modulus E and Poisson's ratio ν for the model are derived from K and shear modulus G (measure of the resistance rock has against shear deformation) using elastic relationships (see e.g. chapter 1.3 Fjær et al. [8]). For the model, this meant that the intact formation actually behaved softer than the failed triangles (the fracture). This induced instability, and was not physical. The formation was then given higher stiffness and shear modulus, from which new E and ν were derived, and as a result the model was stable. Mass balance was now enforced, with full coupling of fracture and flow during fracture initiation and propagation.

4.4.3 Permeability at the Boundary Between Failed and Intact Clusters

The permeability at the boundary between broken clusters (with up-scaled permeability) and their neighbouring intact clusters was previously calculated by an arithmetic average of the initial and up-scaled permeability. This induced artefacts such as parallel fractures and borehole instability during XLOT simulations.

Parallel Fracturing

One issue that was experienced in simulations was parallel fracturing. This was especially seen for high injection rates, which is a result of attaching a well to the MDEM-TOUGH2 simulator. The well will act as a fluid storage container and thereby uphold pressure and induce a larger fracture. Note that "parallel fracturing" does here not refer to a case where the fracture parts and grows separately in parallel, but rather a case where the fracture grows in width by

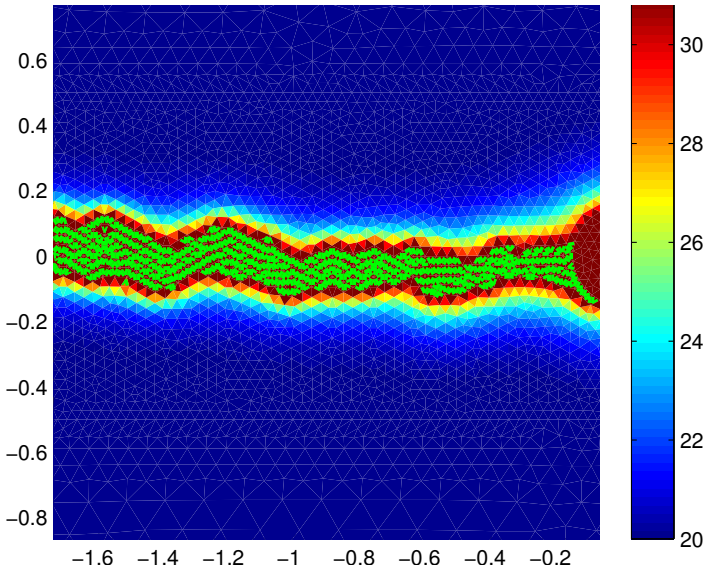

Figure 4.7: Plot of pressure in fracture.

failing new clusters in the fracture walls, instead of displacing these clusters by increasing the aperture in the already broken elements. This is illustrated in Figure 4.7. Another issue attributed to the permeability mean was borehole instability during injection, where clusters in the borehole wall failed in tensile and shear failure, resulting in an unstable and time consuming simulation where MDEM could not find a stable solution. Remember also, that for XLOTs in low-permeable formations, the only volume that fracture can flow into is the fracture space, which means that if fluid percolates into the walls as described in this section, it will be trapped as the well is flowed back for pressure versus time analysis of fracture closure (as this relates to stress determination). In Chapter 4.7.3, a simulation example of how the issue of parallel fracturing as a numerical artefact affected XLOT pressure versus time behaviour.

The modification to how the permeability at the boundary between a failed and an intact cluster was given, was to use harmonic average of permeability instead of arithmetic average. A harmonic average gives more consideration to the smaller value. This was a breakthrough in terms of stability and described the fracturing process and behaviour more realistically. The effect of the change is illustrated in Figure 4.8, on a before/after plot of pore pressure field during an XLOT injection phase. A more stable fracture propagation in length was then seen, while the fracture aperture increased steadily when surfaces were displaced in only a few failed clusters, instead of by the sum of width in several clusters in parallel.

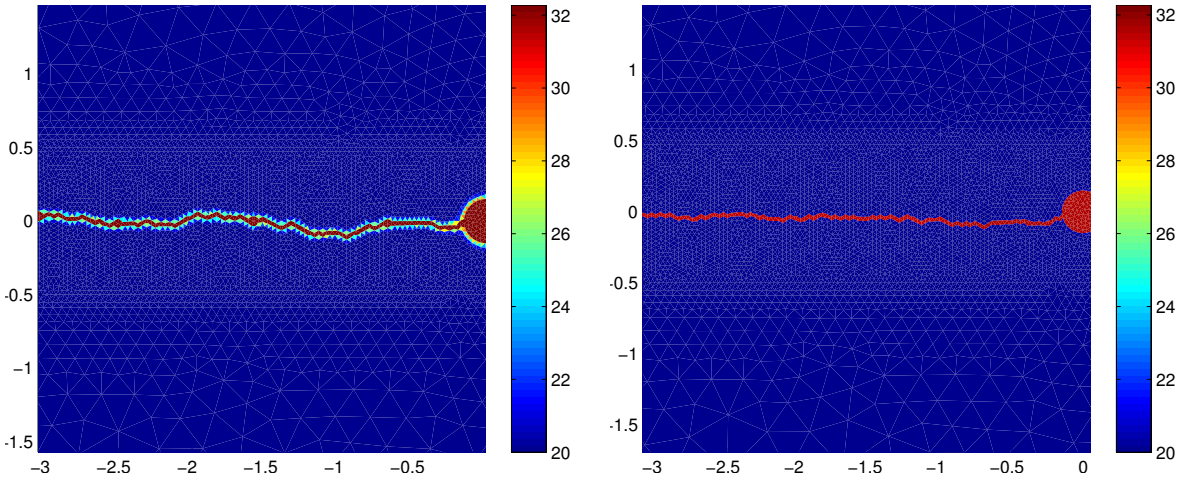

(a) Plot of pore pressure field [MPa]

(b) Plot of pore pressure field [MPa]

Figure 4.8: Plot of pore pressure field in formation and fracture before (a) and after (b) the modification of how permeability at the boundary between failed and intact elements was calculated. The same grid and conditions were used for both simulations.

4.4.4 Numerical Artefacts and Discretization

Recall the criteria for tensile failure, Equation 2.15. Due to their large area (in 2D) or volume (in 3D), large elements need more filling of fluid to fail in tensile failure to overcome the stress concentration on the specific element if the tensile strength is the same. A large surface will in addition carry more stress concentration from the surrounding stress distribution of the formation. Recall that the "saw tooth" behavior observed during fracture propagation in Figure 4.1 is interpreted to be a numerical artefact attributed filling of larger elements far from the well. When working with code modification and implementation to a geomechanical simulation software one has to do thorough testing by simulation to confirm that the implementation works as intended. It is then convenient to do trial testing on coarsely meshed grids, as these require less calculation effort. This may however depend on the type of problem the implementation is to model, but in general if the algorithms run on a course model, it is likely to work on finer grids as well. As a fracture will propagate in the direction of least resistance, it will in a model of isotropic stresses and varying triangle sizes choose to go in the direction of the smaller elements. See Figure 4.9, where this artefact is illustrated in a very coarse grid. The crack initiates on both sides of the well, but as it starts to propagate it chooses to go eastward to the smaller elements. At the point where the fracture has propagated far enough to encounter larger elements, the initiated crack in west will start to propagate. This trend was consistently experienced during trial simulations with different grids that had varying triangle size. The grids of varying triangle size that are used for trials in this thesis work are increasingly fine towards the center. In the center, a circular domain mark the borehole.

Variations in triangle size is not merely for trial simulations and testing. It is also an efficient

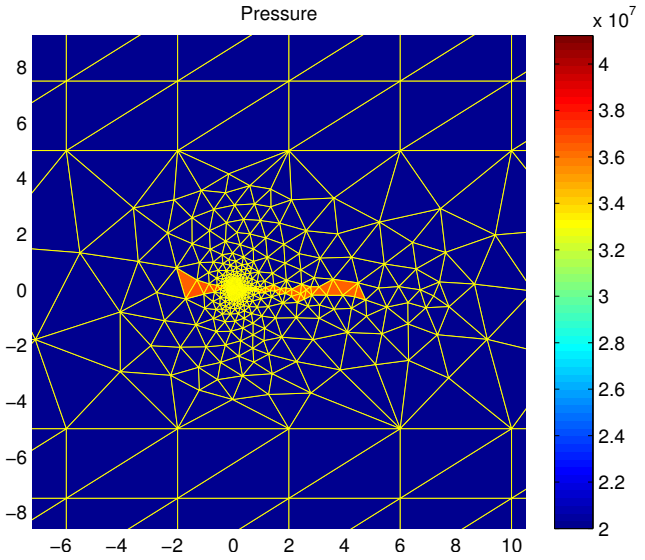

Figure 4.9: Simulation result in a very coursely meshed grid to illustrate an effect of variation in triangle size. Cluster strength is not scaled by triangle size (area), and the fracture grows accordingly: in the direction of least resistance, i.e. to the smaller elements.

way of decreasing simulation time in finer meshed grids. As MDEM-TOUGH2 uses triangles, the user can utilize automatic mesh generation software to construct grids, and specify smaller triangle sizes where discontinuities are expected or predefined, e.g. in cases where the user have an idea of where fractures will propagate. This is in the direction of least resistance. For instance, if an XLOT is to be simulated in a well in a formation of anisotropic stresses, i.e. that $\sigma_H > \sigma_h$, and the formation model is given low heterogeneity, then the fracture can be expected to initiate and propagate perpendicular to the minimum horizontal stress.

For XLOT simulation, the issue of increasing fracture threshold with element size manifested itself in that the fracture propagation pressure did not decrease with length of the fracture, when the model had increasing element size away from the borehole. Due to the borehole circumferential stresses, the propagation pressure is expected to reduce with length of the fracture, until it is near minimum in-situ stress.

The modification done in MDEM-TOUGH2 to reduce the effect of element size was to make particle bond strength properties a function of triangle size. In 2D it can be explained in a simplistic manner by that the strength of the smallest triangle in the grid is used to scale the strength of every other triangle. The scaling factor considers the ratio of the scaling element's area to the scaled elements' area. The specific equations cannot be disclosed.

Note that the modification does not take away other effects of element size, such as effects on the fracture propagation pressure, specifically fracture toughness effects. Fracture propagation pressure with its different contributions are described in Appendix C section 2.3.3. Fracture toughness is a concept that necessitates length scale, and in MDEM-TOUGH2 this length scale is the cluster size, when these fail in turn (and simultaneously) to form a fracture. Glass is a

very brittle material; it has a very high tensile strength, but once a fracture has been created, it propagates with ease due to glass' very low fracture toughness. Shale, on the other hand, is considered to be a material with more ductile behaviour. MDEM simulates, however, highly brittle fracturing, i.e. the ductility is not modelled.

An issue that was observed during simulations conducted as part of this thesis was as mentioned that fractures propagate faster in finer meshed grids. This is an common issue in modelling. Fracture toughness is at present not implemented in MDEM-TOUGH2, which means that the discretized grid does not model tip stresses and tip tensile strength, which has to be included to realistically model fracture propagation on a small scale. For this to be implemented, then what is referred to as a "sub-grid model" or "sub-grid scale model" could be included in the fracture propagation area, which would allow including analysis models for tip effects. Fracture toughness should then be a function of element size as well. In addition, when MDEM reports that an element has failed, its permeability and porosity is up-scaled to simulate fracture opening, then logically larger elements need more filling than small elements, which is another reason that element size should be a part of the failure criterion. In reality in low permeable shales, the induced space is mostly due to displacing rock surfaces.

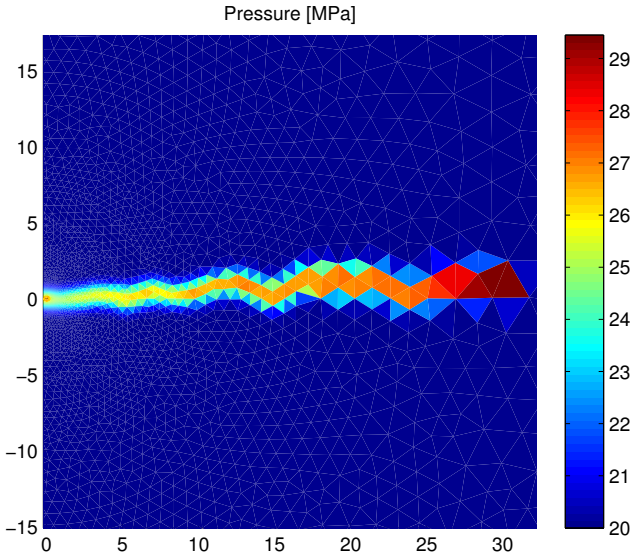

Figure 4.10: Simulation result: Plot of pressure versus radial position from borehole center after 80 minute of shut-in to model linear formation flow. The fracture pressure is plotted for the east wing of the fracture. Notice the trapped fluid pressure and that it decreases towards the well. The fracture aperture, and thus fracture permeability is zero in all elements at the time of the plot.

Triangle size was seen to affect rate of leak-off out of the fracture surfaces, i.e. the rate of pressure decline at a point in the fracture if the well is shut in. At any time when there is an open fracture, the leak-off rate through fracture surfaces will be highest where pressure is the highest in the fracture (where the pressure differential to intact elements is largest, recall Darcy Law for flow between clusters). However, this does not have to be the case if there is variation

in element (here triangle) size. The size of both the fractured elements, and of the elements surrounding them, affects the rate of leak-off. This was concluded after performing a shut-in test to investigate fracture closure by leak-off. The test and its results are discussed in more detail in Chapter 4.7.1.

Triangle size effects can also explain some of the experiences made with XLOT flowback tests. In these it was seen that pressure often got trapped in the fracture due to closure of the fracture flow path near the well, also known as fracture "snap-off", while it maintained hydraulic aperture further away from the borehole. As the fracture is then produced by specifying mass rate out of the borehole domain in the grid center, this near well "snap-off" can be attributed that these small elements near the well need to be a portal of flow to deplete the larger elements away from the borehole. Thus, if the hydraulic aperture slowly reduces near the well, as the pressure is lowered in the borehole from production, then permeability in these elements reduces and the immediate near well radii is depleted faster than the rest of the fracture.

Due to the many numerical artefacts induced by the use of course and varying sized triangles, it would be ideal to only use very finely meshed and large grids of constant triangle size. The limitation lies in the considerable time a simulation takes with such grids. The size of triangles is decided to some extent by the complexity of the problem to be described, but as a general conclusion variation in triangle size should be minimized.

4.5 Coupling of Formation Flow and Well Flow

4.5.1 Coupling to a full scale well

This chapter describes a module that attaches a full scale well to the MDEM-TOUGH2 model. As manifested by discussions and results in the previous chapters, mechanics and hydraulics are intimately connected during initiation and propagation of a fracture. To be able to model fracture development in XLOTs in deep petroleum wells, the well, which will act as a fluid-storage container, needs to be included. The Well Flow Module (WF) code was developed as part of this thesis, to allow realistic simulation of XLOTs in deep petroleum wells. A challenge of the reservoir simulator TOUGH2 when it comes to realistic results, is that it simulates injection with a given rate into a well volume of almost negligible size. MDEM-TOUGH2 sees the borehole as a small circular domain in the centre of a 2D grid of triangles, with a vertical dimension of one unit length to model volume. In MDEM the triangles within this domain are given high permeability and porosity, and then the user specifies injection or production into these. As a result the formation is unit length thick in the fluid simulations, which leaves the intact TOUGH2 borehole, herein segment, with a volume of A x unit length filled by a stiff fluid system.

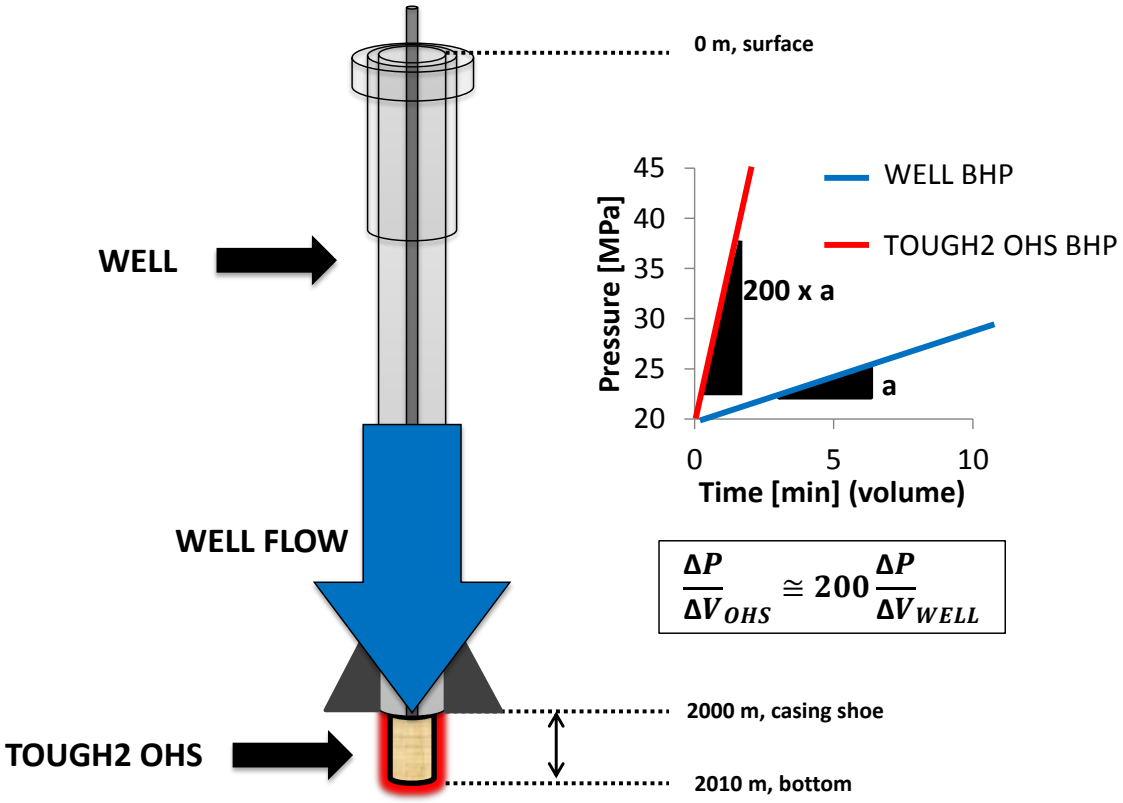

Figure 4.11: Illustration of a full scale well of 2000 meters attached to a 10 meter TOUGH2 open hole segment (OHS). The schematic plot shows pressure versus volume (time x rate) for an injection test, to illustrate the difference in compliance. After casing is set, cement is drilled out together with a few meters of fresh formation.

All XLOT simulations in this thesis assume a 10 meter rat hole below the casing shoe, and the well pump-in stiffness is scaled accordingly to extend the TOUGH2 segment to 10 meters length, as illustrated in Figure 4.11

The WF module consists of two parts, the Decompression Model, WFD, and the Fluid Pipe Flow Model, WFF. The task of the WF Decompression Model is to add a full well volume to the well segment that the reservoir simulator TOUGH2 works with. The effect of having a full well volume is easily illustrated by considering the situation in the present TOUGH2/MDEM 2D software with a well volume in the open hole segment of only around 60 litres low-compressible fluid: The leaked off volume during pressurization of such a small segment, although small, will have considerable effect on the pressure in the segment, whereas in the context of injecting into a well of e.g. two thousand meters depth, the effect of the same leak-off rate will be almost negligible. This is illustrated in Figure 4.12 which shows a LOT simulation result after constant injection into a 10 m open hole segment for 500 seconds. Note that the well is not coupled to the open hole segment in Figure 4.12, rather the corresponding pressure of the well due to the leak-off rate (that is responsible for the pressure drop at 250-300 seconds) is plotted. The problem is illustrated in Figure 4.11. The same logic applies to the injection rate: a 2000 meter

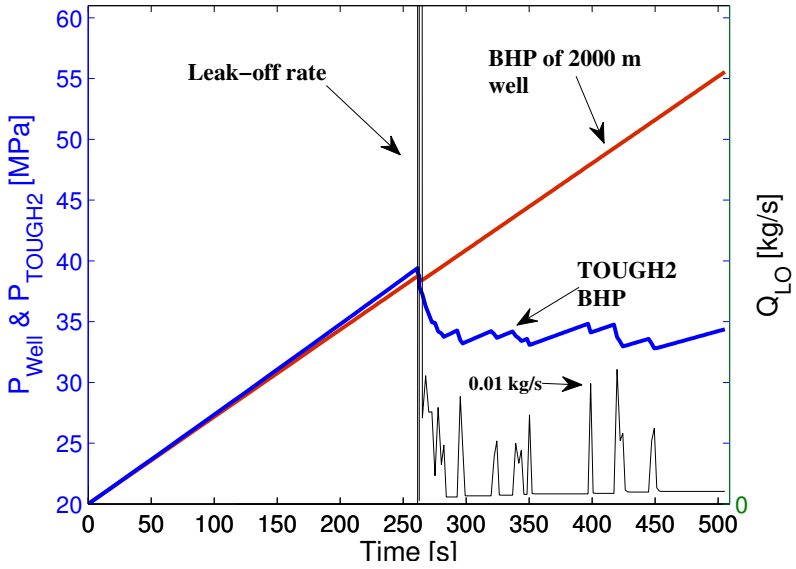

Figure 4.12: Simulation result: Left axis: Plot of pressure versus time for a constant rate injection LOT into a 10 m open hole segment, without coupling to a well. Right axis (increments of 0.05 kg/s): Recorded leak-off rate is plotted on the right. For comparison, the effect of the same leak-off volume on BHP of a 2000 m well is plotted. During formation breakdown starting at 250 seconds, leak-off rate averaged around 4 kg/s at timesteps of 2.5e-4 s, but peaked at 50 kg/s. Notice that these rates are barely sensed by the well, where only a small drop in well BHP is seen.

well with 13 3/8" casing and a hollow bottom drill string of 5" has a compliance of around 70 litres/MPa. If we assume that this is constant, then 70 litres can be injected per MPa BHP increase, whereas the 10 m TOUGH2 open hole segment will give the same pressure increase for 70/200 = 0.35 litres/MPa.

The problem

To couple a well to the MDEM-TOUGH2 unit length segment necessitates that we inject much more volume into TOUGH2, because the well will act as a fluid storage container to uphold the BHP. If we again consider the plots in Figure 4.12, the problem can be described as fitting the red curve, which is BHP of the well, to the blue curve, which is BHP of the open hole segment. This will require the fracture volume to be orders of magnitude higher.

Two main approaches on coupling to a well are proposed:

- An iterative technique where leak-off is calculated and iteratively matched to that of the well. Staggered coupling to TOUGH2. BHP of the segment and the well is then matched in every step.
- Use of a gain controller system to separate the TOUGH2 open hole segment and the well. The interaction between these (the flux) is controlled by the error in BHP, i.e. the difference in BHP of segment and well. The error is input to a gain controller that adjusts

injection rate into TOUGH2, and flux out of the well.

For the well model implemented in the well coupling algorithms, is that the well is assumed to be in hydraulic equilibrium at all times, i.e. that there are no flow-induced pressure gradients in the well. This basically means that if a unit of mass is injected into the well, then it is considered to be instantly and equally distributed in the well volume. The speed of a sound wave propagating through water is around 1500 m/s. The well length used in the simulations in this thesis is at or below 2000 meters. In more advanced well flow simulators this may be included, and a sketch of such a problem is described in the end of the chapter. In the present model flow-induced pressure gradients are neglected due to their minor effect, and the focus is rather set on achieving a stable and convergent well flow coupling to the fracture simulator MDEM-TOUGH2.

4.5.2 Well Flow Decompression Model (WFD)

The WFD model uses an iterative procedure to, for every global timestep, match the BHP in a full scale well with that of the small TOUGH2 segment during injection with a given surface injection rate. If volume is lost by leak-off during injection, it will have a tremendous effect on the pressure in the, initially very stiff, TOUGH2 well segment, whereas in a full scale well a large volume is stored or compressed and the effect of the same volume will be significantly less. The WFD model includes TOUGH2 to simulate pressure in each iteration towards matching the well BHP and the TOUGH2-well-segment pressure to within a specified maximum error, and can thus be considered to be the proper way to include a full well. It is, however, time consuming, as the iterative coupling converges towards a solution.

Note that whenever TOUGH2 simulates pressure, it includes MDEM to do a trial simulation where number of failed elements (cracks) is counted. If the number of new failed elements N is above a specified number N_2, then the timestep length is reduced to reduce number of failed elements. This is done to ensure that fluid is allowed to be updated during fracture extension, and thereby have an intimate and more correct hydro-mechanical coupling during fracturing. In addition the user can specify a minimum number of new failed elements N_1. TOUGH2 will redo the pressure simulation according to a MDEM/TOUGH coupling algorithm (developed at SINTEF) until $N_1 \leq N \leq N_2$. When the criteria is fulfilled, pore pressure data are handed over to MDEM to update the model with the updated permeability and porosity field to be used in following timestep.

Input into WFD is the expected leak-off rate, which as a first guess equals that of the last timestep. With this rate, WFD estimates the expected bottom hole pressure BHP* after a timestep of injection. TOUGH2/$MDEM_{trial}$ is then run and the actual pressure change is recorded. The error between BHP* and the actual BHP is checked, as well as whether there was significant change in leak-off rate from guess to actual rate, and if these errors are larger than

a specified value, the actual leak-off mass rate is calculated and saved into a matrix along with the error, and given back to the WF Decompression Model. A new BHPguess is calculated, by which the TOUGH2 injection rate is modified, and pressure is again simulated in TOUGH2.

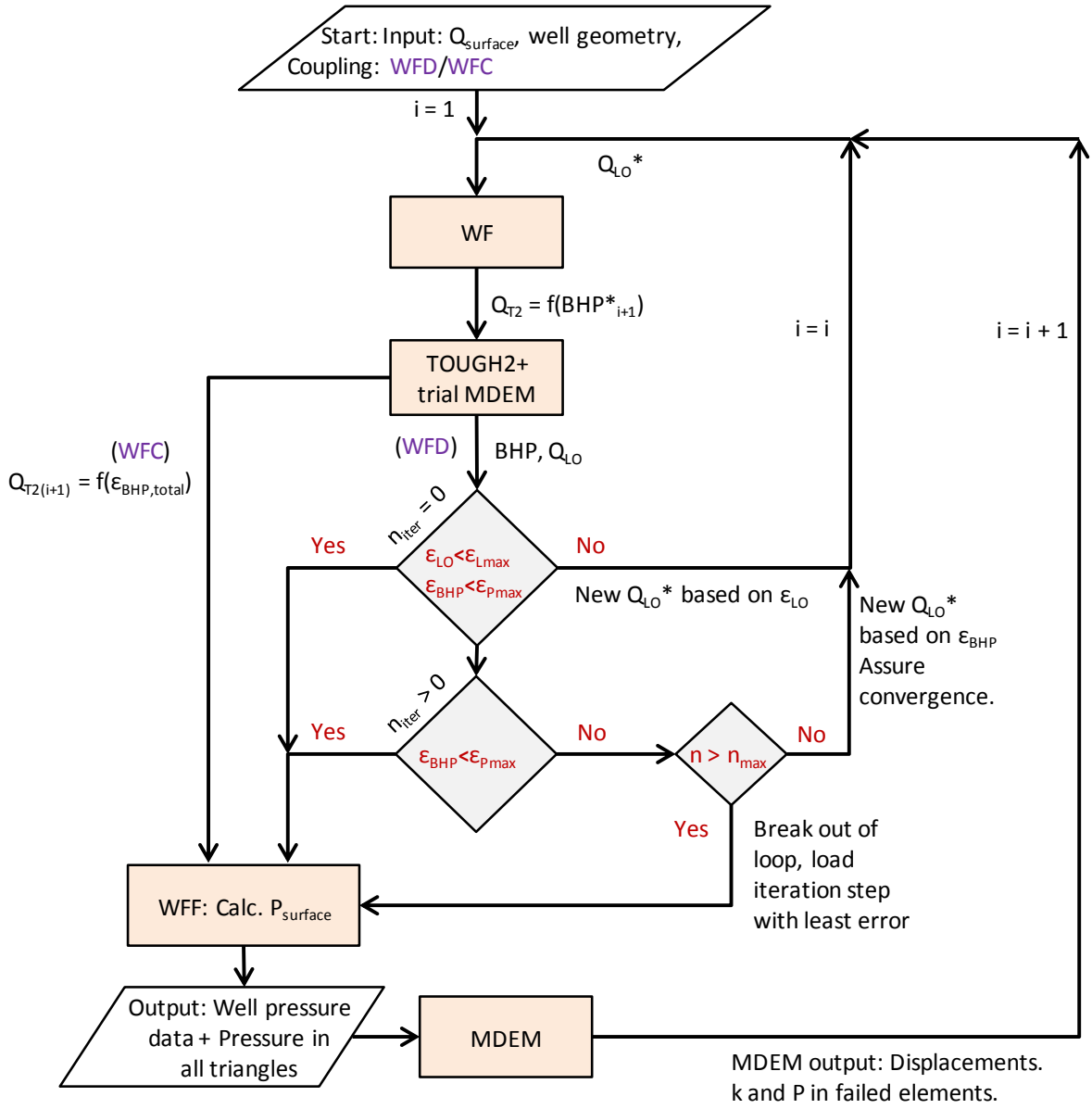

Figure 4.13: Flow chart showing how well coupling algorithm is implemented in the MDEM-TOUGH2 sequental coupling.

A module that checks for error convergence and error is active throughout the iterative process. The convergence algorithm is there to avoid too many iterations, any oscillation, as well as to regain convergence if this was lost during looping.

The following stepwise description explains the WFD model coupling to TOUGH2 and MDEM, during injection. Lower case, "q", represents mass rate and upper case, "Q", represents volume rate, while the star exponent, "*", means that the variable is the guess for the coming simulation.

1. The script "WFsetsys" sets up the well geometry and calculates well system compliance based on input well completion data and fluid data.

2. The initial TOUGH2 segment fluid compliance is then calculated using the sum of pore volume and compressibility in all triangles in the borehole domain.

3. A base TOUGH2 injection rate is defined for the first global timestep assuming that with negligible leak off to formation, the pressure change versus time in the well is equal to the pressure change versus time in the TOUGH2 segment, when the rate into the segment is scaled by the ratio of volume in the segment to the well, i.e. that

$$(\frac{\mathrm{d}P}{\mathrm{d}t})_{\text{Well}} = (\frac{\mathrm{d}P}{\mathrm{d}t})_{\text{T2 segment}} \tag{4.8}$$

when

$$Q_{\text{T2, (i=1)}} = Q_{\text{surf}} \frac{V_{\text{segment}}}{V_{\text{well}}} \tag{4.9}$$

where Q_{surf} is the surface injection rate in l/s, which is constant during the injection phase.

During pressurization of the borehole, before any fractures are formed, and with barrier integrity intact, leak off volume is likely to be negligible in a shale of low permeability. This is indicated by a linear slope on a plot of pressure versus time. Under these conditions Eq. 4.9 would be valid, and a constant injection rate could be given to TOUGH2. However, because pressurization of the open hole segment is modelled by TOUGH2, which simulates compressible fluid flow, the pump-in stiffness of the open hole segment is not constant, and will increase with increasing pressure.

4. After the first timestep, Equation 4.9 is thus replaced with

$$Q_{\text{T2(i+1)}} = Q_{\text{surf}} \frac{C_{\text{segment}}}{C_{\text{well}}} \tag{4.10}$$

where

- C_{well} is the borehole compliance, i.e. $\frac{\mathrm{d}P}{\mathrm{d}V_{\text{well}}}$,
- C_{segment} is the TOUGH2 segment pump-in compliance $\frac{\mathrm{d}P}{\mathrm{d}V}$, i.e. the inverse of pump-in stiffness.

The latter is calculated for every timestep i, and used to calibrate Equation 4.10 during pressurization of the borehole until fracture initiation, while assuming it is constant over the time increment $\Delta t_{\text{i-1}}$. It is the inverse of pump-in stiffness, which is equated as

$$(\frac{\mathrm{d}P}{\mathrm{d}V})_{\text{T2 segment (i+1)}} = \frac{(BHP_{\text{i}} - BHP_{\text{i-1}})}{Q_{\text{T2, i}} \Delta t_{\text{i}}} \tag{4.11}$$

After fracture initiation, Equation 4.11 is just seen an indicator of fracture + segment stiffness and is not used as calibration. C_{well} is then kept constant.

The reason for this can be summarized in a short version: Firstly, that the stiffness is no longer changing primarily due to changes in fluid bulk modulus, but due to hydraulic pressure communication with the fracture. Secondly, that this hydraulic pressure response is a non-linear function of varying and competing pressure gradients in the fracture, specifically, and most importantly, the imposed gradient at the well due to injection (Q_{T2}), and the changing gradients along the fracture and at newly failed clusters at the tip. During formation breakdown large volumes from the well needs to be injected into the segment, which means that large hydraulic force is applied to the model. At the same time there is a limitation on number of new failed clusters per global timestep. The condition (in combination with large force) result in that timestep increments are reduced, in some cases down to $10^{-}7$ s during breakdown. Essentially this means that the system is highly sensitive to changes in injection rate in a non-linear way, and that during breakdown we have to differ between change in pump-in stiffness and change in system stiffness, where the latter is mainly a function of fracture length. When trying to match the well pressure with that of the TOUGH2 open hole segment, we do not want to vary too many parameters per iteration, and since C_{well} fluctuates from even minor changes in injection rate this value could not be the varying parameter. This was primarily experienced during fracture initiation and formation breakdown, where the pressure gradient is large near the fracture, before the pressure has been allowed to propagate to the tip. In the simulation results presented in Chapter 4.7.4, this gradient is observed.

A scheme is presented, where pressure change is predicted in each global timestep i based on a guess of lost mass in the segment during that timestep. By using Equations 4.12-4.16, the updated (for every iteration and every global timestep) input rate to TOUGH2, Q_{T2}, is damped e.g. as compared to a scheme where the pump-in compliance of the (open hole segment + fracture) is used to update Q_{T2} directly. The scheme is thus able to facilitate convergence towards small well coupling error in volume flux and pressure both when mass balance is enforced (there is a moving pressure gradient in the fracture), and when mass balance is turned off (there is very little gradient along the fracture, but one local gradient at the tip and one near the borehole).

5. WFD calculates a first guess on the well BHP at the start of every timestep, and in each iteration before pressure is simulated in TOUGH2. The first guess is calculated with Eq. 4.12,

$$BHP^{*}_{(i+1)} = \frac{Q_{\text{surf}} - Q^{*}_{\text{LO(i+1)}}}{C_{\text{well}}} \Delta t^{*} + BHP_{\text{i}} \tag{4.12}$$

where

- Δt is the expected injection time based on last step,

- Q^*_{LO} is the estimate on leak-off rate to the formation, with its initial guess to be equal the final leak-off rate in the previous time step (zero at start of injection), defined as

$$\begin{aligned} Q^*_{\mathrm{LO(i+1)}} &= \left(\Delta BHP_{\text{zero leak-off}} - \Delta BHP_{\text{actual in previous step}}\right) \frac{C_{\text{segment}}}{\Delta t^*} \\ &= \left(\frac{q_{\mathrm{T2(i)}} \Delta t_{\mathrm{(i)}}}{\rho} C_{\text{segment}} - \left(BHP_{\mathrm{(i)}} - BHP_{\mathrm{(i\text{-}1)}}\right) \right) \frac{C_{\text{segment}}}{\Delta t_{\mathrm{(i)}}} \end{aligned} \tag{4.13}$$

  where q_{T2} is the mass rate injected into the TOUGH2 segment for pressure simulation in the previous step. The recorded rate of leak-off $\mathrm{Q_{LO}}$, however negligible before fracture initiation (in low permeability formations), is calculated and considered in every timestep throughout the simulation.

Note that Eq. 4.13 is not applied directly in WFD, but is a simplified view to illustrate the method of calculating the lost volume. In WFD, the Mass Calculation Module, (see B) calculates, for all triangles in the borehole domain, the density and compressibility of its fluid as function of pressure and temperature, as well as a mass balance calculation. Then it returns the sum of mass lost from the triangles in the domain during the simulation step as compared to what was injected, to be used in Equation 4.12.

6. The WFD model hands over a mass rate to T2 that consist of two contributions as equated in Eq. 4.14,

$$q_{\mathrm{T2(i+1)}} = \left(Q^*_{\mathrm{LO(i+1)}} + Q_{\mathrm{W}}\right) \rho \tag{4.14}$$

   where $\mathrm{Q^*_{LO}}$ is the guess on leak-off rate, and Q_{W} is the net flux into the full scale well, i.e. the rate that yields the pressure in the well, assuming that $\mathrm{Q^*_{LO}}$ is constant over the timestep. This net flux, either positive or negative, is scaled for the segment, and Q_{W} is equated as

$$\begin{aligned} Q_{\mathrm{W}} &= \frac{Q_{\text{surf}} - Q^*_{\mathrm{LO(i+1)}}}{C_{\text{well}}} C_{\text{segment}} \\ &= \frac{BHP^*_{\mathrm{i+1}} - BHP_{\mathrm{i}}}{\Delta t^*} C_{\text{segment}} \end{aligned} \tag{4.15}$$

   Substituting Eq. 4.15 into Eq. 4.14 yields the mass injection rate handed over to TOUGH2

$$\begin{aligned} q_{\mathrm{T2(i+1)}} &= \left(Q^*_{\mathrm{LO(i+1)}} + \frac{Q_{\text{surf}} - Q^*_{\mathrm{LO(i+1)}}}{C_{\text{well}}} C_{\text{segment}} \right) \rho \\ &\quad or \\ &= \left(Q^*_{\mathrm{LO(i+1)}} + \frac{BHP^*_{\mathrm{i+1}} - BHP_{\mathrm{i}}}{\Delta t^*} C_{\text{segment}} \right) \rho \end{aligned} \tag{4.16}$$

   The assumption is then that $Q^*_{\mathrm{LO(i+1)}}$ equals $Q_{\mathrm{LO(i)}}$ (actual leak-off from simulation is now the new guess), i.e. that the rate is constant throughout the timestep. Under these

conditions the pressure change in the TOUGH2-MDEM$_{\text{trial}}$ simulation equals the pressure change estimated for the well by the WFD model.

7. q_{T2} is then handed over to TOUGH2, which simulates pressure with its own iterative coupling algorithm. When a solution is reached, TOUGH2 returns the actual BHP after simulating with q_{T2} over the actual time step length Δt.

8. BHP* is then recalculated with the actual time step length ($\Delta t_{(i+1)}$ replaces Δt^* in Eq. 4.12), and the sum of actual leak-off volume out of all triangles in the borehole domain during the step is calculated and expressed per time as the actual leak-off rate. Then relative errors in guesses on leak-off rate and BHP is calculated by Eqs. 4.17,

$$\varepsilon_{BHP} = \frac{BHP^* - BHP}{\left(\frac{BHP^* + BHP}{2}\right)} \tag{4.17a}$$

$$\varepsilon_{LO} = \frac{Q_{LO} - Q^*{}_{LO}}{\left(\frac{Q_{LO} + Q^*{}_{LO}}{2}\right)} \tag{4.17b}$$

If the errors $|\varepsilon_{BHP}|$ and $|\varepsilon_{LO}|$ are larger than $\varepsilon_{\text{BHP, max}}$ and $\varepsilon_{\text{LO, max}}$, then the Convergence Module will be active and the pore pressure field will be reloaded as it was prior the simulation step, before the algorithm will run again with an updated input Q^*_{LO} to WFD.

9. The criteria to continue to the next timestep are formulated

$$|\varepsilon_{BHP}| > \varepsilon_{\text{BHP, max}} \tag{4.18a}$$

$$|\varepsilon_{LO}| > \varepsilon_{\text{LO, max}} \tag{4.18b}$$

If Equation 4.18b is violated, then the guess on pressure BHP*, as calculated with Eq. 4.12, is false. This means that, as an example, if the error in rate is high, but the error in BHP is low, then the step will be taken back for a new iteration. The convergence algorithm will take in the actual leak-off rate reported, and give out a new guess $Q^*_{\text{LO(i+1)}}$. Often, this is the case the first time the pressure is simulated by TOUGH2-MDEM$_{\text{trial}}$ in a timestep. The first pressure simulation may as such be considered a calibration of $Q^*_{\text{LO(i+1)}}$. In the subsequent iterations within the same global timestep, only $|\varepsilon_{BHP}|$ is checked, and not $|\varepsilon_{LO}|$. The scheme is illustrated in the flowchart in Figure 4.13. Normally the convergence algorithm finds a solution with reasonable error after 2 iterations, but to illustrate how it converges towards a solution a few examples with several iterations are presented.

Table 4.1: Output Data From the Convergence Module: Data From Iterations Loop.

$Q_{LO^*}[l/s]$	37.921	16.841	45.322	39.626	42.474	44.000	43.237	43.618	43.811
$BHP_{error}[MPa]$	-105.126	0.323	-0.017	0.051	0.016	-0.002	0.007	0.003	0.0001
$\varepsilon_{rate}[-]$	0.863	-0.458	-0.016	-0.080	-0.046	-0.029	-0.038	-0.034	-0.031
$q_{T2}[kg/s]$	28.197	17.028	45.819	40.061	42.940	44.483	43.712	44.097	44.292
$Q_{LO(actual)}$	2.788	45.322	46.753	46.510	46.538	46.654	46.643	46.649	46.653
$dPdV[MPa/l/(v_f m^3)]$	36.929	-76.896	1.474	-5.244	-1.548	0.111	-0.763	-0.322	-0.104

Table 4.1 shows a case where it took 8 iterations to find a solution. Each column contain data after one iteration. In the first column, $Q^*_{\mathrm{LO(i+1)}}$ of 37.9 l/s, is from the last global timestep. In the subsequent iterations, $Q^*_{\mathrm{LO(i+1)}}$ in the first row are the new guesses based on the actual leak off rate in row 5 in the previous column. Notice first that after the first pressure simulation, $Q^*_{\mathrm{LO(i+1)}}$ was reported to be 2.8 l/s, from the guess of 37.9. This change was considerable, and the new guess is therefore damped by the convergence algorithm, and a rate of 16.8 l/s is given back for a new simulation. The second row shows the error from guess to actual BHP, which first is -105 MPa, then after the first iteration to calibrate the rate, then it slowly decreases. Notice how the pump-in stiffness fluctuates from step to step while rate injected into the segment, $\mathrm{q_{T2}}$ in row 4 is damped. 37 MPa/l in the first step to -76 MPa/l in the second step. It is also seen that there is a sign change on $|\varepsilon_{LO}|$ (row 3, column 2) after the first iteration, and the reported $Q_{\mathrm{LO(i+1)}}$ was now 45 l/s, which confirms that damping decision was correct. From now on, new guesses $Q^*_{\mathrm{LO(i+1)}}$ are based on BHPerror convergence alone, and not rate, to avoid oscillation (the flux has been roughly calibrated and will now be fine calibrated). A new rate is sent back, for another iteration (column 3), and the response is a sign change (row 2 column 3) on BHP error, from 0.323 to -0.017 MPa. A sign change in ε_{BHP} implies that the convergence algorithm must go back and reduce the slope of change. On the other hand, if ε_{BHP} did not change sign after the first iteration, then the factor of change is increased to decrease the number of iterations (negative damping). The slope is altered (damped positively negatively depending on ε_{BHP}), until a solution is found in row 9, after 8 iterations.

To monitor the change in Q^*_{LO} during WFD iterations has however shown to be important to reveal whether ε_{LO} is changing merely as a result of change in stiffness, timestep length or numerical artefacts. A numerical artefact that may hinder convergence in the well coupling algorithm is e.g. that the TOUGH2/$\mathrm{MDEM_{trial}}$s coupling algorithm could not find a solution to keep number of new cracks within the specified range, and then changed timestep length in the middle of the well coupling convergence loop, in between iterations. Change in timestep length during iterations will alter the total injected mass, and thus the non-linear pump-in stiffness of the borehole segment.

The above case, with 8 iterations, is just to show how the convergence algorithm works, and the large number of iterations was attributed a combination of abnormally high rates combined with no mass balance (little pressure gradient in the fracture), and small timesteps. Normally

a solution is found after a couple of iterations, and if not, the loop is anyway broken following a condition to keep below a given number of iterations. Then data and pore pressure field are loaded from the step that in the end had the least $|\varepsilon_{BHP}|$.

It should be mentioned that the convergence algorithm was written before the implementation full coupling in MDEM-TOUGH2, and thus developed for cases where numerical instability was a more frequent issue: The staggered mass balance will involve fluctuations in pressure (and aperture, see Chapter 4.4.2) and without mass balance there is as mentioned little pressure gradient in the fracture, and there is essentially very little volume injected into the fracture, which promotes the non-linear behaviour described above. After a global timestep, new cracks have likely appeared in the triangles located at the fracture tips, and when pressure are reduced in these (without full coupling of fracture and flow), a sudden pressure gradient increase was introduced locally at the tip. At the same time, the injection rate induces a gradient at the well. Within a timestep of injection it can thus be said that competing transients are affecting the non linear pressure response recorded in the borehole centre. With full coupling and mass conservation, the crack opens as fluid flows into it to form an open fracture, and as a result there is a smooth pressure gradient along the fracture which is a more correct description of fracture growth in a single phase water system. Enforcing mass conservation requires more fluid to be injected into the formation, which in principle should make it simpler to couple it to a well. The same applies formations of higher permeability (this thesis' scope lies in the range of 10^{-19} to 10^{-21} m^2), where more fluid leaks through the fracture surfaces. Changes in injection rate have less impact, because a smaller percentage of the total leak-off rate goes into pressurization within the fracture, resulting in a more linear pressure behaviour, and thus fewer iterations are needed. Furthermore, fracture aperture and volume have less of an impact on fracture growth and leak-off rates.

It should be pointed out that it is essential to keep the errors in the simulation steps small. Especially during formation breakdown, errors can accumulate over many timesteps (remember that timesteps can be as small as 10-7 s). As an example, if FPP (stable fracture propagation pressure) is reached, but we have accumulated a total BHP error of BHP_{well}- BHP_{T2} = 1 MPa during breakdown and unstable growth, then we have a volume of 1 MPa * 60 l/MPa/100m3, i.e. a volume of 60 litres that should have been injected, and thus a large error in fracture size. A well of 100 m3 volume is then assumed. Coupling of a well by use of the WFD iterative technique is presented in Figure 4.14 and until start of shut-in in Figure 4.16. Note that the saw-tooth behaviour in Figure 4.14 is a numerical artefact due considerable triangle size, and that triangle size dependent strength was not yet implemented, nor mass balance or full coupling of fracture mechanics and flow. A great limitation Condition in the MDEMtrial loop that for each loop to obtain a stable model, an if sentence checks for

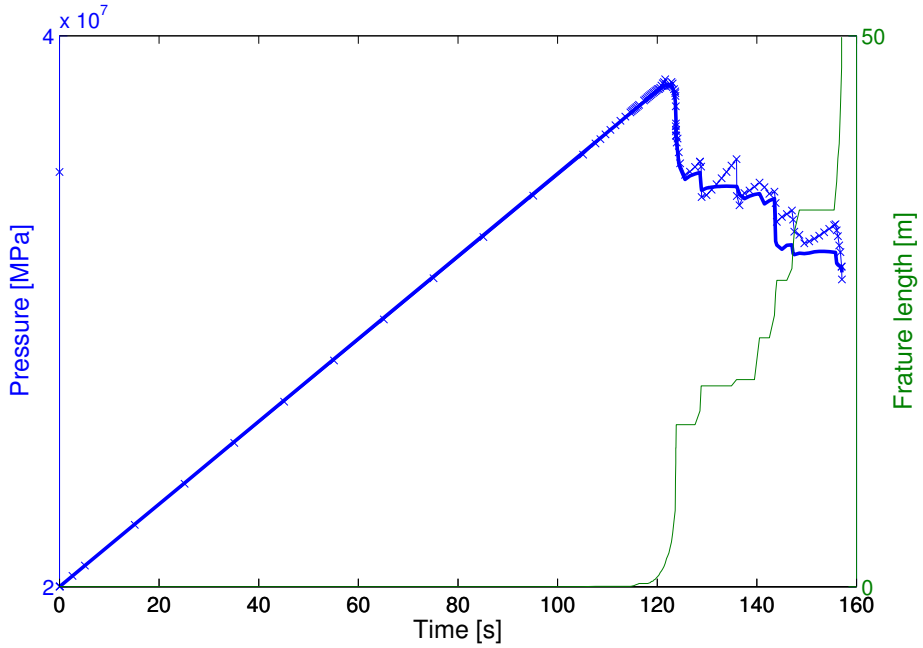

Figure 4.14: Plot of Pressure versus time for well and open hole segment using the WFD iterative technique. The well was 2000 m deep. The solid blue line is the BHP of the 2000 m well, while the cross-dotted line is TOUG2 open hole segment pressure. The saw-tooth behaviour is a numerical artefact (discretization) and not reflective of jumps in fracture length.

4.5.3 Well Flow Gain Controller (WFC)

In this section a second approach on coupling a well to the MDEM-TOUGH2 fracturing simulator is presented: Well coupling by use of a gain controller. As an alternative to the WFD, this is a non-iterative coupling scheme. While the WFD is based on matching the BHP of the well with that of the TOUGH2 open hole segment for every time step, this approach instead keeps track of the BHP error, and uses the error to adjust the injection rate into TOUGH2 like a proportional integral derivative controller (PID). This way, there are no iterations, and the decompressed well volume is injected over a longer time period, which promotes stability in the model. The better part of fracture volume will however be induced later than the initial pressure drop, when error has accumulated and the gain controller increases the injection rate. The injection rate into TOUGH2 is calculated using Equation 4.19,

$$Q_{\mathrm{T2(i+1)}} = Q_{\mathrm{T2(i)}} + G\sum_{1}^{\mathrm{i}} \left(BHP_{\mathrm{i}}^{*} - BHP_{\mathrm{i}}\right) \tag{4.19}$$

where the gain factor G is specified by the user. An example value can of the gain factor is 1/30, but it depends on the how fast the user wants the well decompressed fluid volume to be injected. If the user expects a certain accumulated error during formation breakdown, some trial testing should be done to calibrate the gain factor. This is necessary as an automatic time step reduction will occur in MDEM-TOUGH2 if stability is not reached. A condition will in addition scale G

scaled by timestep length if timesteps are below a certain length (e.g. 1e-5), to avoid error/rate fluctuations. The well injection rate is calculated subsequently as

$$Q_{\text{well(i+1)}} = Q_{\text{surface}} - Q_{\text{T2(i+1)}} \tag{4.20}$$

The updated guess on pressure $\text{BHP}^*_{\text{i+1}}$ is calculated

$$BHP^*_{\text{(i+1)}} = \frac{Q_{\text{well}}}{C_{\text{well}}} \Delta t^*_{\text{(i+1)}} + BHP_{\text{i}} \tag{4.21}$$

After TOUGH2-$\text{MDEM}_{\text{trial}}$ has simulated pressure in the pore pressure field, the guess calculated with Eq. 4.21 is updated with the actual timestep length Δt, which may have changed during the simulation due to the condition to keep within a certain number of new failed triangles over one timestep. If the accumulated error is observed to fluctuate between negative and positive, a damping term can be added to Eq. 4.19, equated as

$$Q_{\text{T2(i+1)}} = \frac{Q_{\text{T2(i)}}}{1-\gamma} + \frac{G \sum_1^{\text{i}} \left(BHP^*_{\text{i}} - BHP_{\text{i}} \right)}{1-\gamma} \tag{4.22}$$

where γ is a damping parameter between 0 and 1, specified by the user (e.g. 0.05 (5 %). The damping parameter will induce some error in every global step, and promote convergent behaviour. In Appendix A a result is shown, where WFC without damping was applied in combination with a high gain factor, see Figure A.6. The stabilizing effect of adding the damping term is illustrated in Figure 4.16. If instabilities are seen during fracture initiation, or fluctuation in rate during breakdown, then the gain factor should be reduced. An example simulation can illustrate the use of a gain controller: In Figure 4.15 pressure and rate is plotted as function of time injected in an XLOT. The gain controller was used to couple a 10 meter open hole segment in MDEM-TOUGH2 to a 2000 meter long well. The well volume specified (by input completion data) was 160 m3, and a well fluid compliance of 66 l/MPa. Surface injection rate was 60 l/min and the gain factor G was set to 0.25. When the error approaches zero, a slope change on the well pressure can be observed. To avoid fluctuation, damping is automatically accelerated at this point, while gain is reduced.

The simulation did not have mass balance and full coupling in place, and thus a large fracture had to be created for the pressured to drop in the fracture. Figure 4.15b shows the fracture length per time during breakdown.

The green dotted line in Figure 4.15 is a plot of the reported leak-off rate in MDEM-TOUGH2. It fluctuates due to the highly stiff system and its non-linear response to variation in injection rate as the fracture initiates and propagates. The red line is the corresponding TOUGH2 injection rate Q_{T2} as calculated by the gain controller with Eq. 4.22.

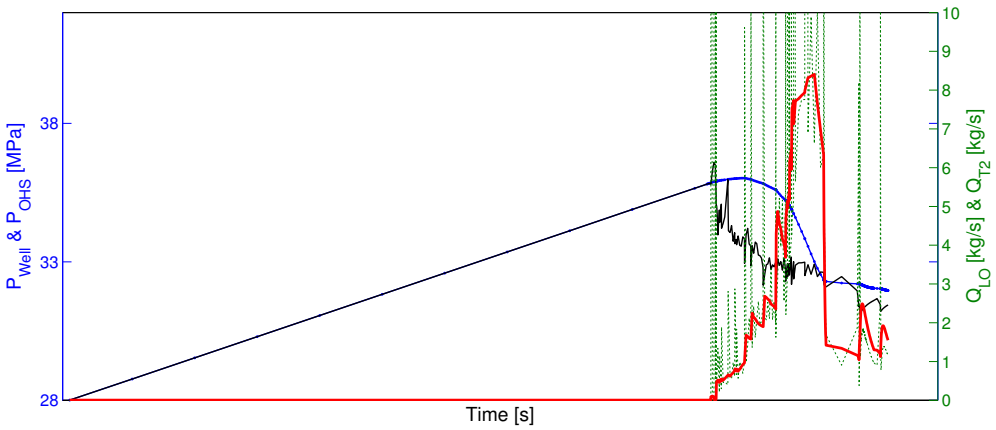

(a) Left axis: The black pressure curve is TOUGH2 segment borehole pressure, and blue curve is the well pressure. Right axis: Green dotted line is the recorded rate of leak-off out of the open hole segment and the overlaid red line is the injection rate into TOUGH2. The peak leak-off rate during breakdown was 60 l/s at a timestep increment of 1e-5 s.

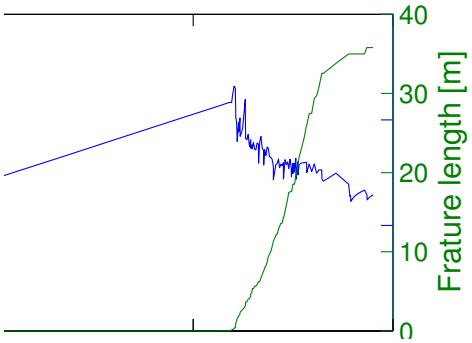

(b) Corresponding growth in fracture length, overlaid plot of borehole pressure versus time for comparison with the plots in (a).

Figure 4.15: Plot of borehole pressure and injection rate development versus time. Coupling to well by a gain controller.

4.5.4 Well Coupling During the Shut-In Phase

During the shut-in phase, the well flow module still needs to be active, and provide flux from the well (the storage container) into the fracture and formation. Shut-in denotes that pump are shut-off on surface, and the pressure versus time development is monitored. For an introduction to how the shut-in phase is used for interpretation in XLOTs, the reader is kindly referred to Appendix C, where this is described. Different approaches on coupling during shut-in were tested for both shut-in simulation and flow-back simulation. As MDEM-TOUGH2, as part of the DrillWell project, is being developed as a tool to "improve precision in stress determination from XLOT, in challenging formations and complex stress regimes". This requires the fracture behaviour to be accurately described, and as a result of this the well coupling approach based on a gain controller would not suffice. It was experienced that the fracture analysis behaviour was masked by the gain controller due to its "lag" in rate and time. The shut-in and flow-back phase are areas where fracture closure analysis is important for stress determination, and this

requires pressure and volume behaviour (recordings) that are in terms with fracture mechanics and hydraulics. XLOT interpretation and field techniques are described in Appendic C.

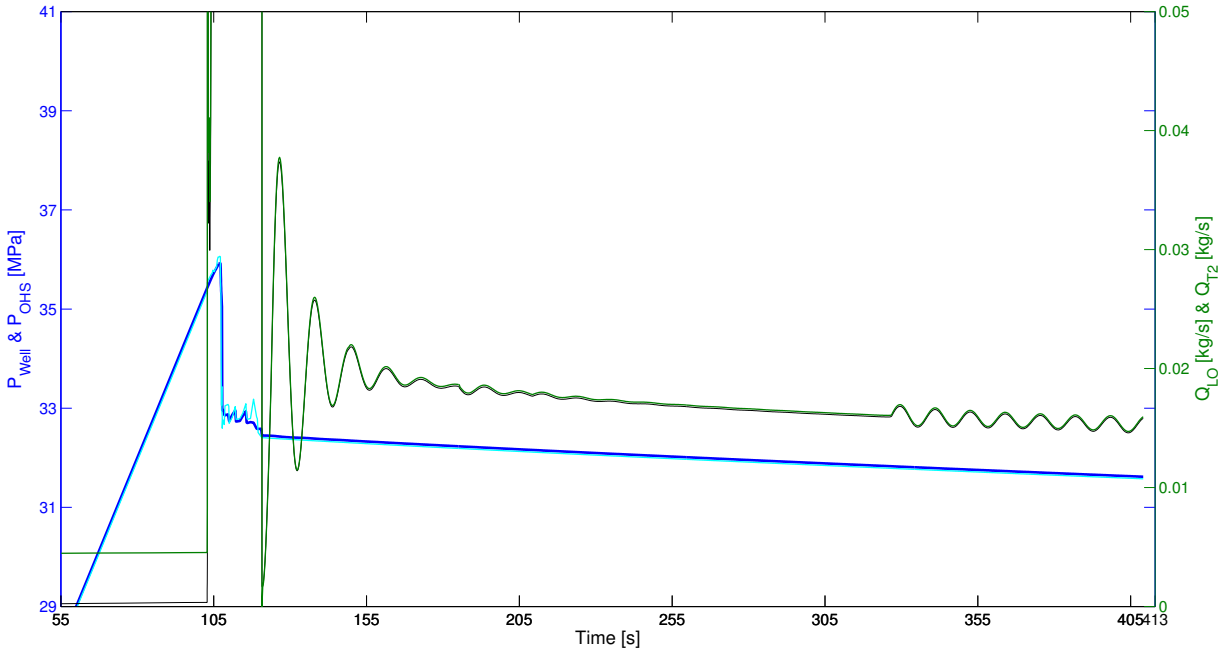

Figure 4.16: Simulation result: Plot of pressure and TOUGH2 injection rate during the shut-in phase of an XLOT. Coupled to a 2000 m deep well.

During testing of the iterative procedure to be used during shut-in and flow-back it was found that iterations were not really needed because the fracture no longer was growing (at least after the pressure gradient in the fracture had equilibrated). No induced fracture extension implies a predictable volume and pressure behaviour. This led to a combined use of the two models WFD and WFC instead of the WFD; the WFDmod uses the equations of the WFD, but the concept of controlling the rate by gain in error. The scheme differs from the WFC gain controller by that in addition to calibration from the error, the flux in or out of the borehole is calculated for each step and used as in the WFD to calculate rates to be sent back to MDEM-TOUGH2 in the next global timestep. Note that "leak-off rate" here describes the flux in/out of the clusters in the borehole domain, i.e. the change in mass of all these clusters combined. This flux does not change much from step to step during shut-in, but to couple a well to the open hole segment implies that a small amount of fluid (depending on the permeability of the formation, and the length of the open fracture) must be injected to uphold the pressure. The system is sensitive to changes, but as the flux changes only by small amounts, then linearisation of this rate can be assumed, i.e. that the coming step's leak-off rate follows the trend of that of the last timestep linearly. If the leak-off rate changes, as for instance due to fracture closure or snap off, error in BHP will be induced, but then quickly regained, as shown in Figure 4.16. In the right axis

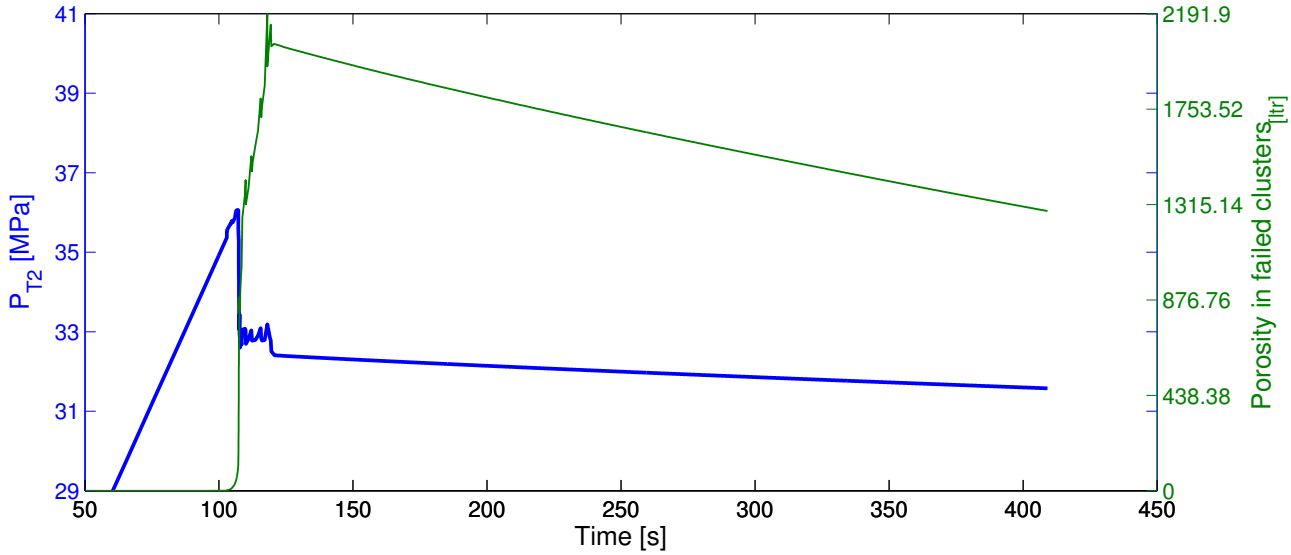

Figure 4.17: Simulation result: Plot of well and open hole segment pressure and sum of induced (upscaled cluster porosity) volume versus time during injection and shut-in phase of an XLOT. Coupled to a 2000 m long well.

injection rate is plotted. Damping makes this method efficient and convergent.

$$Q^*_{\mathrm{LO(i+1)}} = \frac{Q_{\mathrm{LO(i)}}}{1-\gamma} + \frac{G\Sigma^{\mathrm{i}}_{\text{start of shutin}}\left(BHP^*_{\mathrm{i}} - BHP_{\mathrm{i}}\right)}{1-\gamma} \tag{4.23}$$

then input rate into TOUGH2 is calculated with the WFD equation, Equation 4.16. From plots

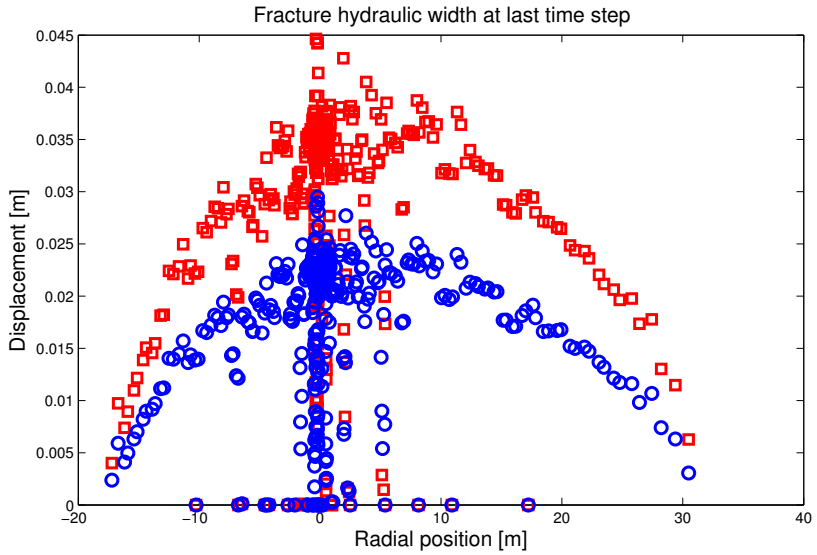

Figure 4.18: Simulation result: Plot of fracture hydraulic width at start and at end of shut-in, for the simulation in Figure 4.16 and 4.17

of borehole pressure (on left axis) and induced fracture porosity (on right axis) in Figure 4.17, a steady porosity decline with time is observed, indicating that the fracture is gradually closing. This is confirmed by in Figure 4.18 in a corresponding plot of hydraulic width at start and at

end of shut-in. The plot indicates that the fracture closes in width while length is maintained until end of the shut-in phase.

4.5.5 Flow Back Through Fixed Choke, Coupled to a Well

"The essence and advantage of the system stiffness approach is that the point of mechanical closure can be isolated in a different plot of system stiffness during closure. The plotting technique is facilitated by how the flow rate through a fixed choke relates to its pressure drop [14]". Flow through a fixed choke is basically flow through a hole of constant size, where the rate is decided by properties of the mud as well as by the pressure differential across the choke. By flowing back over a fixed choke, the surface production rate will decrease with time as the well pressure is reduced. Now, in a sandstone with higher permeability, the leak-off would be larger, and pressure drop faster. Thus it would be harder to spot fracture closure, as the change in stiffness during closure would be less visible. The flow rate through a choke is proportional to the square root of the pressure drop across the choke,

$$\frac{\mathrm{d}V_{\text{flow-back}}}{\mathrm{d}t} = \zeta \sqrt{p(t)_{(\text{upstream pressure})} - p_{(0)}} \tag{4.24}$$

where ζ is dependent on fluid properties and choke setting and can be assumed constant given that fluid density is constant. The upstream pressure is the pressure at time t during flow back, and the downstream pressure, p_0, which for our analysis is atmospheric pressure.

The surface production rate is calculated for each step based on the last steps output BHP. This is done by a simple pipe flow calculation cycle (see Appendix B, script v_WFF.m), which takes in the TOUGH2 BHP, and after each global timestep the algorithm integrates the fluid column, including density variation effects and friction effects. A Newtonian fluid system is assumed, but this can if necessary be scaled by setting a high fluid viscosity, which is a reasonable assumption as drilling fluids often are considered Bingham yield fluids. Friction effects were however seen to be negligible for all simulations done as part of this thesis, and essentially only the weight of hydraulic fluid column is withdrawn to get the surface pressure. In XLOTs the pump-in rate is typically around 50-150 l/min. For a rate of 80 l/min through a 5" drill pipe of inner diameter 4.276", this corresponds to a velocity of 0.144 m/s. Assuming a fluid viscosity of 10 cp and fluid bulk modulus of 2.34 GPa, then the total pressure loss due to friction in the 2000 m deep well can be calculated to be 0.0008 MPa.

If iterations are needed to match well BHP with TOUGH2 reported BHP, then surface production rate is kept constant throughout this iterative process. For flowback it is reasonable for low-permeability formations to assume that we produce with higher rate than we leak off to the formation. Recall that this is a condition for the Statoil ASA's System Stiffness Approach to be successful [14]. During flowback the pressure is reduced according to the flow-back stiffness,

which is increasing as the fracture closes, meaning that with time a lower volume per pressure change will be produced. The point of mechanical closure can then be isolated at the intersection between tangent lines of pressure versus volume at two linear slopes: while the fracture reduces in width while length is constant, and after hydraulic closure. The fracture stiffness, is equated [14].

$$S_f = \frac{\Delta P}{\Delta V_f} = \frac{3E}{16R^3(1-\nu^2)} \tag{4.25}$$

where E is Young's modulus and ν is Poisson's ratio. R is the fracture length. Thus, from Equation 4.25, it is seen that stiffness is more or less given by the fracture length, and a change in stiffness is thus related to a change in fracture length. For a fracture that closes in width while its length is maintained S_f is thus constant. Consequently, as fluid stiffness in the cased part of the system can be assumed constant, and if casing expansion effects are assumed negligible, then during the XLOT, the total system stiffness as derived from pump-in and flowback tests is constant while the fracture closes in width. This facilitates that the point of mechanical closure can be isolated as described. The system stiffness approach is described with field examples in Appendix C, section 2.2.2.

To implement the use of a fixed choke during flowback with WFD coupling to a well, Equation 4.24 is applied directly. The choke setting, ζ, is specified by the user, and the when pressure is updated in the TOUGH2 open hole segment, then the WFF algorithm calculates the corresponding surface pressure upstream the choke, which is near equal the weight of the fluid column for XLOTs. Then the surface production rate is recalculated. This is done at each global timestep, according to the given choke setting, and the current TOUGH2 open hole segment BHP. Flowback using a fixed choke is illustrated in Figure 4.20 and the corresponding

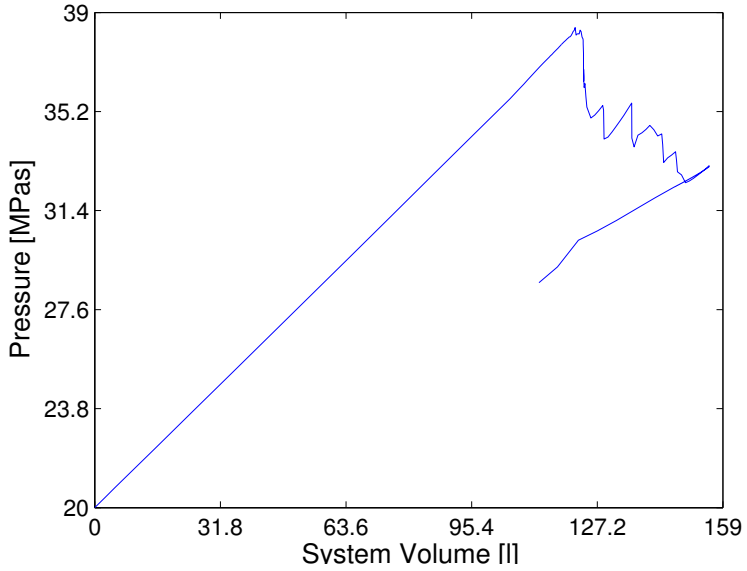

Figure 4.19: Flowback through a fixed choke, will coupling to a well

plot of pressure versus system volume in Figure 4.19 . There is clear indication of fracture

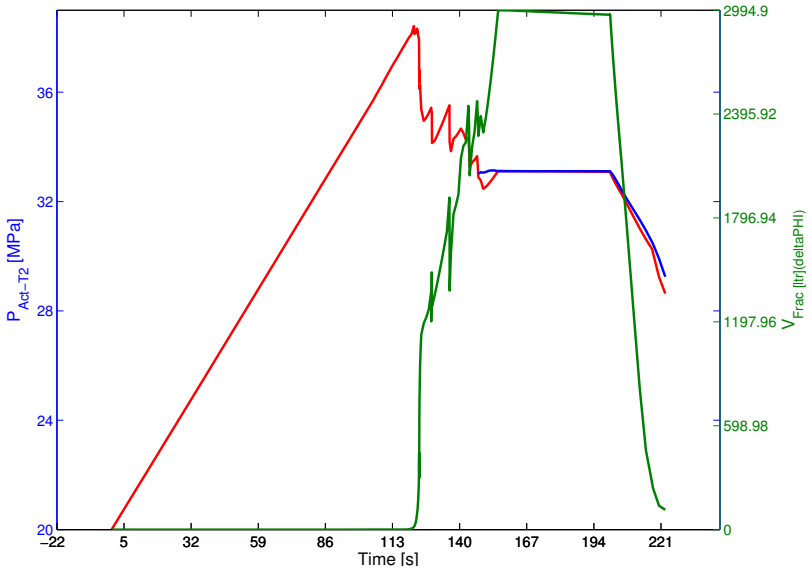

Figure 4.20: Flowback through a fixed choke, with coupling to a well

closure in both plots: On plot of pressure versus time, there is a clear slope change, indicative of closure. Sum of failed cluster porosity supports this interpretation. Although shear failure in the borehole wall prevented further flowback, the functionality of the scheme is shown. The plot of pressure versus system volume (as described for interpretation in Appendix C) further strengthens this. The simulations of flowback through a fixed choke were here run with the coupling scheme as described in shut-in well coupling.

4.6 Results After Modifications of Original MDEM-TOUGH2

Figure 4.21 represents the status of the MDEM-TOUGH2 fracture simulator project per June 2014. Full coupling of fracture mechanics and flow provides a more realistic description of fracture propagation. The width of the fracture is plotted in Figure 4.23. The formation permeability was 3e-21 m2 (1e-9 Darcy), and the injection rate was 0.002 kg/s for . Pressure versus volume is plotted in 4.22, where the point of fracture closure is identified at 680 seconds.

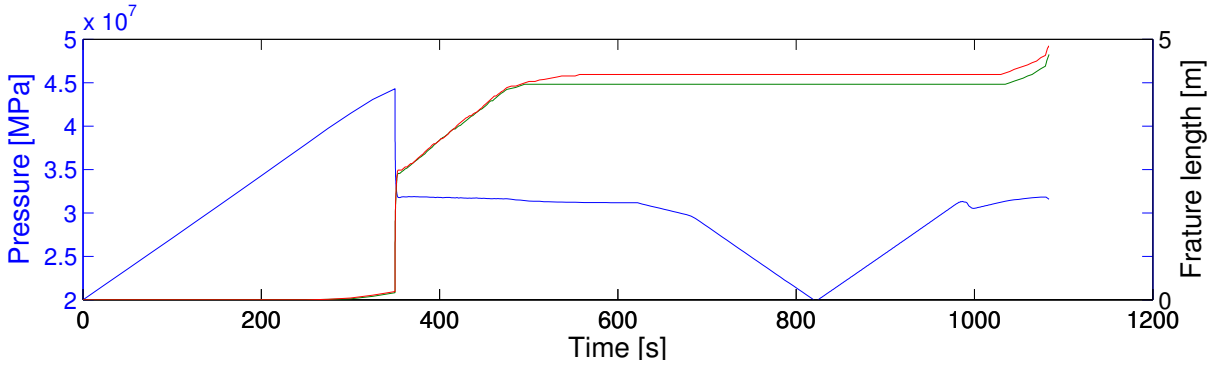

Figure 4.21: Current status of the MDEM-TOUGH2 fracturing simulator XLOT project, per June 2014: XLOT with mass conservation and full coupling of fracture mechanics and flow (with permission from SINTEF Petroleum).

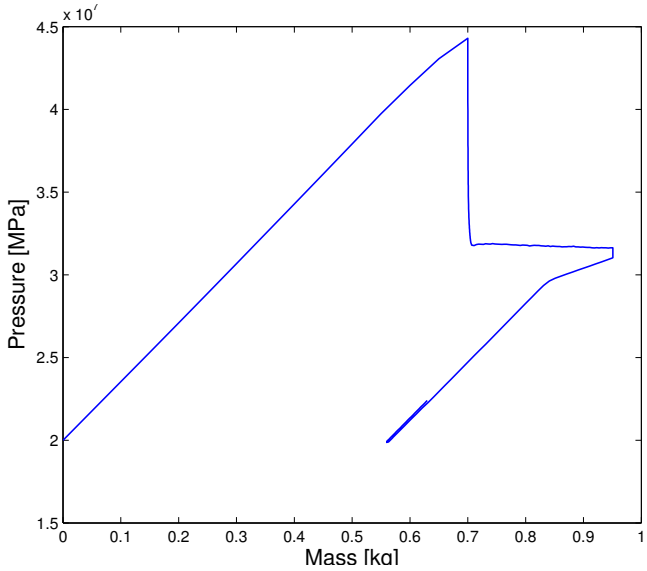

Figure 4.22: Plot of pressure versus volume for the simulation in Figure 4.21.

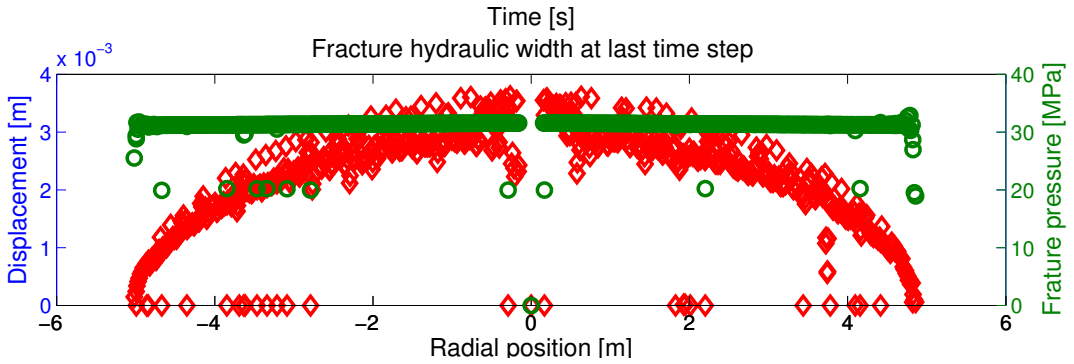

Figure 4.23: Plot of hydraulic width and pressure at the last timestep of fracture of the simulation in Figure 4.21. The fracture has opened hydraulically and mechanically, and the pressure in the fracture is uniformly distributed.

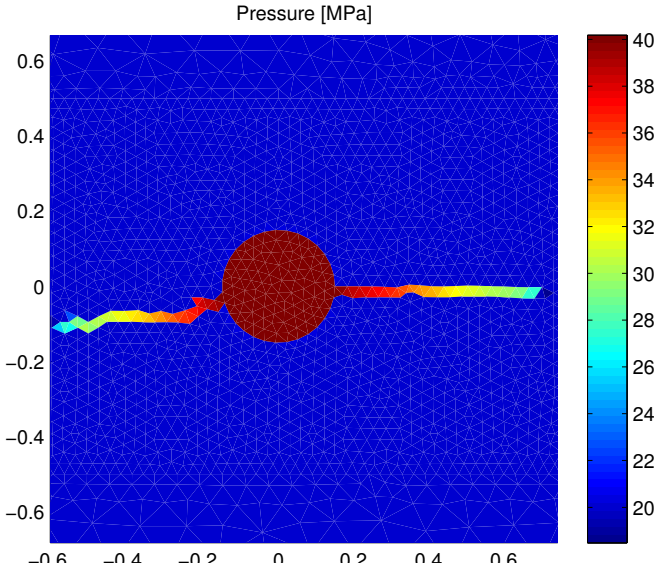

Figure 4.24: Plot of pressure in crack. The pressure transient slowly propagates to the tip of the fracture, at which time the pressure in the well will start reduce until the pressure gradient has equalized at stable fracture propagation pressure.

4.7 Issues

4.7.1 Long Shut-In Well Test

To investigate a purely formation leak-off induced fracture closure process, a long shut-in test was performed after inducement of a large fracture by hydraulic fracturing. The goal was in addition to evaluate how fluid leak-off through fracture surfaces was affected by variation in element size.

Shut-in denotes that pumpes are shut off on surface, and then in a shut-in test, downhole pressure (or surface pressure) is recorded versus time after shut-in. In real XLOTs, the recorded BHP is expected to have an immediate drop after pump-shut off due to the sudden absence of frictional pressure contribution. Assuming that there are no downhole packers to isolate the open hole section, a large well volume would require the fracture surface permeability to be high if a shut-in test is to be used for stress determination. This is explained by the way such a test is analysed for information: one look for the fingerprint of formation linear flow through the fracture surfaces. Then one would want to see a decrease in slope on a plot of pressure versus time when the fracture closes hydraulically. For a further explanation of shut-in analysis, the reader is referred to Appendix C, where in section C.221 the events after pump shut-in test are explained as they regard field XLOT testing.

As XLOTs are mostly done in low permeability formations without downhole packers, such flow regime fingerprints are seldom seen, and fracture closure would take considerable time, i.e. high cost. However, the MDEM-TOUGH2 simulator of unit borehole length (in 2D) can still provide valuable shut-in analysis. As a result of the small open hole segment volume, the pressure response measurement at the borehole is more sensitive to fluid leak-off through the fracture surfaces, and thus ideal for a fracture investigation during shut-in. An advantage of using an advanced numerical simulator is that fracture behaviour can be studied at any point in time during the test, and in addition the borehole circumferential stress can be evaluated during fracture closure.

A long shut-in test was set up to investigate the fracture closure process by shut-in simulated by the MDEM-TOUGH2. Various data were recorded and monitored throughout the test. In addition to pressure in the borehole, these included parameters in the fracture such as permeability, width, volume, total and effective stresses and fluid pressure. Test input and boundary conditions:

- A fracture of considerable size had been induced by constant injection rate 0.17 kg/s for 100 seconds (large fracture surface area, more pressure response on BHP)
- Fracture lengths of 15 m and 30 m in each direction from the borehole domain at pump shut off
- Reasonably fine grid, but increasing triangle size away from well

- Permeability k = 1e-18 m2
- Shear induced dilatency turned off in the fracture permeability model
- Mass balance not included (see Chapter 4.4.2)
- Permeability average updated to harmonic (see Chapter 4.4.3)
- Triangle size not considered in strength calculations.

The fact that mass balance was not included was not critical for this simulation, as the closure process was in focus and no flowback-phase was included. Rather, it allowed a large fracture to be created in a short period of injection, as the pressure never was allowed to drop when new fractures were created.

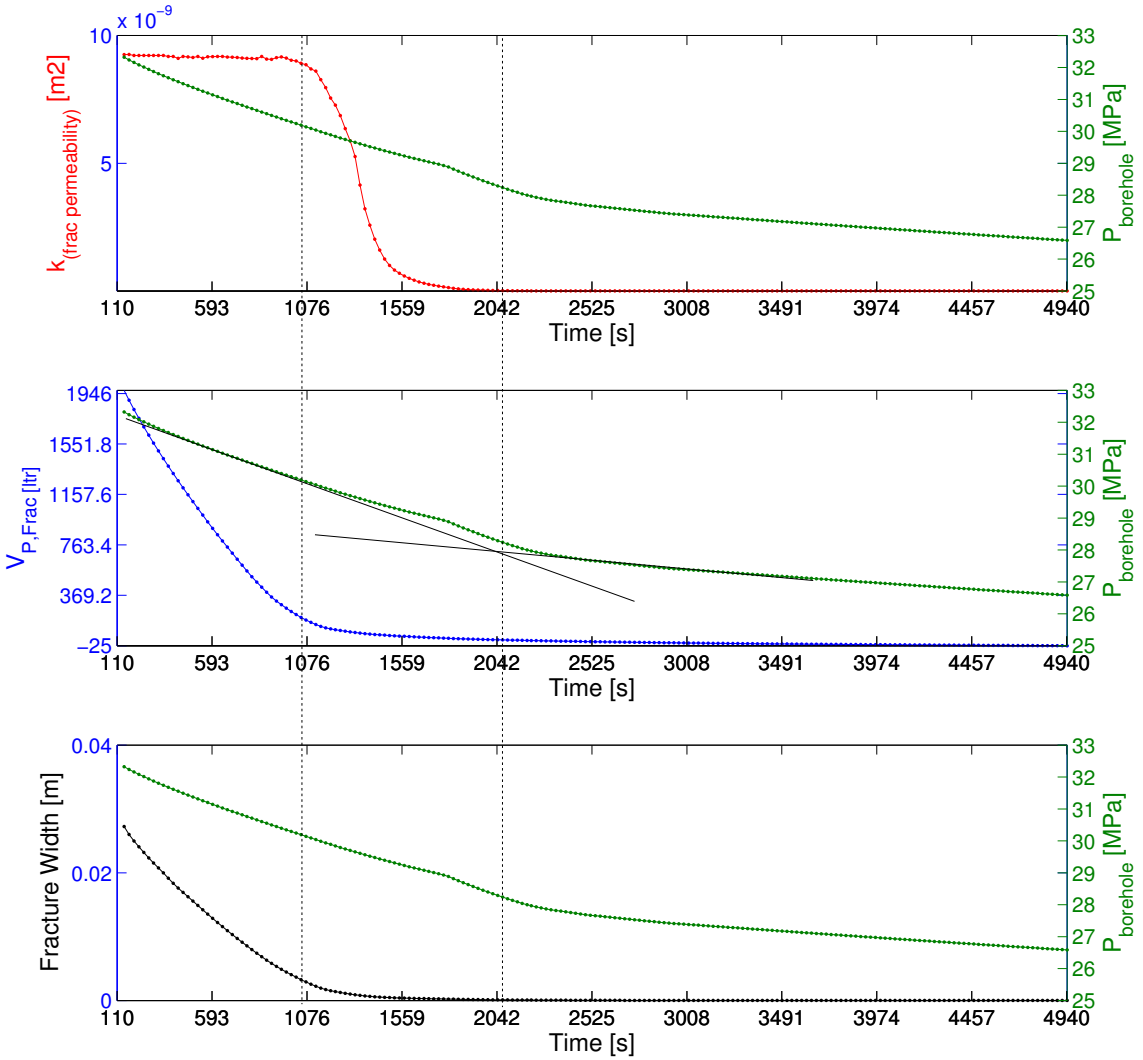

Figure 4.25: Simulation result: Shut-in test in low permeability rock for 80 minutes. Top plot: Plot of average permeability of failed clusters in a radii 2 m from the well center. Middle plot: Plot of fracture up-scaled porosity (initial pore volume minus updated volume due to upscaling of porosity in failed clusters) Bottom: Plot of fracture width (displacement). Borehole pressure versus time is plotted in each subplot for comparison.

Fracture analysis plots of pressure, permeability, aperture, and total stresses in x and y direction are investiated for 4 different times during shut in: at start, at t = 1070 s and t = 2045 s indicated by vertical dotted lines in 4.25, and at end of shut in. These plots are attached in Appendix A. Figure 4.26 illustrates flow from a failed to an intact cluster. At pump-shut off,

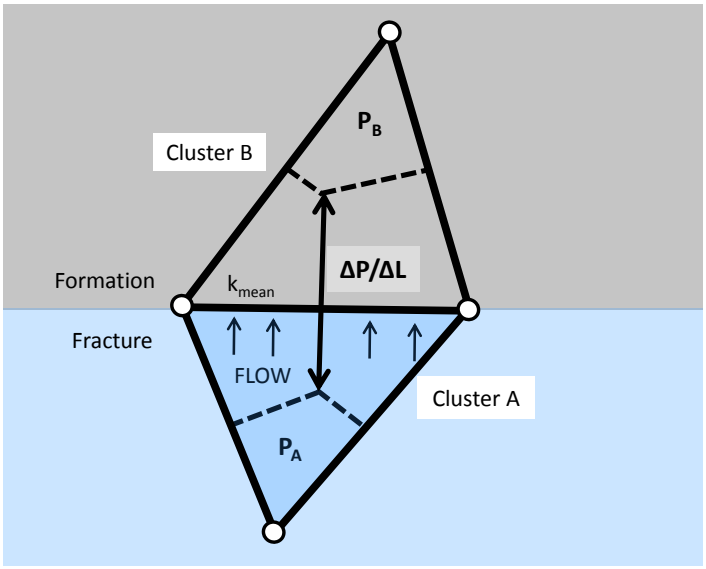

Figure 4.26: Illustration of leak-off flow from a failed to an intact cluster. The cluster size decides the distance L between two clusters, which again decides the rate of pressure decline per volume leaked off to that cluster. Length L is an input parameter to Darcy's Law.

pressure decline is due to pressure equilibration in the fracture and to leak-off to the formation. The pressure decline in an element is strictly due to flow to its neighbouring elements, either these are in intact state or not. Apart from permeability (and the permeability multiplier which is a function of aperture), there are two significant factors that decide rate of pressure decline in a specific cluster during shut-in. If the volume of the cluster is large, then more mass must be leaked off to the formation to "deplete" it. The other factor is that the size of the cluster decides the distance between the two elements, which again decides the rate of pressure decline per volume leaked off to the formation. In Appendix A a simulation result during flowback is shown where two XLOTs with two cycles are compared. One of the tests has a averagely course mesh throughout the grid, and the other has finer mesh at the borehole, and increasingly course outwards. The flowback and fracture closure analysis shows that in this case the point of closure is equally interpreted regardless of the numerical artefacts of triangle size: Variation in strength (failure threshold) and area (volume to be injected).

4.7.2 Shear Induced Fracture Aperture

The fracture permeability model implemented in MDEM, takes into account shear induced fracture dilatency. The term is denoted that due to shearing of asperities on fracture surfaces

(which are never perfectly smooth) some aperture will be induced (displacement perpendicular to the shearing direction). To include this phenomena is a powerful feature of MDEM-TOUGH2, but such a model needs proper calibration. During full XLOT simulations it was seen that shear induced width tended to maintain hydraulic aperture even though the fracture was mechanically closed. A hydraulically open fracture was identifiable by looking at plots

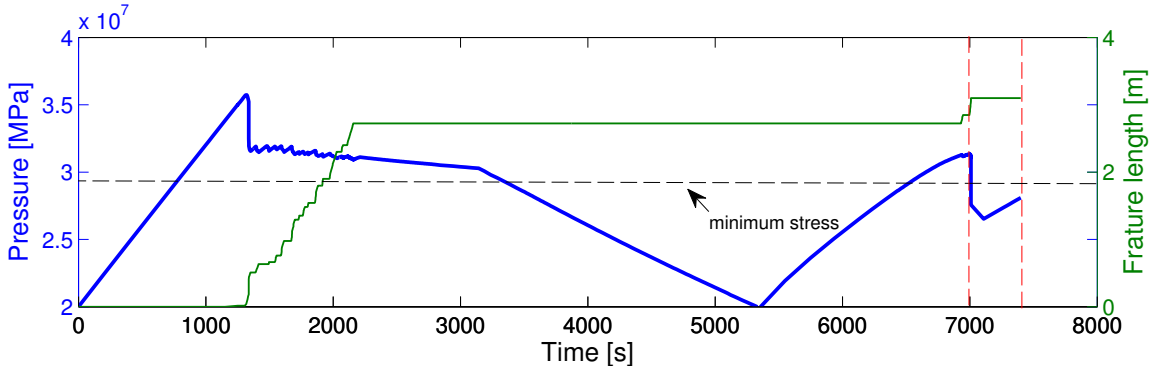

Figure 4.27: Plot of borehole pressure and fracture length.

of permeability, and pressure, and also the conventional methods of XLOT plot interpretation, where a plot of pressure versus time is analysed.

The simulation result presented in Figure 4.27, was done with constant rate injection of 0.0035 kg/s in a formation of permeability k = 1e-19 m2, and 1 meter long open hole segment and formation (2D). At start of bleed phase at 3100 seconds the fracture was mechanically and hydraulically open. This was confirmed by plots of permeability and aperture. Next, pressure is bled down with a rate of 0.003 kg/s. The minimum stress is 29.4 MPa, and fracture closure

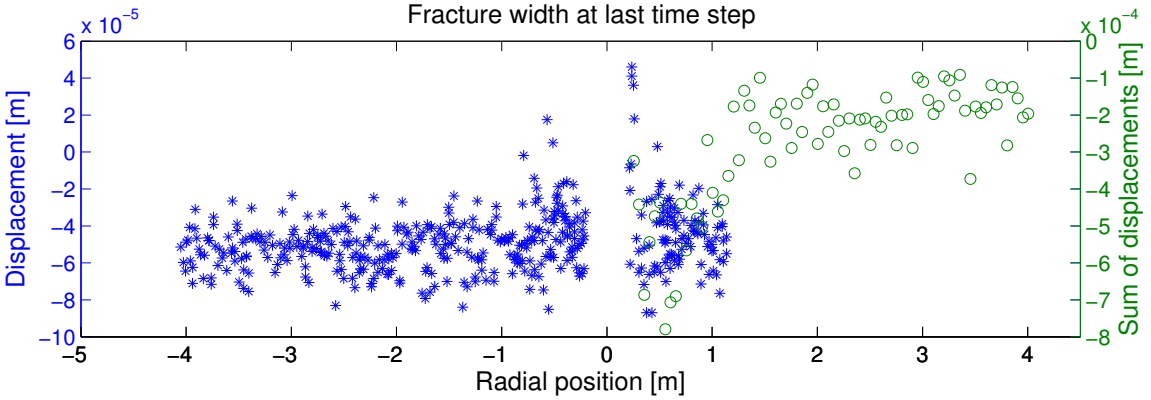

Figure 4.28: Plot of normal displacement versus radial position from the well.

should be indicated by a slope increase around this pressure. However, as seen in Figure 4.27, this is not the case. In Figure 4.28 normal fracture displacement (normal aperture) is plotted versus radial position from well centre, and in Figure 4.29a total stress in y direction is plotted. Both plots indicate a mechanically closed fracture. A plot of permeability however, for the

same timestep, describes a hydraulically fully open fracture with a considerable permeability of 1e-10 m2 (100 Darcy) throughout the fracture. This is confirmed by the re-injection phase in the second cycle in Figure 4.27, where deviation from linearity is observed. The issue of an

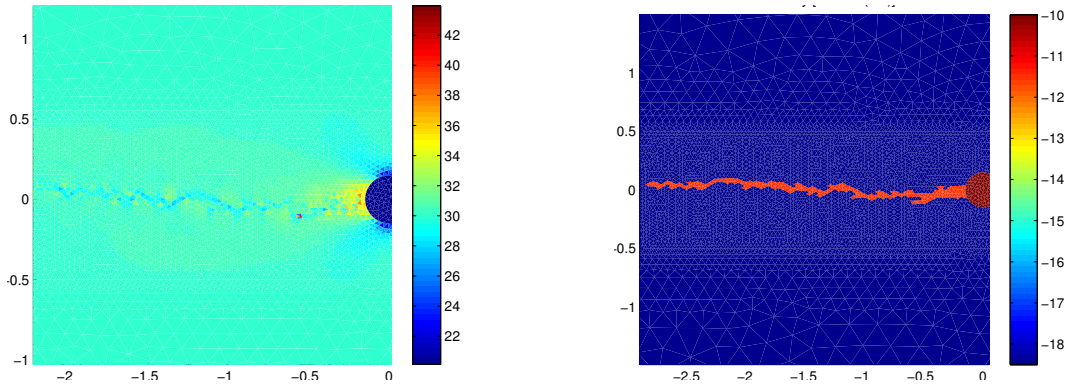

(a) Plot of total stress in y direction [MPa] (b) Plot of permeability [log m2]

Figure 4.29: Fracture analysis plots at end of bleed phase at t=5300. BHP is initial pressure of 20 MPa.

open fracture was attributed that the fracture permeability model calculated aperture including both the normal aperture and the shear aperture. The total stress distributions change during closure, and there will be some shearing of the triangles that model the rock.

4.7.3 Parallel Fracturing as a Numerical Artefact: Effects on XLOT Interpretation

In this section, the simulation result in Figure 4.27 is further investigated to show how the issue of parallel fracturing as a numerical artefact can explain certain features on the pressure versus time plot. Parallel fracturing and borehole instability were issues connected to how the permeability at the boundary of failed and intact clusters was calculated (see Chapter 4.4.3.

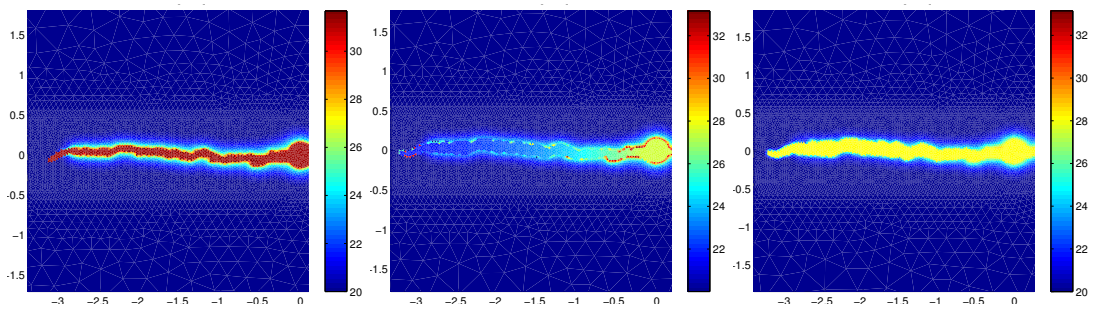

(a) Pressure at t=7000 s (b) Pressure at t=7003 s (c) Pressure at t=7400 s

Figure 4.30: Plot of pressure versus radial position from borehole centre [MPa]

A staggered approach to enforce mass conservation was used in the simulation (see Chapter 4.4.2). In cycle two of the test in Figure 4.27, a large drop in pressure can be seen, which is

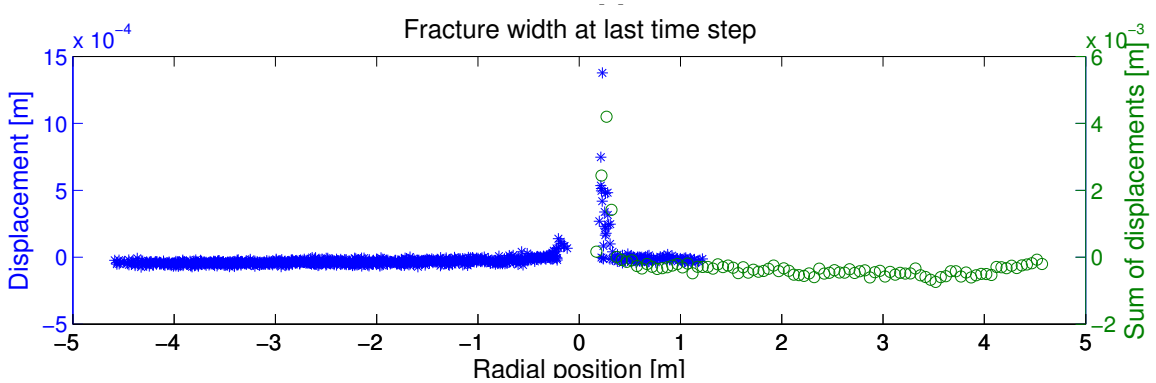

Figure 4.31: Plot of normal displacement and sum of displacement versus radial position from the well at t = 7003 s.

attributed that a layer of intact clusters fail simultaneously in tensile failure along the surfaces in the outer part of the fracture, in addition to at the tip. Recall that in the staggered approach on mass balance, MDEM-TOUGH2 reduces pressure in failed triangles while keeping track of the mass mismatch. The current fracture pressure distribution is presented for three different timesteps, in Figure 4.30. The position in XLOT is indicated by vertical dashed lines in the pressure versus time plot in Figure 4.27. Over 4 seconds of injection the pressure distribution in the fracture had been reduced almost down to initial pressure by the staggered coupling. At the same time a layer of newly failed triangles is spotted along the fracture. When the mass balance algorithm subsequently reduces pressure in all of these triangles, and this while the fracture still is mechanically closed (see figure 4.31), then the fracture could not oscillate, and the pressure is thus reduced a great amount while these newly failed triangles fill.

As a result of the fracture never closed hydraulically, the fracture was pressurized during re-injection, and thus the triangles in the fracture wall was injected into during this time, which again can be attributed how the permeability at the boundary was calculated. The large pressure drop in the second XLOT cycle in Figure 4.27 can be thus be explained by three different issues working together: 1. Shear induced fracture aperture, which keeps the fracture hydraulically open throughout the XLOT simulations. 2. Arithmetic permeability mean at the boundary of failed and intact clusters. 3. A staggered approach on mass conservation.

4.7.4 Effects of Triangle Size: Issues in Well Coupling

Figures 4.32 and 4.33 plot data from the first phase of a test where brine was injected 30 l/min into a 2000 m well for six minutes. It is seen from Figure 4.33 a and c that there is a sudden increase in pressure inside the fracture near the well during fracture propagation, at around 0.5 m on each side. From the plot of well BHP and TOUGH2 box BHP in Figure 4.32, it is observed that error would not accumulate after fracture initiation, because pressure never was allowed to drop in TOUGH2. The large pressure gradient leaves a pressure of 42 MPa in the

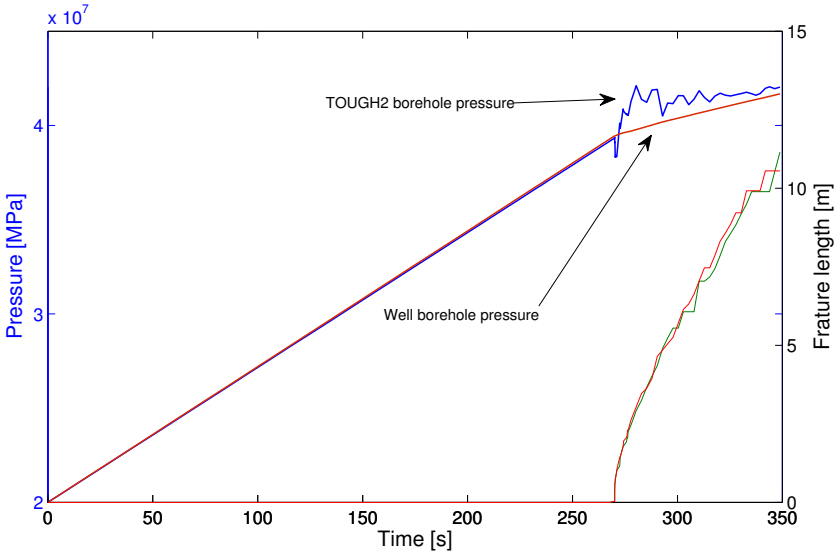

Figure 4.32: Plot of BHP_{well} and BHP_{TOUGH2} after injecting 30 l/min into a 2000 meter long well with for 350 seconds. Well coupling scheme without iterations, but with a gain controller.

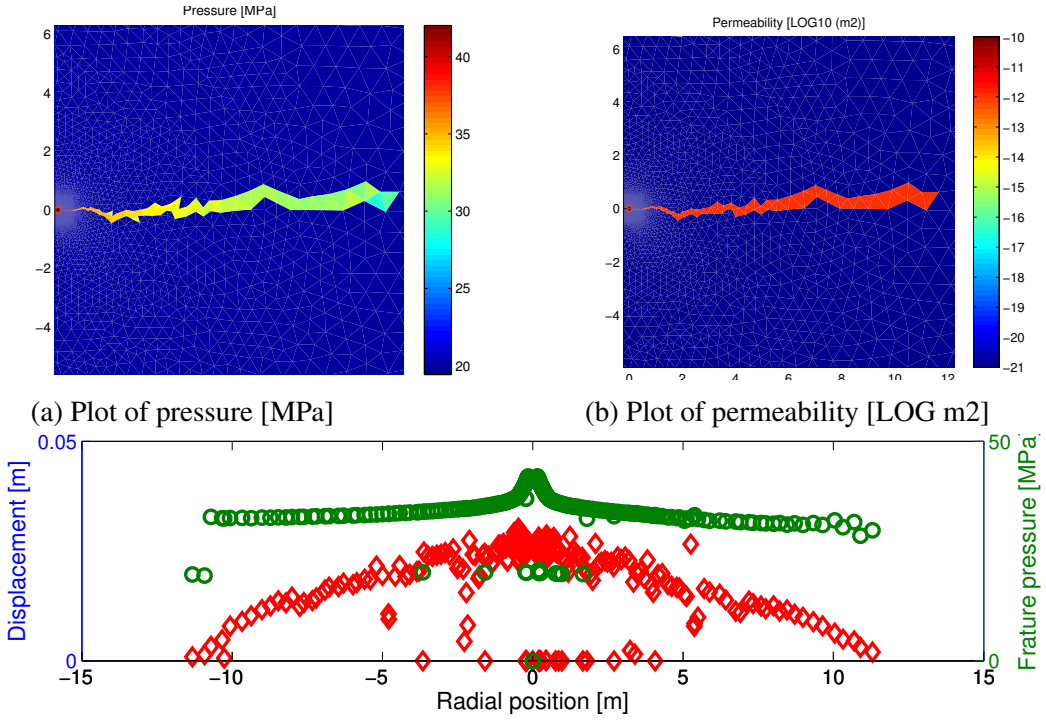

(a) Plot of pressure [MPa]

(b) Plot of permeability [LOG m2]

(c) Plot of width and fracture pressure versus radial position from the well in center.

Figure 4.33: Fracture analysis plots.

borehole, while at the fracture tip the pressure is around 30 MPa, which is the expected fracture propagation pressure. Figure 4.33b shows that the permeability in all clusters throughout the fracture is equal. The problem is that the high well pressure is never transmitted to the fracture tip, meaning that the gradient is never is allowed to even out. A poor approach to fix this issue would be to manipulate the PM value in the smaller triangles, and run the simulation again. Instead the results are analysed, explained, and learning applied for further simulations.

The large near borehole gradient can be attributed to the increase in element size far from the borehole: Remember that the permeability, which is a function of aperture, is not proportional to the up-scaled pore volume of the cluster (see Chapter 4.3). As a result of their area, large triangles require more volume to be injected for the pressure to increase. The volume must flow through smaller triangles near the well, and this conduit will constrain the flux to the larger elements, and act as a choke that prevents the gradient observed in Figure 4.33 from propagating away from the borehole. There are two main reasons for this: 1. The injection rates are high (due to the well coupling). 2. The timestep increments are small. These are of course closely related because of the criteria in MDEM to keep below a certain number of new cracks per timestep. The behaviour is otherwise correct by that the pressure does not increase in the well, until the well pressure has propagated to the tip of the induced fracture. When propagated to the tip, the pressure will start to decrease, and stabilize at the stable fracture propagation pressure, as the fracture has grown away from hoop stress vicinity.

Assumption of Hydraulic Equilibrium

An important assumption for the well model implemented in the well coupling algorithms, is that the whole well length is at all times in hydraulic equilibrium. If the effect of flow induced pressure gradients in the well were to be implemented in the well coupling algorithms some analysis on how the pressure wave travels up the well would be done. The speed of a sound wave propagating through water is around 1500 m/s. The well length used in the simulations in this thesis is at or below 2000 meters. In addition simple fracturing fluid systems have been assumed. For longer wells, with higher compliance, and with a more compressible fracturing fluid, it could be considered. The problem to be solved then, is illustrated by Figure 4.34, for the readers interest.

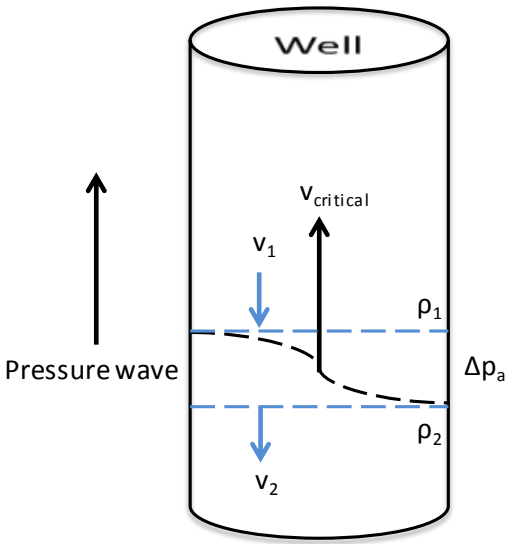

Figure 4.34: Illustration of a pressure wave travelling in a well initiated by a sudden pressure drop.

A pressure wave travelling in a well as shown in Figure 4.34 needs to be evaluated to find increase in flow velocity per time at the source of a pressure drop. The dotted lines mark boundaries of a control volume enclosing the travelling wave. Upstream the control volume, the density of the fluid is ρ_1 travelling with a speed of v_1 + 1500 m/s and downstream it is ρ_2 travelling with speed of v_2 + 1500 m/s. During XLOTs the flow rates through casing are low (50-150 l/min), and thus friction effects can be neglected. In addition the hydrostatic pressure gradient can be neglected across the control volume. The density change can be equated ([16])

$$\begin{aligned} \rho_2 &= \rho_1 e^{P_2 - P_1} \\ &\approx \rho_1 (1 + c(P_2 - P_1)) \end{aligned} \tag{4.26}$$

where c is compressibility. A simple momentum balance (e.g. Reynold's Transport Theorem) across the control volume can then be applied to calculate the increase in flux per time until the wave has reached the end of the well. The effect of such a transient would be larger in a two-phase fluid system, with higher fluid compressibility.

Chapter 5

Conclusions and Outlook

Accurate in-situ formation stress estimates have become crucial for successful petroleum field developments, as formation and well integrity assessments are dependent on these. The accuracy is more and more important due to challenging operations where the drilling margin is narrow. Especially in offshore operations, in-fill drilling, extended reach, high pressure and high temperature wells. Knowledge of stresses are in addition important for assessment of cap rock integrity and evaluation of depletion induced changes in the cap rock and reservoir. The extended leak-off test (XLOT) is considered the most reliable method for estimation of the minimum horizontal stress in deep petroleum wells, but stress data cannot always be ascertained in difficult formations (ductility and plasticity), and in complex stress regimes and geometries (fracture branching). The mentioned challenges present the need for improved interpretation and more reliable stress determination by extended leak-off tests. Numerical modelling may in many cases be the only way to achieve some understanding of the results. These points represent the motivation of the MDEM fracturing simulator development at SINTEF Petroleum.

To become an XLOT simulator, the geomechanical model MDEM which is coupled to a reservoir flow simulator TOUGH2, had to be refined to be able to describe fracture initiation and propagation in low-permeability rock such as shale, including poroelasticity, enforced mass balance, and a fracture permeability model developed at SINTEF Petroleum. The work during this thesis involved running numerical XLOT simulations to test the modifications as they were implemented by the team at SINTEF. Results and discussion from this work have been presented. In addition, the author of this thesis developed schemes on how to couple the MDEM-TOUGH2 fracturing simulator to a well, and implemented these into MDEM. This represents the main objective of the thesis.

The process of coupling the MDEM-TOUGH2 fracturing simulator to a well situated in shale, showed to be more complicated than first anticipated. Numerical instability was a major issue, which was caused primarily by

- An incredibly stiff fluid system: Single phase water has a bulk modulus of around 2GPa.

- That the well is situated in a formation of low permeability (10^{-3} μDarcy), which means that the volume that is induced by hydraulic pressure is the only volume available for the fracturing fluid to flow into. It is thus a strongly hydromechanically coupled system, where fluid flow and fracture mechanics are intimately connected.
- For the very stiff open hole section (unit length long MDEM domain in 2D = the open hole segment) this resulted in a system highly sensitive to changes in injection rate and to leak-off into newly opened fracture volume, in a non-linear way.
- Coupling of a deep petroleum well to a unit length open hole segment implies that large fluid volumes stored in the well will decompress and flow into the formation upon fracture initiation and formation breakdown. The large rate, in combination with the stiff open hole segment showed to induce numerical instabilities due to the highly non-linear behaviour of the system. When fracture volume opens up, and a large pressure drop occurs due to the stiffness in the open hole segment (TOUGH2), the well will provide large flux into the open hole segment. This strong and immediate interaction was difficult to stabilize numerically. The reason for this instability are two things: 1. Changes in flow rate into the open hole segment immediately translates to fracturing rate and number of failed elements. 2. A condition in MDEM reduces timestep length until number of newly failed elements are below a certain value. The condition is there to ensure a stable hydromechanical coupling, and is thus a result of the MDEM to TOUGH2 sequential scheme. Time step lengths were reduced down to $1e^{-7}$ s per timestep, but this was not sufficient.

Nonetheless, two main well coupling schemes were developed and implemented in MDEM: one iterative technique and a technique based on a PID controller system. Simulation results were obtained and have been presented.

Every numerical tool for geomechanical modelling has its disadvantages and advantages. In MDEM a shortcoming is the connected to discretization, specifically that when a grid block has failed, the direction of the crack within that grid block cannot be tracked . As a result the geomechanical model requires finely meshed grids to describe fracture growth.

A general limitation to well coupling is that of the large volumes that needs to be injected during an XLOT to get the pressure down to a stable fracture propagation pressure. At the same time it has been concluded in this thesis that finely meshed grids are required for a correct description of fracture and fracturing behaviour. A large, finely meshed grid will demand considerable time with the current implementation of MDEM-TOUGH2. The high non-linearity of the open hole segment during fracture initiation and propagation, leads to the belief that with the current relatively slow MDEM, the best approach would be a full coupling instead of sequential, where flow equations were directly implemented in MDEM. Currently however, MDEM runs on only one computer core, and with parallellization of the sequential interaction, the simulation time can be reduced significantly. If a faster fluid flow simulator was coupled to MDEM

and the software ran on all cores of a computer, these two contributions would allow efficient 2D simulations, which again would allow large finely meshed grids and thus well coupling to be implemented.

Outlook

In MDEM, the physics remain the same in 2D and 3D. Once the above problems have been solved, an MDEM 3D model can be established and linked to a faster reservoir simulator. MDEM 3D will be a tool that enables us to run 3D simulations in complex stress regimes and complex geometries. From XLOTs in deviated wells the full in-situ stress tensor may be derived from simulations and field data, and phenomena such as fracture twisting may be captured automatically by the model. At this point the development of MDEM looks very promising, but there is still some work to be done.

References

[1] M.A. Addis, T.H. Hanssen, Yassir N., Willoughby D.R., and J Enever. A comparison of leak-off test and extended leak-off test data for stress estimation. *SPE/ISRM*, 1:1–2, 1998.

[2] H.T. Alassi. Modeling reservoir geomechanics using discrete element method: Application to reservoir monitoring. *PHD Thesis, Norwegian University of Science and Technology (NTNU)*, 2008.

[3] H.T. Alassi, R.M Holt, O-M. Nes, and S. Pradhan. Realistic geomechanical modeling of hydraulic fracturing in fractured reservoir rock. *SPE 149375*, 2011.

[4] Itasca Consulting Group Inc. Software brochures: UDEC 3DEC PFC FLAC. Available: http://www.itascacg.com/software. Last accessed 05.13.2014.

[5] P.A. Cundall and D.O. Potyond. A bonded-particle model for rock. *International Journal of Rock Mechanics and Mining Sciences*, 41:1329—1364, 2004.

[6] P.A. Cundall and O.D.L. Strack. A discrete numerical model for granular assemblies. *Géotechnique*, 29:47—65, 1979.

[7] V. Eide. Pressure integrity tests for subsurface stress determination. *TPG 4520 Project Report, Department of Petroleum Engineering and Applied Geophysics, Norwegian University of Science and Technology*, 2013.

[8] E. Fjær, R.M. Holt, P. Horsrud, A.M. Raaen, and R. Risnes. *Petroleum Related Rock Mechanics*. Developments in Petroleum Science, 53. Elsevier, 2 edition, 2008.

[9] T.B. Gederaas and A.M. Raaen. Precise minimum horizontal stress determination from pump-in/flowback tests with drilling mud. *American Rock Mechanics Association (ARMA)*, 88, 2009.

[10] B.C. Haimson, F.H. Cornet, and ISRM. Suggested methods for rock stress estimation—part 3: hydraulic fracturing (hf) and/or hydraulic testing of pre-existing fractures (htpf). *International Journal of Rock Mechanics & Mining Sciences*, 40:1011–1020, 2003.

[11] L. Ji, A. Settari, and R. Sullivan. A novel hydraulic fracturing model fully coupled with geomechanics and reservoir simulation. *SPE Journal*, 14:423–430, 2009.

[12] L. Jing and J.A. Hudson. Numerical methods in rock mechanics. *International Journal of Rock Mechanics & Mining Sciences*, 39:409–427, 2002.

[13] D. Mas Ivars. Bonded particle model for jointed rock mass. *PHD Thesis, Royal Institute of Technology (KTH), Engineering Geology and Geophysics Research Group*, 2010.

[14] A.M. Raaen, E. Skomedal, H. Kjørholt, P. Markestad, and D. Økland. Stress determination from hydraulic fracturing tests: the system stiffness approach. *International Journal of Rock Mechanics and Mining Sciences*, 38:529–541, 2001.

[15] A.M. Raaen, P. Horsrud, H. Kjørholt, and D. Økland. Improved routine estimation of the minimum horizontal stress component from extended leak-off tests. *International Journal of Rock Mechanics and Mining Sciences*, 43:37–48, 2006.

[16] F.M. White. *Fluid Mechanics*. McGraw-Hill Series in Mechanical Engineering, 6 edition, 2008.

[17] O.C Zienkiewicz, R.L. Taylor, and J.Z. Zhu. *The Finite Element Method Its Basis and Fundamentals*. Elsevier, 6 edition, 2005.

Appendix A

Plots

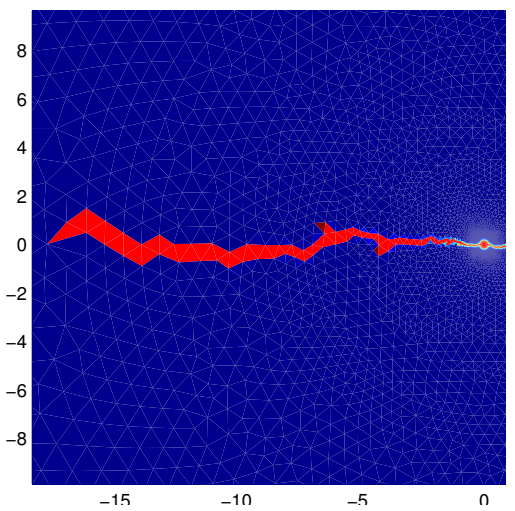

(a) Plot of pressure [MPa]

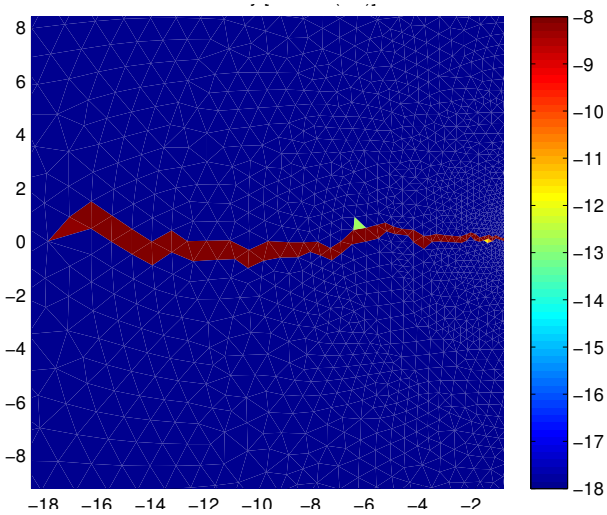

(b) Plot of permeability [LOG m2]

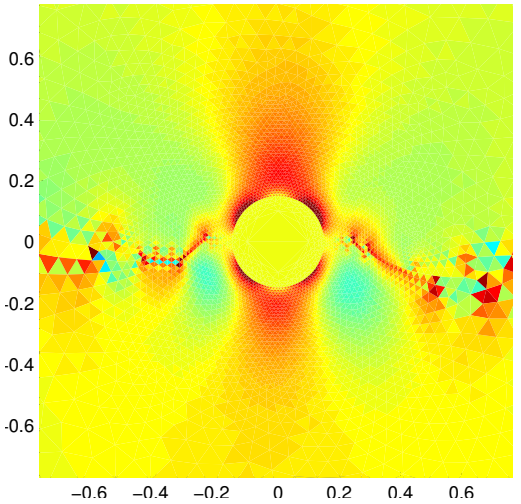

(c) Plot of total stress in y direction [MPa]

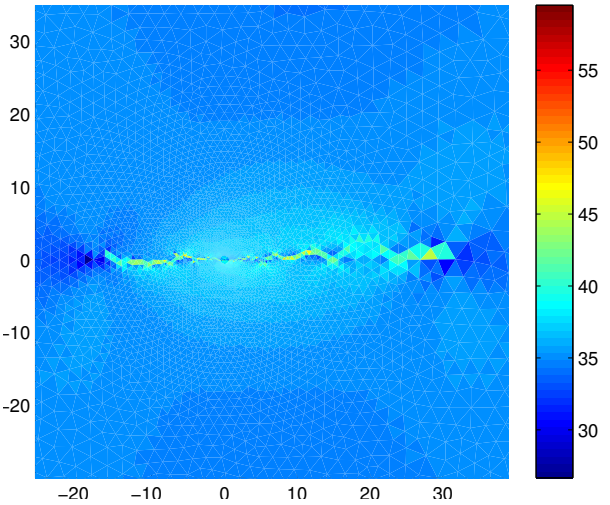

(d) Plot of total stress in X direction [MPa]

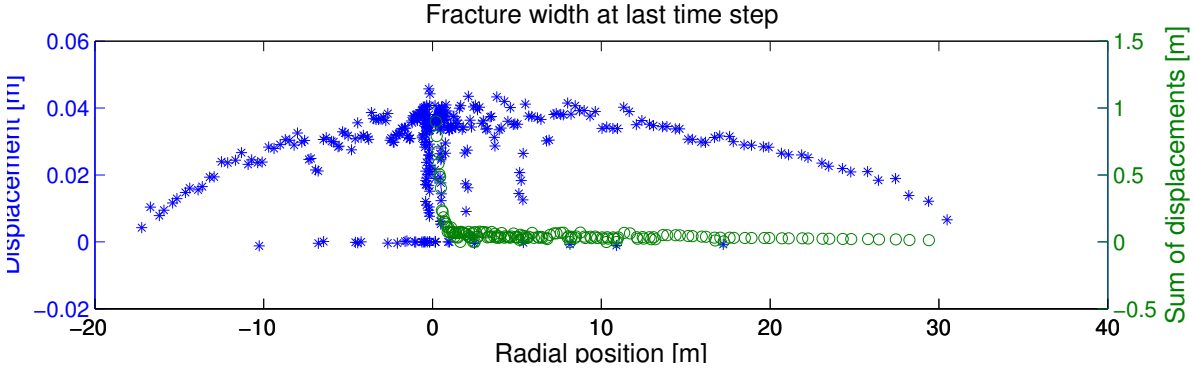

(e) Plot of displacement (width) and sum of displacement versus radial position from the well.

Figure A.1: Fracture analysis plots at start of shut-in.

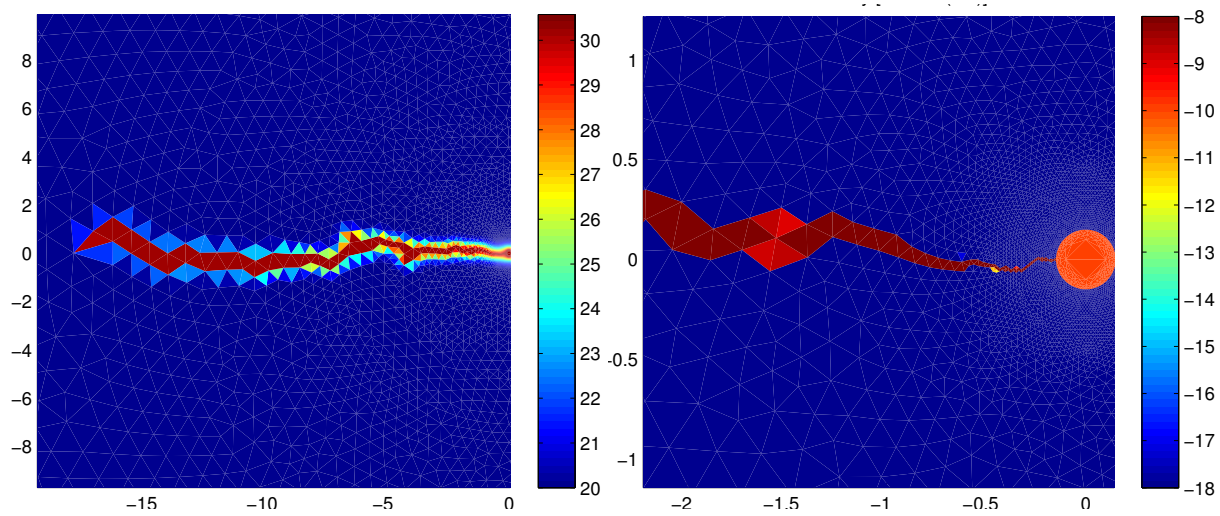

(a) Plot of pressure [MPa]

(b) Plot of permeability [LOG m2]

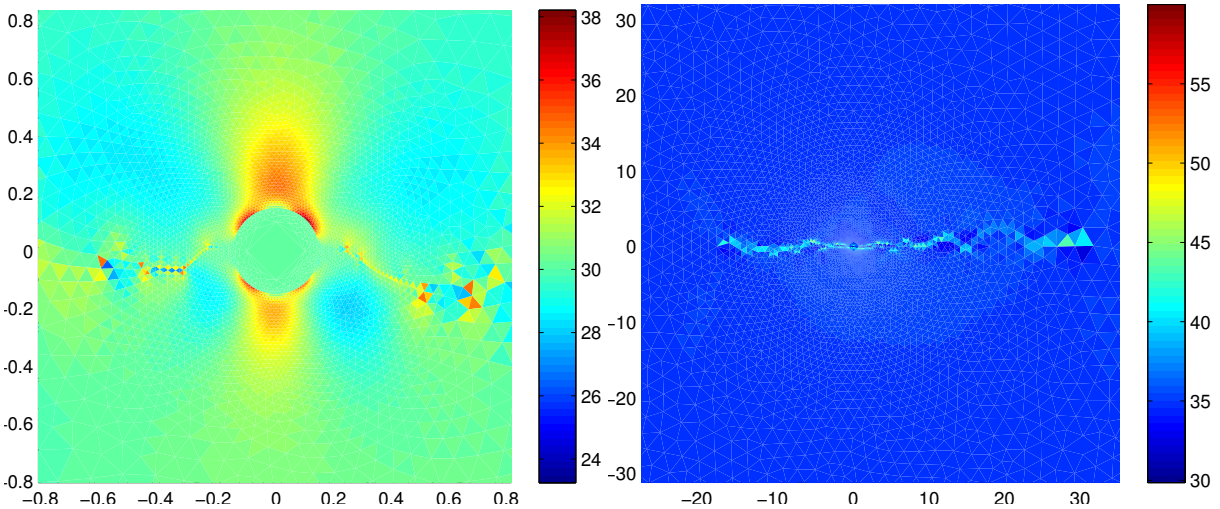

(c) Plot of total stress in y direction [MPa]

(d) Plot of total stress in X direction [MPa]

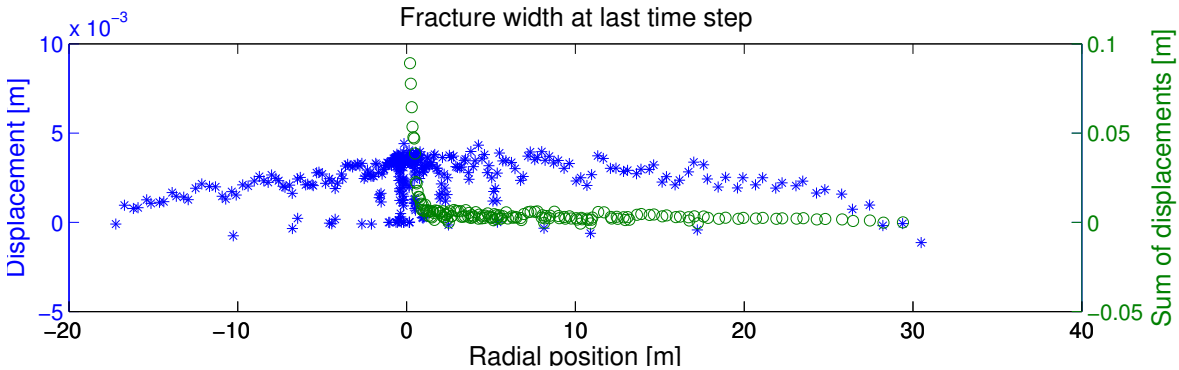

(e) Plot of displacement (width) and sum of displacement versus radial position from the well.

Figure A.2: Fracture analysis plots at t=1070 s of shut-in. Radial position in all plots are in [m] from well center

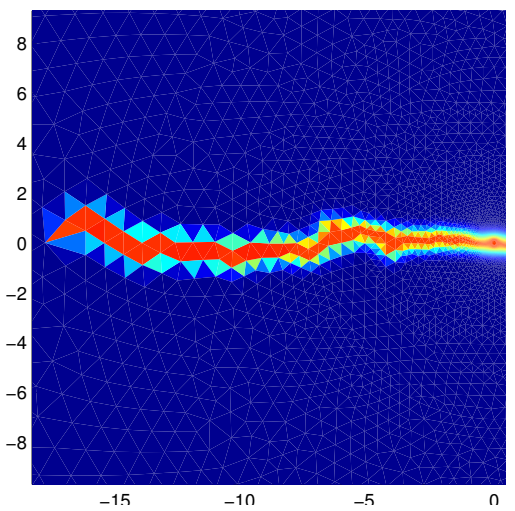

(a) Plot of pressure [MPa]

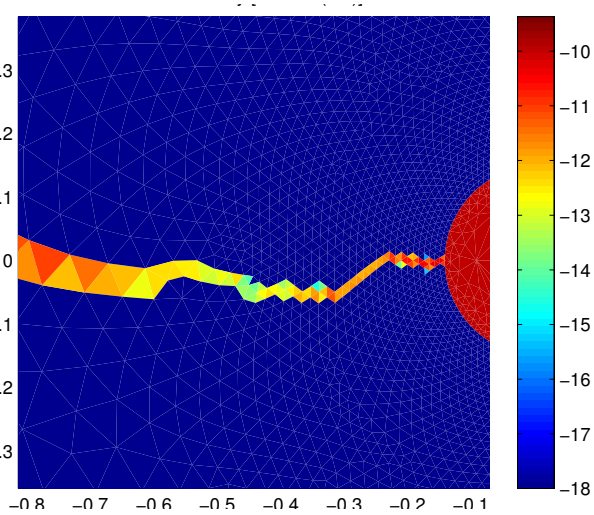

(b) Plot of permeability [LOG m2]

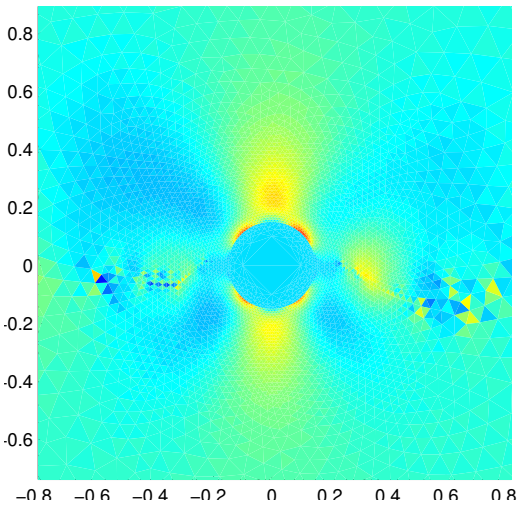

(c) Plot of total stress in y direction [MPa]

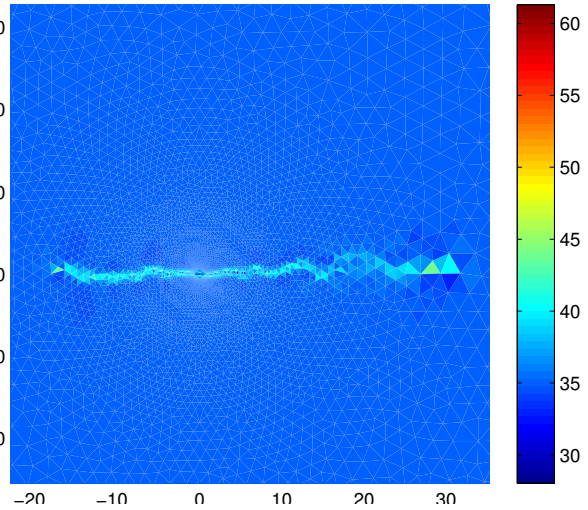

(d) Plot of total stress in X direction [MPa]

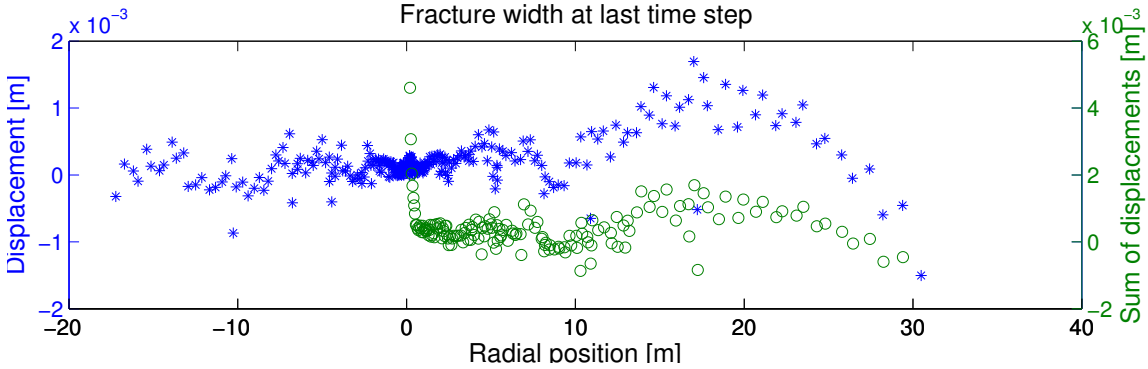

(e) Plot of displacement (width) and sum of displacement versus radial position from the well.

Figure A.3: Fracture analysis plots at t=2045 s of shut-in.

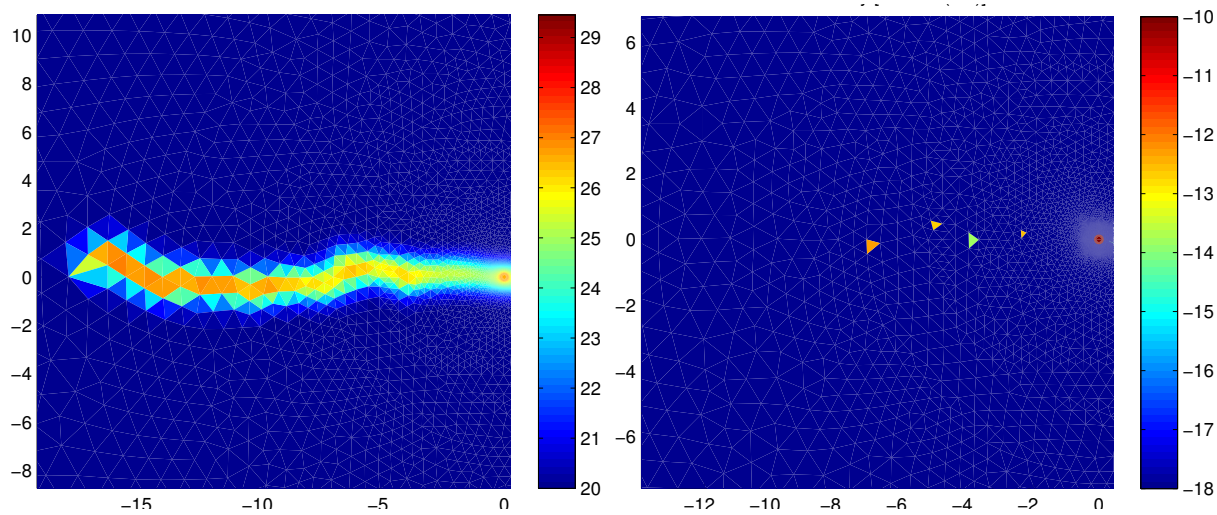

(a) Plot of pressure [MPa]

(b) Plot of permeability [LOG m2]

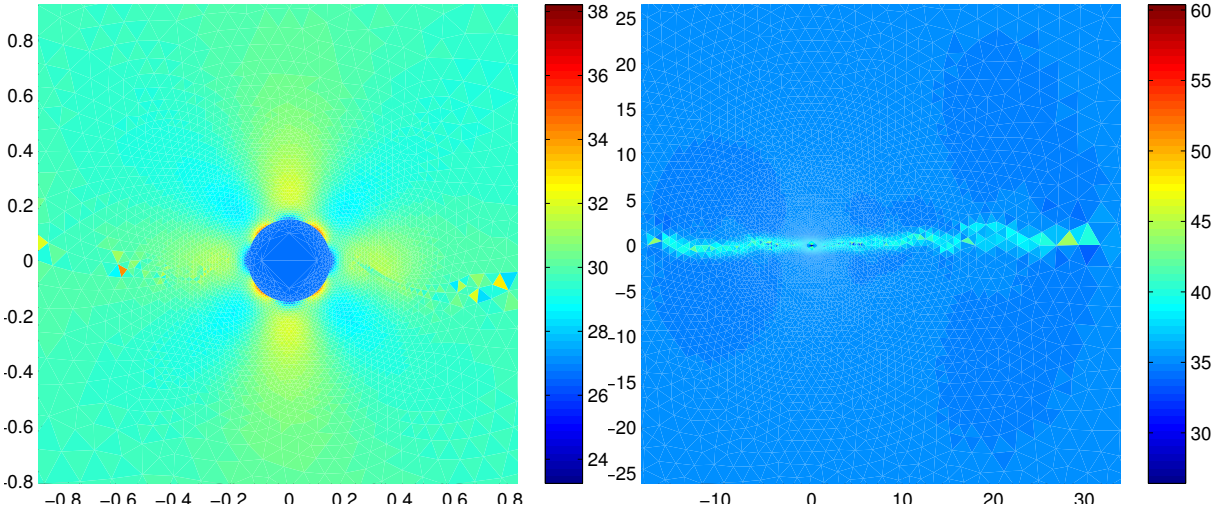

(c) Plot of total stress in y direction [MPa]

(d) Plot of total stress in X direction [MPa]

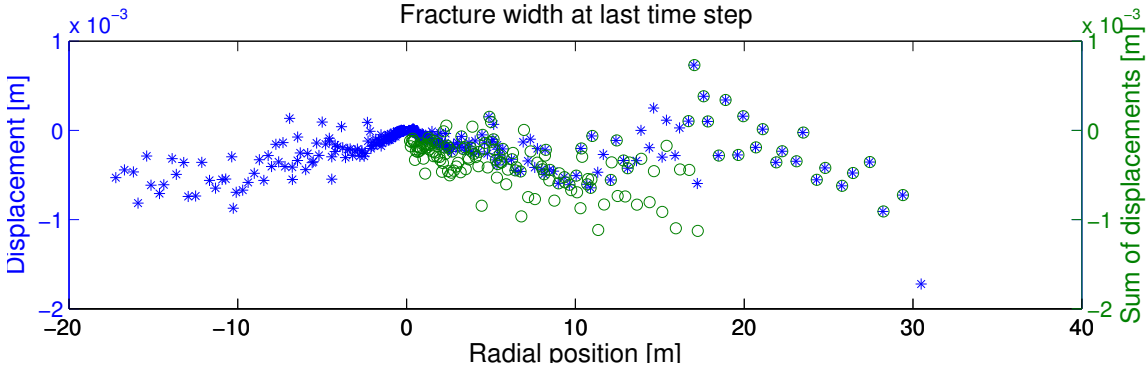

(e) Plot of displacement (width) and sum of displacement versus radial position from the well.

Figure A.4: Fracture analysis plots at end of shut-in.

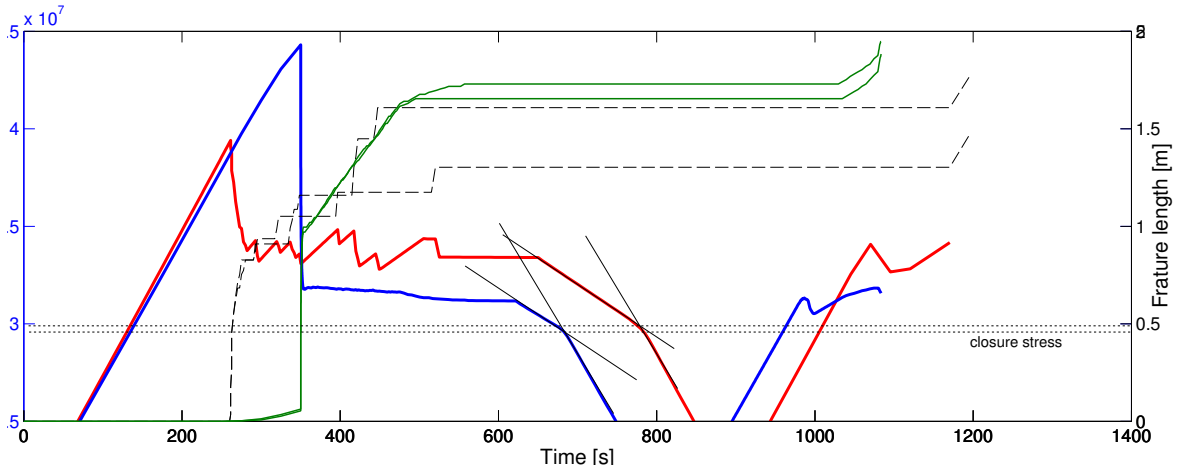

Figure A.5: Simulation result: Constant rate XLOT in finely meshed grid and comparison to evaluate effect of element size on stress estimation by flowback. Pressure and fracture length are plotted for equally sized (blue and green solid lines) and fine grid coarsening outwards (red and black dashed line). The coursening grid has a finer inner grid thus a lower breakdown pressure. The fracture propagation pressure is however higher than that of the equally sized grid. The plot shows that the fracture closure pressure, identified as an increase in slope during flowback (between 700 and 800 s), is obtained to be equal in both simulations, regardless of the numerical artefact of triangle size: Variation in strength (failure threshold) and area (volume to be injected).

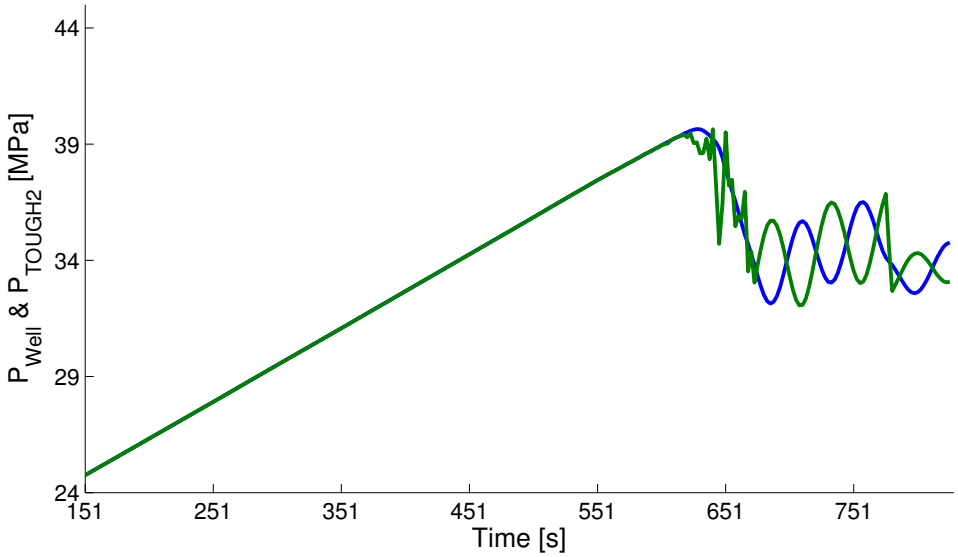

Figure A.6: Plot of Pressure versus time for well and open hole segment using the WFC gain controller without damping in combination with a high gain factor. Without damping to induce some error in the gain controller, the injection rate and thus pressure response will oscillate during stable fracture propagation.

Appendix B

Matlab Code

List of Algorithms

Algorithms B.1: Well Geometry Calculations: WFsetsys.m

```
1     v_IDpipe = 4.276;  %inches (input) Drill pipe inner diameter
2     v_ODpipe = 5;      %inches (input) Drill pipe outer diameter
3     v_IDcsg = 12.715;  %inches (input) Casing inner diameter
4     v_Kw = 1/TOUGH2_model.Fluid_compressibility(1)*10^-9; % GPa (bulk modulus of water)
5     v_ID_pipe = v_IDpipe*0.0254;                %m
6     v_OD_pipe = v_ODpipe * 0.0254;              %m
7     v_D_csg = v_IDcsg*0.0254;
8     v_Acsg = v_D_csg^2/4*pi;
9     v_dAsteel = (v_OD_pipe^2-v_ID_pipe^2)*pi/4;   % Area taken up by steel m2
10    v_Afluid = v_Acsg-v_dAsteel;                  % Area taken up by fluid m2
11    v_Lwell = 2000;                               % Well length meter
12    v_Vfluid = v_Afluid*(v_Lwell-v_heightz);
13    v_WellCompliance = v_Vfluid/(v_Kw*1e6)/10;
14    if v_bleed == 1 && (v_fixedchoke == 0 || v_wellCoupling == 0)
15        v_VolRateSurf = -v_VolRateSurf
16    elseif v_shut == 1
17        v_VolRateSurf = 0;
18    elseif v_bleed == 1 && v_fixedchoke == 1
19        if i == firstFBstep
20            v_VolRateSurf = -v_VolRateSurf
21        elseif i > firstFBstep % Calculate surface production rate from last steps ...
              output bottomhole pressure.
22            v_VolRateSurf = v_zeta*(v_SurfacePressurei-0.101325*1e6)^0.5
23            disp(['Surface Production rate through fixed choke is ',num2str(...
                  v_VolRateSurf*60), 'l/min']);
24        end
25    end
26    rho0 = 1.0131;
27    v_GenRateSurf = v_VolRateSurf*rho0;
28    v_SegmentVolume = v_heightz*sum(TOUGH2_model.Area((TOUGH2_model.Tdom == 2)).*...
          TOUGH2_model.Por((TOUGH2_model.Tdom == 2))); %m3
29    v_SegmentVolume0 =  v_heightz*sum(TOUGH2_model.Area((TOUGH2_model.Tdom == 2)).*...
          TOUGH2_model.Por((TOUGH2_model.Tdom == 2))); %m3
```

```
30      if 0 %i>1 && v_leakoffpressures(11,i-1)>0
31          v_SegmVolOld = v_SegmentVolume;
32          v_SegmentVolume = (v_heightz*sum(TOUGH2_model.Area((TOUGH2_model.Tdom == 2)).*...
                TOUGH2_model.Por((TOUGH2_model.Tdom == 2)))*1000 + v_leakoffpressures(11,i...
                -1))/1000; %m3
33          v_SegmentStiffness = v_Kw*1e6/v_SegmentVolume;
34      end
35      v_SegmentStiffness = v_Kw*1e6/v_SegmentVolume
36      Fluidstiffness0 = v_Kw*1e6/v_SegmentVolume0;
37      Fluidstiffness = v_SegmentStiffness;
38      if v_bleed == 1 %IF FLOWING BACK: segment stiffness is updated live, to give a rate ...
            corresponding to surface production rate.
39          if i == firstFBstep
40              Fluidstiffness;
41          else
42          v_SegmentStiffness = Fluidstiffness;
43          end
44      end
45      v_GenerationRateSteady = v_GenRateSurf / v_WellCompliance / v_SegmentStiffness;
46      v_continue = 1;
47      v_AllowedBHPerror = 0.0009;
48      v_AllowedQloRELchange = 0.001;
49      v_convRemoval = 0;
50      v_gradient = 0;
51      v_QloRELchange = 0
```

B

Algorithms B.2: Well Coupling Algorithm, Iterative: v_WFD.m

```
    if (i<2)
        v_WellBHP = 20*1e6;
        v_BHPERRORACCUMULATION = 0;
        TOUGH2_model.Por = MDEM_model.Porosity;
        v_initialPorevolume = v_heightz*sum(TOUGH2_model.Por.*TOUGH2_model.Area)*1e3;
        v_leakoffpressures = zeros(15,N_iter);
        TOUGH2_parameters.GenerationRate = v_GenerationRateSteady;
            disp(['Generation rate: ',num2str(v_GenerationRateSteady),' kg/s.']);
        sc_couplingAlgorithm;
        v_Pactual = display_element_properties(TOUGH2_model,...
            TOUGH2_parameters.ElementName);
        v_dP = v_Pactual-Outputvalues.Element_pressure(i);
        v_dPdV = v_dP/(TOUGH2_parameters.GenerationRate/rho0*out_time);
        v_dT = out_time;
        v_dP_LO = TOUGH2_parameters.GenerationRate*v_dT/rho0*v_SegmentStiffness-v_dP;
        v_qleakoff =  v_dP_LO/(v_SegmentStiffness*v_dT)
        v_qleakoff_actual = v_qleakoff;
        v_BHPguessUPD = (v_VolRateSurf-v_qleakoff/rho0)*v_dT/v_WellCompliance + 20*1e6;
        v_dPdT = v_dP/v_dT;
        v_BHPerrorstep = (v_BHPguessUPD - v_Pactual);
        v_SystemVolume = 0;
        FPPstart=0;
        newfracks = 0;
    else
        v_dP_LO = TOUGH2_parameters.GenerationRate*v_dT/rho0*v_SegmentStiffness-v_dP;
        v_qleakoff = v_qleakoff_actual;
        disp(['v_qleakoff is ',num2str(v_qleakoff),' l/s']);
        v_loopcounter = 1;
        v_firststep=1;
        v_exit = 1;
        v_convergeQ = zeros(4,50);                  % Convergence Check Algorithm
        v_convergeQ(1,v_loopcounter)= v_qleakoff;  % Sets the qLO at index 1 to the ...
            initial QLO*.
       while v_continue == 1
            %%
            a = v_loopcounter > 1;
            b = v_dPdV > 0 && v_dPdV < 50*1e6;
            c = i > 4;
            d = FPPstart == 0;
            e = v_bleed == 0;
            %f = newfracks == 0;
            if (a && b && c && e && d) || d & c %(f && e) % (c && b && e)
                disp('Floating Stiffness');
               v_SegmentStiffness = v_dPdV
               if count_tensile_cracks > 0
               calib = 1;
               else
               calib=0;
               end
               v_WFGenerationRate = calib*v_qleakoff*rho0 + (v_VolRateSurf-calib*...
                   v_qleakoff)*rho0/v_WellCompliance/v_SegmentStiffness; % Stiffness is ...
                   floating, thus QLO taken into account by "stiffness" in right term.
            elseif e
               if c
               v_SegmentStiffness = Fluidstiffness;
               v_WFGenerationRate = v_qleakoff*rho0 + (v_VolRateSurf-v_qleakoff)*rho0/...
                   v_WellCompliance/v_SegmentStiffness;
               v_lockStiffness = 1;
               else
               v_WFGenerationRate = v_VolRateSurf*rho0/v_WellCompliance/...
                   v_SegmentStiffness;
               end
            elseif e==0 %Bleed
               v_qleakoff = v_FBTweakParQlo*v_qleakoff;
               v_WFGenerationRate = v_qleakoff*rho0 + (v_VolRateSurf-v_qleakoff)*rho0/...
                   v_WellCompliance/v_SegmentStiffness
            end
         TOUGH2_parameters.GenerationRate = v_WFGenerationRate;
         if TOUGH2_parameters.GenerationRate > 0 && v_bleed == 1
             disp('Warning: GenerationRate > 0');
             break;
         end
```

```
66          disp(['Q_T2 is ',num2str(TOUGH2_parameters.GenerationRate),' kg/s']);
67          %%%%%%%%%%%%%%%%%%%%%
68          sc_couplingAlgorithm;  % Simulate pressure in TOUGH2-MDEMtrial
69          %%%%%%%%%%%%%%%%%%%%%
70          v_Pactual = display_element_properties(TOUGH2_model,...
                TOUGH2_parameters.ElementName);
71          v_dP = v_Pactual-Outputvalues.Element_pressure(i);   % Update dP
72          v_dT = out_time;
73          v_dPdV = v_dP/(TOUGH2_parameters.GenerationRate/rho0*out_time);
74          disp(['dPdV ',num2str(v_dPdV*1e-6),' MPa/l and T2 stiffness was calc to be ',...
                num2str(v_SegmentStiffness*1e-6), ' MPa/l']);
75          v_dPdT = v_dP/v_dT;
76          v_BHPguessUPD = (v_VolRateSurf-v_qleakoff)*v_dT/v_WellCompliance + ...
                Outputvalues.Element_pressure(i);
77          format long
78          v_dP_LO = TOUGH2_parameters.GenerationRate*v_dT/rho0*v_SegmentStiffness-v_dP;
79          StepAvgStiffness = (v_dPdV+v_SegmentStiffness)/2;
80          v_qleakoff_actuals =  (TOUGH2_parameters.GenerationRate*v_dT/rho0*...
                StepAvgStiffness-v_dP)/(StepAvgStiffness*v_dT);
81          %%%% Run calculation to estimate lost mass:
82          v_lostVolWFD;
83          v_qleakoff_actual = v_qleakoff_mass;
84          v_convergeQ(5,v_loopcounter)= v_qleakoff_actual;
85          v_QloRELchange = (v_qleakoff-v_qleakoff_actual)/(v_qleakoff+v_qleakoff_actual); ...
                % EpsilonQ_LO
86          if v_QloRELchange > 0 && v_bleed == 0
87              if v_firststep
88                  v_dampingFact = 1.5;
89             disp('Reported QLO > QLO* Set negative damping on rate change');
90              elseif v_bleed==0
91                      v_dampingFact =1;
92                      if v_BHPerrorstep > 0
93                          v_dampingFact = 3;
94                      end
95              disp('Reported QLO > QLO* Set negative damping on rate change');
96              end
97          elseif v_QloRELchange < 0 && v_bleed == 0
98              if v_firststep
99                  if abs(v_QloRELchange) > 0.6
100                 else
101                 v_dampingFact = 1.5;
102                     if v_BHPerrorstep > 0
103                         v_dampingFact = 2;
104                     end
105                 end
106                  disp('Reported QLO > QLO* Set negative damping on rate change');
107             elseif v_bleed==0
108                 v_dampingFact = 1;
109             disp('Reported QLO > QLO* Set negative damping on rate change');
110             end
111         end
112         v_BHPerrorstep = v_BHPguessUPD - v_Pactual;
113         v_BHPrelErr = abs(v_BHPerrorstep)/((v_BHPguessUPD+v_Pactual)/2)
114         format shortg
115         v_convergeQ(4,v_loopcounter) = TOUGH2_parameters.GenerationRate; %Save Data
116         v_convergeQ(3,v_loopcounter) = v_QloRELchange;
117         v_convergeQ(6,v_loopcounter) = v_dPdV*1e-6;
118         v_convergeQ(2,v_loopcounter) = 1e-6*(v_BHPguessUPD - v_Pactual);
119         disp(['BHP error in step ',num2str(v_BHPerrorstep*1e-6),' MPa:']);
120         disp(['Leak off rate relative change after sim. Qleakoff = ',num2str(v_qleakoff)...
                ,' kg/s is ',num2str(v_QloRELchange),'']);
121         disp(['Updated qLO is ',num2str(v_qleakoff_actual),' l/s']);
122         aa = abs(v_BHPerrorstep) > v_BHPerrMax;
123         bb = FPPstart==1;
124         cc = (abs(v_QloRELchange) > v_AllowedQloRELchange);
125         dd = (v_firststep==1 || v_firststep == 2);
126         ee = v_chErr == 1;
127         ff = 1;%v_bleed == 0 && v_HydClosure==0;
128         gg = v_shut == 0;
129          if (aa && bb && ee && ff && gg) || (cc && bb && dd && ff && gg)
130             disp(['Error too large - Run loop to iterate. Relative error in BHP between ...
                    WF and TOUGH2 is  ',num2str(1e-6*(v_BHPguessUPD - v_Pactual)),'']);
131             v_continue = 1;
```

```
            if ff == 0 % Bleed
                v_ConvergenceModuleBLEED;
            elseif gg == 0 % Shut in
                v_ConvergenceModuleSHUTIN;
            else
                v_ConvergenceModule;
            end
            v_loopcounter = v_loopcounter + 1;
            if v_firststep == 1 && cc
            v_firststep =2;
            else
            v_firststep = 0;
            end
           if v_continue == 1
            %% LOAD ORIGINAL DATA FOR NEW LOOP
            clear MDEM_model;
            clear TOUGH2_model;
            load('MDEM_model_v.mat');
            load('TOUGH2_model_v.mat');
            delete('MESH');
            delete('INCON');
            delete('SAVE');
            copyfile('MESH_v','MESH','f');                  % Make a copy of the MESH ...
                file (backup)
            copyfile('INCON_v','INCON','f');                    % Make a copy of the ...
                INCON file (backup)
            copyfile('SAVE_v','SAVE','f');                  % Make a copy of the INCON ...
                file (backup)
           end
        else
            v_continue = 0;
            disp('Found a solution, matched well BHP with TOUGH2 BHP.')
            v_convergeQ=v_convergeQ(:,any(v_convergeQ))
            if v_bleed == 0
                save(['v_convergeQfinal_',num2str(i),'.mat'],'v_convergeQ');
            end
            v_convergeQ(:,any(v_convergeQ));
        end
        end
    end
```

Algorithms B.3: Monitor Well and TOUGH2 Interaction: v_MonitoringMatrix.m

```
%Assign results to monitoring matrix
        disp(['...
            %%%%%%%%%%%%%%%%%%%%%%%%%%%%%%%%%%%%%%%%%%%%%%%%%%%%%%%%%%%%%%%%%%%%%%%%%%'...
            ]);
        disp(['Final v_dP was ',num2str(v_dP*1e-6),' MPa']);
        disp(['Final injection time was ',num2str(v_dT),' s']);
        disp(['Final dP/dT was ',num2str(v_dPdT*1e-6),' MPa/s']);
        disp(['Final Q_T2 was ',num2str(TOUGH2_parameters.GenerationRate),' kg/s']);
        disp(['Final BHP error between WF estimate and T2 result was ',num2str(...
            v_BHPerrorstep*1e-6),' MPa']);
        v_SystemVolume = v_SystemVolume + v_VolRateSurf*v_dT;
if v_UseModel == 2 % IF WFC :
        if i > 1 && count_tensile_cracks > 2 %Two system with controller
            v_WellBHP = v_WellBHP + (v_VolRateSurf-TOUGH2_parameters.GenerationRate/rho0...
                )*v_dT/v_WellCompliance;
            v_BHPERRORACCUMULATION = v_BHPERRORACCUMULATION + v_BHPerrorstep;
            FPPstart=1;
        else
            v_WellBHP = v_Pactual;
        end

elseif v_UseModel == 1 || v_UseModel == 3 || v_shut == 1 %IF WFD:
        if  i<4
            v_WellBHP = v_Pactual;
            v_BHPERRORACCUMULATION = 0;
        elseif i > 1 && count_tensile_cracks > 4
            FPPstart=1;
            v_WellBHP = v_WellBHP + (v_VolRateSurf-v_qleakoff)*v_dT/v_WellCompliance;
```

```
            v_BHPERRORACCUMULATION = v_BHPERRORACCUMULATION + v_BHPerrorstep;
        else
            v_WellBHP = v_WellBHP + (v_VolRateSurf-v_qleakoff)*v_dT/v_WellCompliance;
            v_BHPERRORACCUMULATION = v_BHPERRORACCUMULATION + v_BHPerrorstep;
        end
end
%%% Calculate surface pressure upstream choke:
f_Pbtm = Outputvalues.Element_pressure(i+1)*1e-6; % To be used in WFF
v_WFF;
v_SurfacePressurei = f_Ptop*1e6;
        v_leakoffpressures(1,i)= i;
        v_leakoffpressures(2,i)= v_qleakoff_actual;
        v_leakoffpressures(3,i)= TOUGH2_parameters.GenerationRate;
        v_leakoffpressures(4,i)= v_dT;
        v_leakoffpressures(5,i)= v_BHPerrorstep*1e-6;
        v_leakoffpressures(6,i)= v_dP*1e-6;
        v_leakoffpressures(7,i)= v_dPdT*1e-6; % dP/dT
        v_leakoffpressures(8,i)= v_SurfacePressurei*1e-6;
        v_leakoffpressures(9,i)= v_BHPERRORACCUMULATION*1e-6;
        v_leakoffpressures(10,i)=v_WellBHP*1e-6;
        v_leakoffpressures(11,i)=(sum(TOUGH2_model.Por.*TOUGH2_model.Area)*v_heightz*1e3...
            -v_initialPorevolume); %Fracture volume at Time_inj
        v_leakoffpressures(12,i)= Outputvalues.Time_inj(i)+out_time;
        v_leakoffpressures(13,i)= v_Pactual*1e-6;
        v_leakoffpressures(14,i)= v_dPdV*1e-6;
        if i>1 % Calc. mean k of failed clusters within 2m radius.
        v_leakoffpressures(15,i)= mean(averageperm(1,:));
        else
            v_leakoffpressures(15,i)=NaN;
        end
        v_leakoffpressures(16,i)= v_SystemVolume;% Record current system volume for step
        if v_bleed == 1                          % Record time since start of flowback.
            v_FBmon(1,i+1-firstFBstep) = v_leakoffpressures(12,i) - v_FBtimestart;
            v_FBmon(2,i+1-firstFBstep) = v_dT;
            v_FBmon(3,i+1-firstFBstep) = v_Pactual*1e-6;
            v_FBmon(4,i+1-firstFBstep) = v_VolRateSurf/v_zeta; % Square root of P/choke
            v_FBmon(5,i+1-firstFBstep) = v_dPdV*1e-6;
            v_FBmon(6,i+1-firstFBstep) = (v_SurfacePressurei*1e-6);
            if (i+1-firstFBstep) == 1
            v_FBmon(7,i+1-firstFBstep) = 0;
            else
            v_FBmon(7,i+1-firstFBstep) = v_dP/(v_FBmon(1,i+1-firstFBstep)^0.5-v_FBmon(1,...
                i-firstFBstep)^0.5); % dPdsqrtt
            end
            v_FBmon(8,i+1-firstFBstep) = v_dP;
%             if (i+1-firstFBstep) == 1                % Flowback volume
%                 v_FBmon(9,i+1-firstFBstep) = v_VolRateSurf * v_dT;
%             else
%             v_FBmon(9,i+1-firstFBstep) =  v_FBmon(9,i+1-firstFBstep-1)+ v_VolRateSurf ...
    * v_dT;
%             end
        end
        disp(['...
            %%%%%%%%%%%%%%%%%%%%%%%%%%%%%%%%%%%%%%%%%%%%%%%%%%%%%%%%%%%%%%%%%%%%%%%%%%%%'...
            ]);
        disp(['BHPw-BHPt2 is ',num2str(v_leakoffpressures(10,i)-v_leakoffpressures(13,i)...
            ),' MPa, and BHPerrorStep is ',num2str(v_BHPerrorstep*1e-6),' MPa']);
        disp(['...
            %%%%%%%%%%%%%%%%%%%%%%%%%%%%%%%%%%%%%%%%%%%%%%%%%%%%%%%%%%%%%%%%%%%%%%%%%%%%'...
            ]);
```

Algorithms B.4: Well Coupling Algorithm, Shut-in: v_ShutIn.m

```
%v_ShutIn: SHUT UNTIL v_qleakoff has stabilized.
        if i == firstSIstep
            v_qleakoff = 0;
           % TOUGH2_parameters.TimeStep = 0.01*TOUGH2_parameters.TimeStep0; %Calibrate ...
              with short timestep.
        else
            if i == (firstSIstep+1)
            v_BHPERRORACCUMULATION = 0
```

```
            end
            v_gainFact = 0.5;
            v_gainDamping = 0.1;
            v_qleakoff = v_qleakoff_mass;
            v_qleakoff = v_qleakoff*(1+v_gainDamping) + v_gainFact*...
                v_BHPERRORACCUMULATION*1e-6
        end
        v_BHPguess = v_VolRateSurf*(v_dT)/v_WellCompliance - v_qleakoff*v_dT/...
            v_WellCompliance + Element_pressure(i);
        disp(['v_BHPguess is ',num2str(v_BHPguess*1e-6),' MPa, which is a change in ...
            pressure of ',num2str((v_BHPguess - Element_pressure(i))*1e-6),' MPa']);
        if v_wellCoupling
        TOUGH2_parameters.GenerationRate = v_qleakoff*rho0 - v_qleakoff*rho0/...
            v_WellCompliance/Fluidstiffness;
        else
        TOUGH2_parameters.GenerationRate = 0;
        end
         sjekk = TOUGH2_parameters.GenerationRate
        %%%%%%%%%%%%%%%%%%%%%%
        sc_couplingAlgorithm;          % Simulate pressure in TOUGH2
        %%%%%%%%%%%%%%%%%%%%%%
        v_Pactual = display_element_properties(TOUGH2_model,...
            TOUGH2_parameters.ElementName);
        v_dP = v_Pactual-Element_pressure(i);    % Update dP
        %Pressure_Change_in_Tough2 = v_dP*1e-6
        v_dT = out_time;
        v_dPdT = v_dP/v_dT;
        % Update guesses with actual timestep length:
        v_BHPguessUPD = (v_VolRateSurf-v_qleakoff)*v_dT/v_WellCompliance + ...
            Element_pressure(i);
        % Run calculation to estimate sum of flux in borehole domain triangles:
        v_lostVolWFD;
        v_dPdV = v_dP/((TOUGH2_parameters.GenerationRate-v_qleakoff_mass)/rho0*out_time)...
            ;  %v_SegmentStiffness, Pa/l
        v_qleakoff_actual = v_qleakoff_mass;
        disp(['v_qleakoff_actual = ',num2str(v_qleakoff_mass),' l/s']);
        v_QloRELchange = (v_qleakoff-v_qleakoff_actual)/(v_qleakoff+v_qleakoff_actual);
        v_BHPerrorstep = v_BHPguessUPD - v_Pactual;
        format shortg
        disp(['Segment stiffness is recorded to be = ',num2str(v_dPdV*1e-6),' MPa and ...
            was in the previous step calculated with volume to be ',num2str(...
            v_SegmentStiffness*1e-6),'']);
        disp(['Leak off rate is recorded to be ',num2str(v_qleakoff_actual),' l/s and ...
            relative change in leak-off rate to actual rate is ',num2str(v_QloRELchange)...
            ,'']);
        v_BHPrelErr = v_BHPerrorstep/((v_BHPguessUPD+v_Pactual)/2);
```

Algorithms B.5: Well Coupling Algorithm, Hybrid: WFCWFD.m

```
if i == 1
        v_WellBHP = 20*1e6;
        yy=0;
        v_BHPERRORACCUMULATION = 0;
        TOUGH2_model.Por = MDEM_model.Porosity;
        v_initialPorevolume = sum(TOUGH2_model.Por.*TOUGH2_model.Area)*1e3;
        v_leakoffpressures = zeros(15,N_iter);
        TOUGH2_parameters.GenerationRate = v_GenerationRateSteady;
            disp(['Generation rate: ',num2str(v_GenerationRateSteady),' kg/s.']);
        sc_couplingAlgorithm;
        v_Pactual = display_element_properties(TOUGH2_model,...
            TOUGH2_parameters.ElementName);
        v_dP = v_Pactual-Outputvalues.Element_pressure(i);
        v_dPdV = v_dP/(TOUGH2_parameters.GenerationRate/rho0*out_time);
        v_dT = out_time;
        v_dP_LO = TOUGH2_parameters.GenerationRate*v_dT/rho0*v_SegmentStiffness-v_dP;
        v_qleakoff =  v_dP_LO/(v_SegmentStiffness*v_dT)
        v_qleakoff_actual = v_qleakoff;
        v_BHPguessUPD = (v_VolRateSurf-v_qleakoff/rho0)*v_dT/v_WellCompliance + 20*1e6;
        v_dPdT = v_dP/v_dT;
        v_BHPerrorstep = (v_BHPguessUPD - v_Pactual);
        v_SystemVolume = 0;
```

```
22          v_newT2GenRate = TOUGH2_parameters.GenerationRate;
23          FPPstart=0;
24  else
25      v_loopcounter = 1;
26      v_continue = 1;
27  while v_continue == 1
28  v_qleakoff = v_qleakoff_mass;
29      if v_wellCoupling && FPPstart == 1
30          if v_bleed == 1
31              if i == firstFBstep
32              v_qleakoff = 0;
33              v_gainFact = 0;
34              v_gainDamping = 0;
35              else
36              if v_bleed == 1 && i == (firstFBstep+1) % Restart BHP error
37              v_BHPERRORACCUMULATION = 0;
38              end
39              v_gainFact = v_gainFact0;%0.5;
40              v_gainDamping = v_gainDamping0;
41              end
42          elseif v_bleed == 0
43              if v_leakoffpressures(11,i-1) > 0.3
44                  disp('Average of last three BHP errors used as calibration to eliminate ...
                        error');
45                  v_BHPERRORACCUMULATION = sum(v_leakoffpressures(5,(i-3):(i-1)))*1e6; % ...
                        gain
46                  v_gainFact = v_gainFact0;%0.5;
47                  v_gainDamping = v_gainDamping0;
48              else v_leakoffpressures(11,i-1) < 0.3
49                  v_gainFact = 0;
50              end
51          end
52          v_SegmentStiffness = Fluidstiffness;
53      elseif FPPstart==0
54              v_BHPERRORACCUMULATION = 0;
55              v_gainDamping = 0.0;
56              if i > 2
57              v_SegmentStiffness = v_dPdV;
58              end
59              v_gainFact = 0;
60      end
61          v_qleakoff = v_qleakoff/(1+v_gainDamping) + v_gainFact*v_BHPERRORACCUMULATION*1e...
                -6
62          if v_wellCoupling && FPPstart == 1 && v_bleed == 0 && v_qleakoff < 0
63              v_qleakoff = 0;
64              disp('Warning: New guess on qleakoff rate is below zero due to gain. QLO* ...
                    set to zero. Consider reducing gain.');
65          end
66          v_BHPguess = v_VolRateSurf*(v_dT)/v_WellCompliance - v_qleakoff*v_dT/...
                v_WellCompliance + Outputvalues.Element_pressure(i);
67          disp(['v_BHPguess is ',num2str(v_BHPguess*1e-6),' MPa, which is a change in ...
                pressure of ',num2str((v_BHPguess - Outputvalues.Element_pressure(i))*1e-6),...
                ' MPa']);
68          if v_wellCoupling
69          TOUGH2_parameters.GenerationRate = v_qleakoff*rho0 + (v_VolRateSurf-v_qleakoff)*...
                rho0/v_WellCompliance/v_SegmentStiffness;
70          else
71          TOUGH2_parameters.GenerationRate = v_GenerationRateSteadyCST
72          end
73           sjekk = TOUGH2_parameters.GenerationRate
74          %%%%%%%%%%%%%%%%%%%%%%
75          sc_couplingAlgorithm;          % Simulate pressure in TOUGH2
76          %%%%%%%%%%%%%%%%%%%%%%
77          v_Pactual = display_element_properties(TOUGH2_model,...
                TOUGH2_parameters.ElementName);
78          v_dP = v_Pactual-Outputvalues.Element_pressure(i);    % Update dP
79          v_dT = out_time;
80          v_dPdT = v_dP/v_dT;
81          % Update guesses with actual timestep length:
82          v_BHPguessUPD = (v_VolRateSurf-v_qleakoff)*v_dT/v_WellCompliance + ...
                Outputvalues.Element_pressure(i);
83          %%%% Run calculation to estimate lost mass:
84          v_lostVolWFD;
```

```
85          v_dPdV = v_dP/((TOUGH2_parameters.GenerationRate)/rho0*out_time)
86          insitustiffness = v_dP/((TOUGH2_parameters.GenerationRate-v_qleakoff_mass)/rho0*...
                out_time)
87          v_qleakoff_actual = v_qleakoff_mass;
88          disp(['v_qleakoff_actual = ',num2str(v_qleakoff_mass),' l/s']);
89          v_QloRELchange = (v_qleakoff-v_qleakoff_actual)/(v_qleakoff+v_qleakoff_actual); ...
                % Relative change Q_LO* to Q_LO. If present, then pressure error is ...
                incorrect.
90          v_BHPerrorstep = v_BHPguessUPD - v_Pactual;
91          format shortg
92          disp(['Leak off rate is recorded to be ',num2str(v_qleakoff_actual),' l/s and ...
                relative change in leakoff rate to actual rate is ',num2str(v_QloRELchange),...
                ''']);
93          v_BHPrelErr = v_BHPerrorstep/((v_BHPguessUPD+v_Pactual)/2)
94          aa = abs(v_BHPerrorstep) > v_BHPerrMax;
95          bb = v_bleed == 0;
96          cc = FPPstart == 1 && v_loopcounter == 1;
97          dd = v_wellCoupling;
98          if aa && bb && cc && dd
99              % Go back with the updated v_qleakoff = v_qleakoff_mass
100             %% LOAD ORIGINAL DATA FOR NEW LOOP
101             clear MDEM_model;
102             clear TOUGH2_model;
103             load('MDEM_model_v.mat');
104             load('TOUGH2_model_v.mat');
105             delete('MESH');
106             delete('INCON');
107             delete('SAVE');
108             copyfile('MESH_v','MESH','f');      % Make a copy of the MESH file (backup)
109             copyfile('INCON_v','INCON','f');    % Make a copy of the INCON file (backup)
110             copyfile('SAVE_v','SAVE','f');      % Make a copy of the INCON file (backup)
111             v_loopcounter = 2;
112         else
113             v_continue = 0;
114         end
115
116
117 end
118 end
```

Algorithms B.6: Fluid Pipe Flow Calculations: v_WFF.m

```
1
2  %%%%%%% Fluid Pipe Flow Model: CALCULATES PRESSURE READ AT SURFACE, I.E. PIPE PRESSURE: ...
       CALCULATES PRESSURE DROP WHILE ACOUNTING FOR DENSITY VARIATION WITH PRESSURE %%%%
3  %INPUT: v_Pbtm and surface flux
4  disp(['%%%%%%%%%%%%%%%%%%%%%%%%%%%%%%%%%%%%%%%%%%%%%%%% Fluid Pipe Flow Model: ...
       Backcalculate Stand Pipe Pressure. %%%%%%%%%%%%%%%%%%%%%%%%%%%%%%%%%%%%']);
5  f_c = 1/(v_Kw*1e3);     % 1/MPa
6  f_P0 = 0.101325;  % MPa
7  f_viscinput = 10;  % cp
8  f_visc = f_viscinput*0.001; % kg/m/s
9  f_d = 4.276*0.0254;  % m
10 f_relrough = 0.004 ;
11 f_Pbtm; %%%%%%%%%%%%%%%%%%%%%%%%%%%%%%%%%%
12 f_A = pi/4*f_d^2;   % m2 DRILL PIPE INNER CROSSECTIONAL AREA
13 f_g = 9.81;         % m/s2
14
15 f_dev = 100;
16 f_Ptop = 0;
17 while f_dev > 0.001
18 f_Pt_guess = f_Ptop;
19 f_dP_guess = 0;
20 f_inter = 100;
21 f_di = (v_Lwell-v_heightz)/f_inter;
22 f_Pin = zeros(1, f_inter);
23 f_Pout = zeros(1, f_inter);
24 f_iter = 1;
25 f_depthI = 0:f_di:(v_Lwell-v_heightz);
26
27 for depth = f_depthI
```

```
28          f_test = 1000;
29          while f_test > 0.001
30          if f_iter == 1
31          f_Pin(f_iter) = f_Pt_guess;
32      else
33          f_Pin(f_iter) = f_Pout(f_iter-1);
34      end
35          f_Pout(f_iter) = f_Pin(f_iter) + f_dP_guess;
36      f_P = (f_Pin(f_iter)+f_Pout(f_iter))/2;
37          f_rho=rho0*1000*exp(f_c*(f_P-f_P0));                    % kg/m3
38      f_v = abs(v_VolRateSurf)/1000/f_A;                                  % m/sec
39      f_Re = f_rho*f_v*f_d/f_visc;                              % [-] = kg/m3 * m/s * m / ...
            0.001 kg/m/s where cP = 0.001 kg/m/s
40      if f_Re > 2300
41      f_finv = - 1.8 * log((f_relrough/3.7)^1.11+6.9/f_Re); %Haaland friction factor
42      f_f = (1/f_finv)^2;
43      else
44      f_f = 64/f_Re;
45      end
46      f_phi = 90;
47      f_dPdZ_el = f_g*f_rho*sind(f_phi)*10^-6;              % Hydrostatic pressure drop, ...
            MPa/m
48      f_dPdZ_f = f_f*f_rho*f_v^2/(2*f_g*f_d)*10^-6;         % Frictional pressure drop, ...
            MPa/m
49      f_dPdZ = (f_dPdZ_el + f_dPdZ_f);                      % Total pressure drop, MPa/m
50      %Pout(iter) = Pin(iter) + dPdZ;
51      f_dPint = f_dPdZ*f_di;
52      f_deviationInterval = abs(f_dPint-f_dP_guess);
53      f_dP_guess = f_dPint;
54      f_test = f_deviationInterval;
55      end
56      f_iter = f_iter + 1;
57  end
58  f_dev = f_Pbtm - f_Pout(f_inter+1);
59  f_Ptop = f_Ptop + 0.8*f_dev;
60  end
61  disp(['Upstream pressure read at choke in step ',num2str(i),' is ',num2str(f_Ptop),' MPa...
        , and total frictional pressure drop in pipe: ',num2str(f_dPdZ_f*(v_Lwell-v_heightz)...
        ),' MPa. Pressure to top is ',num2str(f_dPdZ*(v_Lwell-v_heightz)),' MPa, with a ...
        gradient of ',num2str(f_dPdZ),' MPa/m']);
62  %%%%%%%%%%%%%%%%%%%%%%%%%%%%%%%%%%%%%%%%%%%%%%%%%%%%%%%%%%%%%%%%%%%%%%%%%%%%%%%%
```

Algorithms B.7: Well Coupling Algorithm, Gain Controller: WFCmod.m

```
1   format shortg;
2   if (i<2) % Well flow model not active. Set up data.
3   %see WFD
4   else
5       if FPPstart == 0
6           v_BHPERRORACCUMULATION = 0;
7       elseif FPPstart==1 && Outputvalues.Element_pressure(i) < 34*1e6 && ...
            v_BHPERRORACCUMULATION < 2.5*1e6 % Approaching fracture propagation pressure
8            v_gainFact = v_gainFact/2;
9            disp('p < 35 and error < 2.5, flatten out');
10
11          if (v_leakoffpressures(9,i-2) > 0 && v_leakoffpressures(9,i-1) < 0) && ...
                Outputvalues.Element_pressure(i)%|| v_BHPERRORACCUMULATION < 0.2*1e6 % ...
                Controller has eliminated error, and damping is applied.
12              v_gainDamping = 0.1;
13
14          end
15      elseif FPPstart==1
16      if v_qleakoff_mass < 0.009
17      v_gainVol = v_gainFact/10; %1/60/4;
18      else
19      v_gainVol = v_gainFact;
20      v_gainFact_tlow = 1/(5);
21      end
22          v_gainDamping = 0;
23      end
24      if FPPstart==1
```

```
    %v_gainVol = min(v_gainFact*v_dT,v_gainFact)
             v_gainVol = v_gainFact;
        v_newT2GenRate = v_qT2last/(1+v_gainDamping) + v_gainVol*v_BHPERRORACCUMULATION...
            *1e-6;
        a = v_newT2GenRate < 0 && v_bleed == 0;
        if a
            disp(['Consider reducing gain, WFC calculates negative T2 rate for step',...
                num2str(i),'']);
            v_newT2GenRate = v_qT2last + v_gainVol/(1+v_gainDamping)/10*...
                v_BHPERRORACCUMULATION*1e-6; % Early breakdown, then rate may become ...
                zero if high gain, and if so then override and reduce change.
            if a
                v_newT2GenRate = v_qT2last*0.8;
            end
        end
        disp(['BHP error is present, Control increasing last injection rate with ',...
            num2str((v_newT2GenRate/TOUGH2_parameters.GenerationRate-1)*100), ' %, to ',...
            num2str(v_newT2GenRate/rho0), 'l/s']);

        TOUGH2_parameters.GenerationRate = v_newT2GenRate;
        disp('%%%%%%%%%%%%%%%%%%%%%%%%%% Rate Control Module Active ...
            %%%%%%%%%%%%%%%%%%%%%%%%%%%%%%%%');
    end
        v_qT2last = v_newT2GenRate;           % For next step
        %%%%%%%%%%%%%%%%%%%%%%
        sc_couplingAlgorithm;% Simulate pressure in TOUGH2
        %%%%%%%%%%%%%%%%%%%%%%
        v_Pactual = display_element_properties(TOUGH2_model,...
            TOUGH2_parameters.ElementName);
        v_dP = v_Pactual-Outputvalues.Element_pressure(i)     % Update dP
        v_dT = out_time
        v_dPdT = v_dP/v_dT;
        v_dPdV = v_dP/(TOUGH2_parameters.GenerationRate/rho0*out_time);
                % Update guesses with actual timestep length:
        v_qleakoff_actual =  (TOUGH2_parameters.GenerationRate*v_dT/rho0*...
            v_SegmentStiffness-v_dP)/(v_SegmentStiffness*v_dT);
        v_BHPguessUPD = (v_VolRateSurf-v_newT2GenRate/rho0)*v_dT/v_WellCompliance + ...
            Outputvalues.Element_pressure(i);
        disp(['Q_T2 is ',num2str(TOUGH2_parameters.GenerationRate),' kg/s']);
        v_BHPerrorstep = (v_BHPguessUPD - v_Pactual);
end
format shortg;
```

Algorithms B.8: Well Coupling Algorithm, Template into MDEM: MDEM_XLOT.m

```
    % Backup Files for Coupling to Well Loop.
        copyfile('MESH','MESH_v','f');                  % Make a copy of the MESH file (...
            backup)
        copyfile('INCON','INCON_v','f');                % Make a copy of the INCON file ...
            (backup)
        copyfile('SAVE','SAVE_v','f');                  % Make a copy of the SAVE file (...
            backup)
        % Objects
        save('MDEM_model_v.mat','MDEM_model');
        save('TOUGH2_model_v.mat','TOUGH2_model');      % The file contains the Tough2 ...
            triangle name, porosity, pressure and temperature ...
                                                                % The file ...
            contains the Tough2 triangle name, porosity, pressure and temperature

%%%%%%%%%%%%%%% WELL FLOW MODEL: Accounts for fluid compression/decompression ...
    %%%%%%%%%%%%%%%%%%
% In v_WFsetsys the following parameters are specified: Well geometry
% Important to set; 1 for WFD (iterative coupling to well) 2 for WFC (PID controller), 3...
     for WFC mod (WFC/WFD, no iterations).
v_UseModel = 1;          %%%%
v_fixedchoke = 1;        %%%%
firstFBstep = 217;       %%%% % Surface flux rate [l/s]
SurfaceRate = 28.8/60;   %%%%
v_wellCoupling = 0;      %%%%
%%%%%%%%%%%%%%%%%%%%%%%%%%%%%
% If choke setting v_zeta not set, then
```

```
    v_bleed = 1;                % Set to one to activate flowback in WFD
    v_VolRateSurf = abs(SurfaceRate)
    v_gainFact = 1/130    % Set if WFC
    v_dampingFact = 1;    % (Damping in BHP loop)
    v_shut = 0;           % Set to zero when not shut in.;
    v_ShutIn;
    v_gainFact0 = 1/200;
    v_gainDamping0 = 0.01;
    v_WFsetsys;
    v_BHPerrorstep = 0;
    v_criticalBHPerror_PID = 0.001;
    v_dQdP_PIDlim = 0.05;
    v_MaxNoOfIter = 3; % Max number of iterations during WFD BHP matching. 4 for Nicelot...
         grid (fine), 7 for Rabbit (course).
    v_BHPerrMax = 0.005;
    %Set choke setting:
    Zeta = 0;  % If choke setting is set to zero, it is set to max value automatically (...
        i.e. specified production rate)
    if v_bleed == 1
    if v_UseModel == 2 % USE WFC: i.e. controller coupling, not iterations.
        if i == firstFBstep
            v_qleakoff_actual = 0; %Set leakoff to zero in the first step
            v_BHPERRORACCUMULATION = 0.001; % Restart erroraccumulation to use ...
                controller (WFC)
            v_qT2last = -v_GenerationRateSteady;
        end
         v_WFCBleed;
    elseif v_UseModel == 1 % Use WFD: i.e. iterative coupling.
        if v_bleed == 1 && v_fixedchoke == 1 && i == firstFBstep % Calculate max Zeta if...
             not specified
            TOUGH2_parameters.GenerationRate = v_GenerationRateSteady;
            TOUGH2_parameters.TimeStep = 0.001*TOUGH2_parameters.TimeStep0;
            f_Pbtm = Element_pressure(i)*1e-6 % To be used in WFF
            v_WFF;
            if Zeta == 0
            v_zeta = v_VolRateSurf/(f_Ptop*1e6-0.101325*1e6)^0.5;
            end
            v_qleakoff = 0.9*v_GenerationRateSteady;
            v_HydClosure = 0;
            v_FBtimestart = Outputvalues.Time_inj(i);
        end
         %v_WFDm;
         WFCWFD;
    end
    elseif v_shut == 1/130
    v_ShutIn
    elseif v_shut == 0 && v_bleed == 0
    if v_UseModel == 1
         v_WFDm;
        % WFCWFD;
    elseif v_UseModel == 2
         v_WFCmod;
    end
    end
```

Algorithms B.9: Convergence Module: v_ConvergenceModule.m

```
%%%%%%%%%%%%%%% CONVERGENCE CHECK ALGORITHM %%%%%%%%%%%%%%%
signchange = 0;
a = (v_loopcounter == 1);
if a==0
b = abs(v_convergeQ(2,v_loopcounter))-abs(v_convergeQ(2,v_loopcounter-1))<0;
c = v_convRemoval≠ 3;
d = abs(v_convergeQ(3,v_loopcounter))-abs(v_convergeQ(3,v_loopcounter-1))<0;
e = v_firststep == 1;
f = v_firststep == 2;
g = v_convRemoval == 0;
h = v_lockStiffness == 1;
end
if v_loopcounter > 1 && h && v_bleed == 0;% Check sign(), adjust gradient to prevent ...
    oscillation.
```

```
14    SignChange = (v_convergeQ(2,v_loopcounter)<0 && v_convergeQ(2,v_loopcounter-1)>0) || ...
          (v_convergeQ(2,v_loopcounter)>0 && v_convergeQ(2,v_loopcounter-1)<0);
15    SignChangeR = (v_convergeQ(3,v_loopcounter)<0 && v_convergeQ(3,v_loopcounter-1)>0) ||...
           (v_convergeQ(3,v_loopcounter)>0 && v_convergeQ(3,v_loopcounter-1)<0);
16    RRchMagnitudeLow = abs(v_convergeQ(3,v_loopcounter))<0.01 && abs(v_convergeQ(3,...
          v_loopcounter-1))<0.01;
17    RRchMagnitude = abs(v_convergeQ(3,v_loopcounter))<0.1 && abs(v_convergeQ(3,...
          v_loopcounter-1))<0.1;
18       if v_loopcounter == 2 && SignChange==0 && b % If first set did not change sign, ...
             then increased change gradient on guess.
19           if RRchMagnitudeLow % If low rate change consistent, then compensate.
20              v_dampingFact = 60;
21           elseif RRchMagnitude
22              v_dampingFact = 10;
23           end
24       elseif v_loopcounter == 3 && v_signChange == 0 && SignChange == 0 && b
25           if RRchMagnitudeLow % If low rate change consistent, then compensate.
26              v_dampingFact = 65;
27           elseif RRchMagnitude
28              v_dampingFact = 12;
29           end
30       elseif v_loopcounter == 4 && v_signChange == 0 && SignChange == 0 && b
31           if RRchMagnitudeLow % If low rate change consistent, then compensate.
32              v_dampingFact = 70;
33           elseif RRchMagnitude
34              v_dampingFact = 15;
35           end
36       end
37       if v_signChange == 0 && (SignChange) && v_loopcounter > 2
38                b=0;
39                d=0;
40                v_signChange = 1;
41       elseif v_signChange == 1 && SignChange && v_loopcounter > 2
42           xx =(v_convergeQ(2,v_loopcounter)<0 && v_convergeQ(2,v_loopcounter-1)>0 && ...
                v_convergeQ(2,v_loopcounter-2)<0);
43           yy = (v_convergeQ(2,v_loopcounter)>0 && v_convergeQ(2,v_loopcounter-1)<0 && ...
                v_convergeQ(2,v_loopcounter-2)>0);
44           if xx || yy
45           a = 1;
46           end
47       elseif v_signChange == 1 && SignChange == 0 && v_loopcounter > 2
48           disp(['Take gradient and increase for next step ',num2str(v_convergeQ(2,...
                v_loopcounter)),'']);
49             a = 1;
50             b = 2;
51       end
52    end
53    if v_loopcounter > v_MaxNoOfIter
54          v_convRemoval = 2;
55          a=0;
56          b=0;
57          d=0;
58    end
59    if a || (b && c) || ((d && c)  && (e || f))
60                     if v_loopcounter == 1
61                       v_gradient = (v_dampingFact*((v_qleakoff_actual/v_qleakoff)-1)+1);
62                       v_qleakoff = v_qleakoff*v_gradient;
63                       v_convergeQ(1,v_loopcounter+1)= v_qleakoff;
64                       disp(['Relative change in leak off rate from initial guess too ...
                             large, new q_leakoff is ',num2str(v_qleakoff),' (l/s):']);
65                     if (v_qleakoff*rho0 + v_GenerationRateSteady - v_qleakoff*rho0/...
                           v_WellCompliance/v_SegmentStiffness)< 0 && v_bleed == 0
66                         v_qleakoff = 2;
67                         v_convRemoval= 3
68                     elseif (v_qleakoff*rho0 + v_GenerationRateSteady - v_qleakoff*rho0/...
                           v_WellCompliance/v_SegmentStiffness)< 0 && v_bleed == 0
69                         v_qleakoff = 0.1;
70                         v_convRemoval= 3;
71                     end
72                     elseif v_convRemoval == 0
73                         v_qleakofflast= v_qleakoff;
74                         numissue1 = v_convergeQ(2,(v_loopcounter)) > 0 && v_convergeQ...
                               (3,(v_loopcounter)) > 0;
```

```
75                          numissue2 = v_convergeQ(2,(v_loopcounter)) < 0 && v_convergeQ...
                                (3,(v_loopcounter)) < 0;
76                          if v_loopcounter > 2 && v_signChange == 0 && SignChange == 0 && ...
                                SignChangeR || (v_convergeQ(2,(v_loopcounter-1)) > 0 && ...
                                v_convergeQ(3,(v_loopcounter-1)) > 0 && (v_convergeQ(1,(...
                                v_loopcounter))-v_convergeQ(1,(v_loopcounter-1))) > 0 ) || (...
                                v_convergeQ(2,(v_loopcounter-1)) < 0 && v_convergeQ(3,(...
                                v_loopcounter-1)) < 0 && (v_convergeQ(1,(v_loopcounter))-...
                                v_convergeQ(1,(v_loopcounter-1))) < 0)
77                          disp('Converge on pressure.');
78                          v_gradient = (1.4*((v_convergeQ(1,(v_loopcounter))/v_convergeQ...
                                (1,(v_loopcounter-1)))-1)+1)
79                          v_qleakoff = v_gradient*v_convergeQ(1,(v_loopcounter));
80                          elseif (numissue1 || numissue2)
81                              if numissue1
82                                 v_gradient = 0.7
83                              elseif numissue2
84                                 v_gradient = 1.3
85                              end
86                          disp('Converge on pressure..');
87                          v_qleakoff = v_gradient*v_convergeQ(1,(v_loopcounter));
88                          else
89                          v_gradient = (v_dampingFact*((v_qleakoff_actual/v_qleakoff)-1)...
                                +1);
90                          v_qleakoff = v_gradient * v_qleakoff;
91                          end
92                          v_convergeQ(1,v_loopcounter+1)= v_qleakoff;
93                       disp(['Converging, send back new leakoff rate of ',num2str(...
                             v_qleakoff),' l/s']);
94                      if (v_qleakoff*rho0 + v_GenerationRateSteady - v_qleakoff*rho0/...
                            v_WellCompliance/v_SegmentStiffness)< 0 && v_bleed == 0
95                            v_qleakoff =2;
96                            v_convRemoval= 3
97                      elseif (v_qleakoff*rho0 + v_GenerationRateSteady - v_qleakoff*rho0/...
                            v_WellCompliance/v_SegmentStiffness)< 0 && v_bleed == 0
98                            v_qleakoff = 0.1;
99                            v_convRemoval= 3;
100                     end
101                     elseif v_convRemoval > 0
102                       v_gradient = (1/2*((v_convergeQ(1,(v_loopcounter))/v_convergeQ(1,(...
                              v_loopcounter-1)))-1)+1);
103                       v_qleakoff = v_gradient*v_convergeQ(1,(v_loopcounter-1));
104                       if b == 2
105                           v_gradient = (1.1*((v_convergeQ(1,(v_loopcounter))/v_convergeQ...
                                  (1,(v_loopcounter-1)))-1)+1)
106                           v_qleakoff = v_gradient*v_convergeQ(1,(v_loopcounter));
107                       end
108                       disp(['Second try, lower gradient, now converging, send back new ...
                              leak-off rate of ',num2str(v_qleakoff),' l/s']);
109                     v_convergeQ(1,v_loopcounter+1)= v_qleakoff;
110                     if (v_qleakoff*rho0 + v_GenerationRateSteady - v_qleakoff*rho0/...
                            v_WellCompliance/v_SegmentStiffness)< 0 && v_bleed == 0
111                           v_qleakoff = 2;
112                           v_convRemoval= 3
113                     elseif (v_qleakoff*rho0 + v_GenerationRateSteady - v_qleakoff*rho0/...
                            v_WellCompliance/v_SegmentStiffness)< 0 && v_bleed == 0
114                           v_qleakoff = 0.1;
115                           v_convRemoval= 3;
116                     end
117                     end
118                     latestConvIndex = v_loopcounter;
119     elseif v_convRemoval == 0
120                 if  v_signChange == 1
121                     v_gradient = (v_gradient-1)*0.6+1;
122                     v_qleakoff = v_gradient * v_convergeQ(1,(latestConvIndex));
123                     v_convergeQ(1,v_loopcounter+1)= v_qleakoff;
124                 else
125                 disp('Not converging, update w/smaller change ');
126                 v_dPdV = v_convergeQ(6,latestConvIndex)*1e6;
127                 v_gradient = (v_dampingFact/2*((v_convergeQ(1,(v_loopcounter))/...
                        v_convergeQ(1,(latestConvIndex)))-1)+1);
128
129                 v_qleakoff = v_gradient * v_convergeQ(1,(latestConvIndex))
```

```
130                 end
131                 if (v_qleakoff*rho0 + v_GenerationRateSteady - v_qleakoff*rho0/...
                        v_WellCompliance/v_SegmentStiffness)< 0 && v_bleed == 0
132                     v_qleakoff = 0;
133                     v_convRemoval = 2;
134                 end
135                 v_convRemoval = 1
136                 v_convergeQ(1,v_loopcounter+1)= v_qleakoff;
137                 v_convergeQ(:,any(v_convergeQ));
138     elseif v_convRemoval == 1
139                 if  v_signChange == 1
140                     disp('Sign change (decrease further)');
141                     v_gradient = (v_gradient-1)*0.5+1;
142                     v_qleakoff = v_gradient * v_convergeQ(1,(latestConvIndex));
143                     v_convergeQ(1,v_loopcounter+1)= v_qleakoff;
144                 else
145                 v_dPdV = v_convergeQ(6,(latestConvIndex))*1e6;
146                 v_gradient = (v_dampingFact/2*((v_convergeQ(1,(v_loopcounter))/...
                        v_convergeQ(1,(latestConvIndex)))-1)+1);
147                 v_qleakoff = v_gradient * v_convergeQ(1,(latestConvIndex))
148                 end
149                 if (v_qleakoff*rho0 + v_GenerationRateSteady - v_qleakoff*rho0/...
                        v_WellCompliance/v_SegmentStiffness)< 0 && v_bleed == 0
150                     v_qleakoff = 0;
151                     v_convRemoval = 2;
152                 end
153                 v_convRemoval = 2;
154                 v_convergeQ(1,v_loopcounter+1)= v_qleakoff;
155                 disp(['Q_LO    ';'BHPerror';'dQlo/Qlo';'Q_T2    ';'q_lo_act']);
156                 v_convergeQ(:,any(v_convergeQ))
157     elseif v_convRemoval == 2
158                 disp(['Q_LO    ';'BHPerror';'dQlo/Qlo';'Q_T2    ';'Q_LO_Act';'dPdV    '...
                        ]);
159                 disp(['',num2str(v_convergeQ(:,any(v_convergeQ))),'']);
160                 v_convergeQ=v_convergeQ(:,any(v_convergeQ));
161                 save(['v_convergeQ_',num2str(i),'.mat'],'v_convergeQ');
162                 if abs(v_convergeQ(2,v_loopcounter)) < v_minErr
163                     v_continue = 0;
164                     disp(['No solution, continues with BHPerror = ',num2str((...
                            v_BHPguessUPD - v_Pactual)*1e-6),' MPa, eps_rate ',num2str(...
                            v_QloRELchange),' l/s/l/s']);
165                 else
166                 disp(['BHP error =  ',num2str((v_BHPguessUPD - v_Pactual)*1e-6),' MPa, ...
                        and relative leak off error of ',num2str(v_QloRELchange),' l/s/l/s'...
                        ]);
167                 disp('Still not converging, load step with least error (after ...
                        calibration step) and break out of loop, at v_convRemoval = 2');
168                 clear MDEM_model;
169                 clear TOUGH2_model;
170                 load('MDEM_model_vloop.mat');
171                 load('TOUGH2_model_vloop.mat');
172                 delete('MESH');
173                 delete('INCON');
174                 delete('SAVE');
175                 copyfile('MESH_vloop','MESH','f');  % Make a copy of the MESH file (...
                        backup)
176                 copyfile('INCON_vloop','INCON','f');% Make a copy of the INCON file (...
                        backup)
177                 copyfile('SAVE_vloop','SAVE','f');  % Make a copy of the INCON file (...
                        backup)
178                 load(['v_loopTMP.mat'])
179                 delete(['v_loopTMP.mat'])
180                 disp(['No solution, loads model from previous simulation, continues with...
                         BHP error =  ',num2str((v_BHPguessUPD - v_Pactual)*1e-6),' MPa, and...
                         relative leak off error of ',num2str(v_QloRELchange),' l/s/l/s']);
181                 v_continue = 0;
182                 end
183               elseif v_convRemoval == 3
184                 v_continue = 0;
185                 disp(['No solution, continues with BHP error =  ',num2str((v_BHPguessUPD...
                         - v_Pactual)*1e-6),' MPa, and relative leak off error of ',num2str(...
                        v_QloRELchange),' l/s/l/s']);
186     end
```

```
187 if v_loopcounter > 1 %Save simulation with lowest pressure error:
188     if v_loopcounter == 2
189         v_minErr = abs(v_convergeQ(2,v_loopcounter)); %Save min error
190         copyfile('MESH','MESH_vloop','f');
191         copyfile('INCON','INCON_vloop','f');
192         copyfile('SAVE','SAVE_vloop','f');
193         save(['v_loopTMP.mat']);
194         save('MDEM_model_vloop.mat','MDEM_model');
195         save('TOUGH2_model_vloop.mat','TOUGH2_model');
196     elseif abs(v_convergeQ(2,v_loopcounter)) < v_minErr
197         v_minErr = abs(v_convergeQ(2,v_loopcounter));
198         copyfile('MESH','MESH_vloop','f');
199         copyfile('INCON','INCON_vloop','f');
200         copyfile('SAVE','SAVE_vloop','f');
201         save(['v_loopTMP.mat']);
202         save('MDEM_model_vloop.mat','MDEM_model');
203         save('TOUGH2_model_vloop.mat','TOUGH2_model');
204     end
205 end
```

Algorithms B.10: Well Coupling Algorithm, Shut-in: v_ShutIn.m

```
1     Outputvalues.Time_inj(i+1) = Outputvalues.Time_inj(i) + out_time;
2     Fracture_parameters.TimeStep = out_time;
3     Outputvalues.Element_pressure(i+1) = display_element_properties(TOUGH2_model,...
          TOUGH2_parameters.ElementName);
4     if abs(Outputvalues.Element_pressure(i+1) - Outputvalues.Element_pressure(i)) < 1e-6
5         TOUGH2_parameters.ConvergenceRelativeError = max(...
              TOUGH2_parameters.ConvergenceRelativeError/10,1e-9);
6     end
7     [rho_brine,k_brine] = TOUGH2_model.calculateFluidProperties(0);
8     TOUGH2_model.Fluid_compressibility = 1./k_brine; % Calulated according to Batzle and...
          Wang
9     TOUGH2_model.Fluid_density = rho_brine;          % Density of water
10    TOUGH2_model.Por = MDEM_model.Porosity;
11    Mass_balance.Fluid_mass_injected(i+1) = Mass_balance.Fluid_mass_injected(i)+...
          TOUGH2_parameters.GenerationRate*out_time;
12    Mass_balance.Excess_pressure(i+1) = sum(...
          TOUGH2_model.Delta_porosity_out_of_mass_conservation);
13    Mass_balance.TOUGH2_volume(i+1) = sum(TOUGH2_model.Por.*TOUGH2_model.Area);
14    Mass_balance.Fluid_mass_added_to_MDEM(i+1) = sum(TOUGH2_model.Fluid_density.*...
          TOUGH2_model.Por.*TOUGH2_model.Area) - Mass_balance.TOUGH2_Mass0;% + ...
15    Mass_balance.Mass_missing(i+1) = -sum(...
          TOUGH2_model.Delta_porosity_out_of_mass_conservation.*TOUGH2_model.Area.*...
          TOUGH2_model.Fluid_density);
16    Mass_balance.Borehole_Mass(i+1) = sum(TOUGH2_model.Fluid_density(TOUGH2_model.Tdom...
          ==2).*TOUGH2_model.Por(TOUGH2_model.Tdom==2).*TOUGH2_model.Area(...
          TOUGH2_model.Tdom==2));
17    Mass_balance.Mass_lost_from_borehole(i+1) = Mass_balance.Fluid_mass_injected(i+1)+...
          Mass_balance.Borehole_Mass(1)-Mass_balance.Borehole_Mass(i+1);
18    %Output to well coupling modules:
19    v_ΔLostMass = (Mass_balance.Mass_lost_from_borehole(i+1)-...
          Mass_balance.Mass_lost_from_borehole(i));
20    v_qleakoff_mass = v_ΔLostMass/rho0/out_time;
```

Appendix C

Literature Review

Appendix C is meant to provide the necessary understanding and overview of the different types of pressure integrity tests (chapter C.1) and their applicability for stress determination during drilling, as well as of recent and conventional XLOT theory and methods of interpretation (chapter C.2). Section C.2.3 gives a run-through of the theoretical framework of fracture mechanics in rock. The literature review was written by the undersigned as preparation for this thesis, as part of the semester report in TPG4520 at the Norwegian University of Science and Technology, 2013.

Appendix C Contents

C.1 Pressure Integrity Tests

Different terms are used in the literature, for the same procedures of pressure integrity testing. This is mainly due to the different nomenclature present within companies. Abbreviations often seen are FIT (formation integrity test), PIT (pressure integrity test) or LOT (leak-off test) and XLOT/ELOT (extended leak-off test).

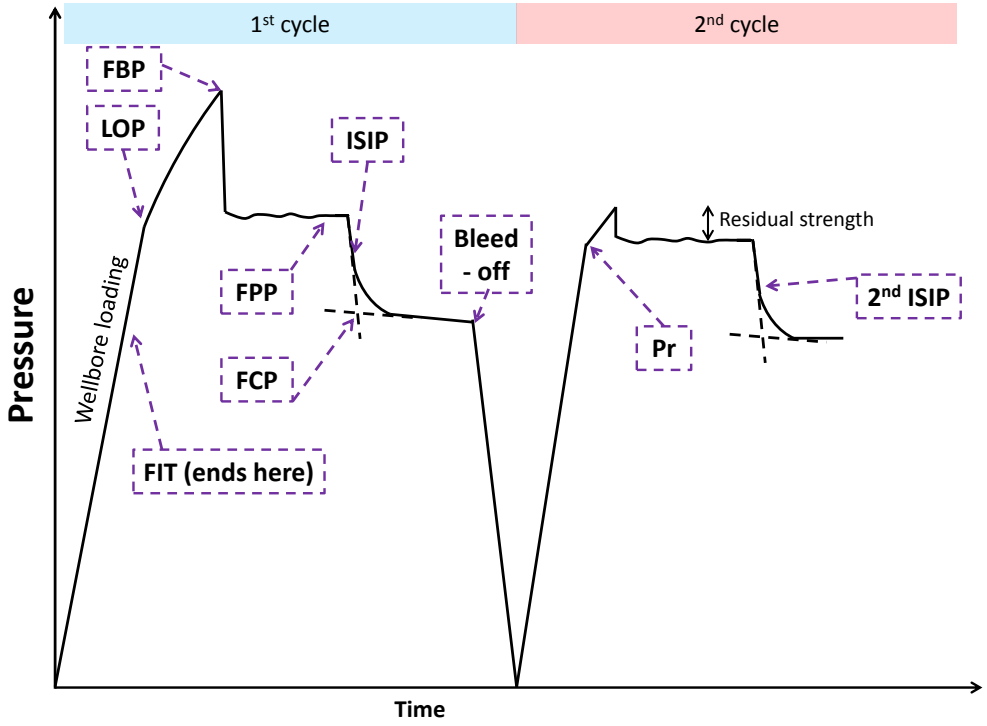

Figure C.1: Characteric pressure response of an idealized extended leak off test with two cycles (schematic plot).

The formation integrity test (FIT) is regularly performed during drilling operations, to verify casing shoe integrity and well stability for the subsequent section. After a section has been drilled and the casing has been run and cemented, the shoe cement is drilled out (around 10 meters) together with about three meters of fresh formation below the cement. The annulus is then shut, before mud is pumped into the well at a fixed rate, allowing pressure to build up in the open hole section. The test is performed without downhole packers, i.e. the entire drill string and annulus volumes are pressurized [11]. The procedure up to this point is similar for most downhole pressure tests performed while drilling, not only the FIT. The well is then steadily pressurized to a pre-determined level, ideally without initiation of a fracture and with the sole purpose to verify the cement shoe's integrity. As new formation is approached below the cement, the FIT consequently is used to confirm that the planned mud weight allows safe

drilling without leak off, thus avoiding lost circulation problems in the section. The pressure response of the FIT is shown in the early phase of Fig. C.1, where the FIT, as indicated, ends prior to deviating from linearity. The FIT preferred over the leak-off test at depths where the operator is confident in the local fracture gradient estimate.

The leak-off test (LOT/PIT) is a continuation of the formation integrity test, and is essentially a measure of the formation fracture gradient at depth in question. The borehole is pressurized until deflection from linearity is seen, i.e. that the rate of pressure increase declines. This point is marked as "LOP" (leak-off pressure) on Fig. C.1, and reflects the point where fluid starts to enter permeable paths somewhere in the system. Its significance is discussed in Chapter C.2.1.1, along with the leak-off test's limitations, development and relevance for stress determination. Although LOTs normally are terminated between the LOP and the formation breakdown point (FBP), some leak-off tests are run past the FBP, before pumps are shut off and pressure decline is monitored. At the FBP there is a sudden drop in pressure, which reflects the situation where system volume grows faster than what the pumps provide. Different variants of the LOT procedure exist, which are summarized in Table C.1.

Table C.1: Classification of pressure tests performed at the casing shoe (adapted from Addis et al. [1])

Pressure test	**Procedure**	**Value for Stress Determination**
Formation Integrity Test (FIT)	The test is run until planned maximum mud weight is reached but does not reach LOP	Little
Leak-Off Test (LOT)	The test is run beyond LOP (See Fig. C.1), and leak-off pressure is determined.	Poor
Leak-Off Test (LOT)	The test is run beyond LOP but shut-in before FBP and the pressure decline is monitored.	Poor
Leak-Off Test (LOT)	The test is run past point FBP (See Fig. C.1), and formation breakdown pressure is determined, then shut-in and the pressure decline is monitored.	Moderate
Extended Leak-Off Test (XLOT/ELOT)	The well is shut in well past FPB, and the pressure decline is monitored. Repressurization with shut-in one or more cycles is performed.	Good
XLOT with flow-back/Flow-Back Test [12]	Pumping is stopped well past FPB, and the pressure decline is monitored. Post shut-in, the well is allowed to flow back injected volume at rates regulated by a fixed choke. Repressurization, *without shut-in*, but with flowback one or more cycles is performed.	Good/Very good

The extended leak-off test (XLOT or ELOT) in its simplest form is a LOT which is repeated with two or more pressurization cycles. In an extended leak-off test the pumping is continued well beyond the FBP, as illustrated in Fig. C.1, where clear indication of fracture growth is observed in the pressure versus time plot. Pumps are shut off when pressure stabilizes at what is called the fracture propagation pressure (FPP), normally after a few minutes, where the pumping volume equals increase in fracture volume. When pumps are shut off, the pressure drops/equilibrates instantly, and the "Instantaneous Shut-In Pressure" (ISIP) is recorded. Also described as the point where the sharp pressure break after shut off starts decreasing gradually with time (See Fig. C.1), i.e. an inflection point. The fracture closure pressure (FCP) is the most important parameter recorded in the XLOT, and is obtained e.g. as shown in Fig. C.1, by intersecting the tangent lines of the immediate ISIP drop and the stabilized pressures as the fracture is believed closed. Both ISIP and FCP have been assumed to reflect the minor in-situ stress magnitude, but FCP is recognized as the best-known indicator [8]. The physical meaning of the FCP and ISIP response and how they differ is discussed in Chapter C.2.2.1. Pressure is then bled down, and two or more cycles are performed.

Pressure is normally recorded at surface and corrected to downhole pressure, as is done in FITs and LOTs (traditionally by manual reading 1-2 samples/min, but recently every 5s or

shorter by digital monitoring). A downhole pressure gauge is however preferred if high accuracy is needed, and can record pressure by memory every second ([13]) (e.g. as hydrostatic head of mud often is higher than the actual downhole pressure due to thermal expansion Addis et al. [1]).

A modification of the XLOT, where the shut in phase in the second and subsequent cycles is replaced by a phase of flowing back volume using a fixed surface choke, has shown to ease and improve interpretation of FCP under certain conditions. This approach is explained and discussed in Chapter C.2.2.2.

C.2 Literature Review

The key papers that have been given most emphasise in the review are

- Addis et al. [1], 1998: "A comparison of leak-off test and extended leak-off test data for stress estimation."
- Raaen et al. [12], 2001: "Stress determination from hydraulic fracturing tests: the system stiffness approach"
- Økland et al. [8], 2002: "The importance of extended leak-off test data for combatting lost circulation"
- Raaen et al. [13], 2006: "Improved routine estimation of the minimum horizontal stress component from extended leak-off tests"
- Gederaas and Raaen [6], 2009: "Precise minimum horizontal stress determination from pump-in/flowback tests with drilling mud"
- Couzens-Schultz and Chan [2], 2010: "Stress determination in active thrust belts: An alternative leak-off pressure interpretation"

Please be referred to the last two pages for a complete reference list.

C.2.1 The Leak-Off Test

The industry has in recent years, due to reasons briefly mentioned in the introduction (Ch.1), recognized how accurate stress data strengthen exploration and drilling planning, as well as planning to avoid completion and production problems. This has led to that the LOT, a test meant to assess casing integrity has been used beyond its original purpose, to determine the minimum horizontal stress [1].

Addis et al. [1] (1998) for the first time compared the use of leak-off test and extended leak-off test data for stress estimation. Data from the two areas, the North West Shelf of Australia and the Norwegian North Sea, were evaluated and it was found that the minimum in-situ stress estimates determined from XLOTs formed a lower bound to leak off pressure values in both areas. Fig. C.2 shows a scatter plot of leak-off pressure data from vertical wells in Oseberg, where the red line is the minimum stress gradient estimate from extended leak-off tests in the

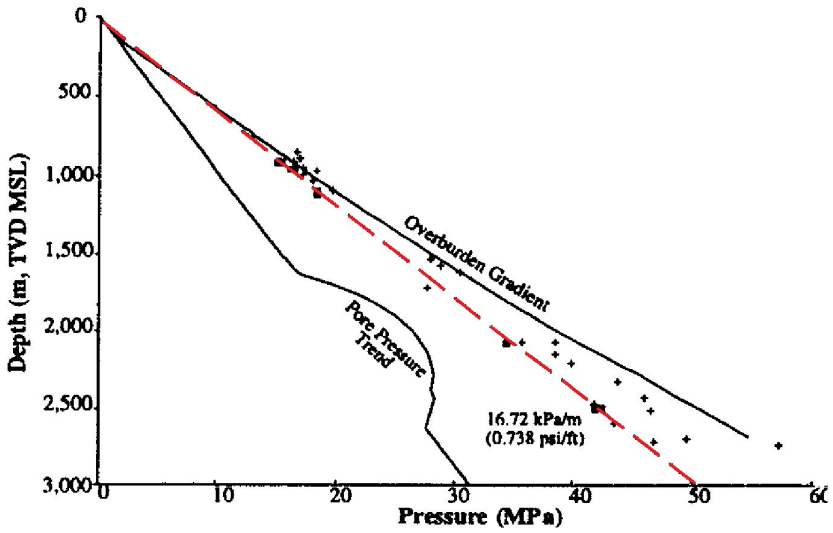

Figure C.2: Scatter plot of leak-off pressures from standard LOTs in vertical wells on the Oseberg field, North Sea (adapted from Addis et al. [1]).

same area. The XLOT is discussed in Chapter C.2.2. It was drawn that if a sufficient quantity of LOT data is available, such a set of LOTs can be used to estimate the minimum horizontal stress with sufficient accuracy, as well as to develop empirical correlations for further use in the area. The authors explain that this is probably due to presence of favourably oriented *pre-existing* fractures, which opens with pressures near the minimum horizontal stress (see Ch. C.2.3.2 on fracture initiation). They emphasize however, that the basinal approach should only be applied in absence of more reliable XLOT data. Their stress gradient estimates from basinal datasets in the Ekofisk field showed lower magnitudes than XLOT estimates in the same area. It was concluded that this was grounded in complexity of the Ekofisk formation, and as such that the applicability of the basinal approach depends on complexities such as near by salt diapirs or tight folds. Awareness must also be given to that the minimum horizontal stress is not a function of pore pressure and thus the gradient should not be extrapolated across or to depths with overpressure [1]. Use of correlations can be especially dangerous for reservoir sandstones if the formation pressure has been reduced by depletion [1].

Numerous papers have questioned the validity of the LOT as a stress determination test (e.g. [1, 8, 9, 11, 13]). Addis et al. [1] state major drawbacks of the LOT for stress determination to be

- its lack of procedure standards in the industry
- the limited understanding of the test's relevant mechanics and test artifacts as a stress determination test, which does not allow robust interpretation.

- that as fracture breakdown is highly dependent on rock properties such as permeability, fracture gradients can not be extrapolated across lithologies.

Most LOTs have traditionally been performed in low-permeability rocks such as shales, which generally have the highest fracture gradients [1]. In the absence of a perfect mud cake on the borehole wall, however, near wellbore pore pressure will increase when exposed to a greater well pressure during drill-out, thus the fracture pressure is reduced. The mechanism is part of what is referred to as poroelastic time effects, which is described in Chapter C.2.3.2.

C.2.1.1 Physical significance of the LOP

Addis et al. [1] refer to Postler [9] when further listing LOT properties that compromise and limit its applicability for stress determination: The leak off pressure (LOP) may not reflect fracture initiation, but rather be an artefact of casing expansion, leakage in casing cement, fluid compressibility, and pump rate. Doing only one cycle, the LOP can be dominated by tensile strength, near wellbore cracks (no contribution to the fracture initiation threshold from inherent tensile strength, as discussed further in Ch. C.2.3), instability due to rat hole over-gauge, or the presence of a plastic and unstable cone around the wellbore. Such a plastic cone can be reflected by a characteristic pressure versus time response, where the FPP is not constant, but rather has two distinct magnitudes: The lesser initially, due to a near well region of lower strength resulting from plastification[1] during drill out, followed by a higher FPP in the outer and unaffected elastic zone [9].

In addition to hoop stress, near wellbore effects include geometrical, thermal, chemical and poroelastic properties of the borehole wall, fracture toughness, sealing ability of the mud, as well as altered near wellbore pore pressure, all of which influence fracture initiation and can vary with depth and exposure time [8]. The ability of some drilling fluids to seal off the fracture tip and thereby add to fracture toughness i.e. the fracture propagation threshold pressure, is discussed in Chapter C.2.3.3 about fracture growth.

The list of different mechanisms that are influential on the LOP in varying degree is extensive, and explains the limited consistency and varying accuracy often seen in the literature when LOT applicability for stress determination is discussed. Many of the effects are however

[1] Plastic deformations/strains in a rock are permanent, i.e. not recovered to its initial state after unloading, as it is seen within limits of elasticity (within the "strength" of the rock). Plastic deformations promote borehole stability during drilling and production, and are included in stability models. In the context of this paragraph, the term describes breaking of cement bonds between grains near wellbore, which reduces the tensile failure threshold.

not directly influential on the minimum stress estimate from repeated cycles: These methods base their estimations on a far field pressure response, i.e. where borehole effects are less (if at all) influential, and not on fracture initiation as defined by linear elasticity theory (Chapter C.2.3.2). Some phenomena are however still relevant for improved interpretation of the test as a whole, especially for cases with uncharacteristic and unexpected pressure responses. Thorough understanding of the full picture may allow, and more importantly, trigger interest in, further development of the tests to yield additional and more information. Some phenomena will be described more in detail where relevant in later chapters when XLOTs are reviewed.

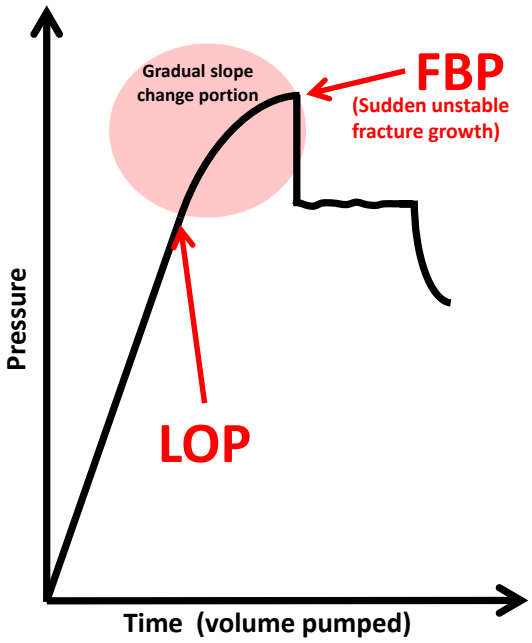

Figure C.3: Schematic plot of a typical LOT, starting with linear pressurization before a gradual slope change starts at LOP and continues until FBP.

Raaen et al. [13] discussed the conventional assumption that the LOP reflects fracture initiation. Specifically for some cases, where the slope of the pressure versus volume curve changes gradually between the LOP and the FBP, as highlighted with red in Fig. C.3, they argue that it does not reflect the creation of an hydraulic fracture, but rather is due to leakage upwards between cement/formation annulus. When cement sets, it shrinks, thus a micro annulus is formed between the formation and the cement. As the space is in pressure communication with the borehole, the annulus outer wall is pressurized during a pressure test, and will expand accordingly. Raaen et al. [13] proposed, based on simple theory of geometry and frictional losses, that such a channel can be sufficiently conductive to be consistent with the slope change in a pressure test. It can be questioned though, whether a void of this magnitude will allow filling with mud, and if not the response can come from other phenomena such as presence of a plastic deformation zone around the wellbore, which in theory can limit growth. Severe fluid lag into fracture may appear as stable growth as well. Gederaas and Raaen [6] illustrated with a field example how a cement conduit's presence can be proved by multiple pressurization cycles with flowback. The case is described in Chapter C.2.2.2.

Postler [9] stated that cement channels are the most common cause of unusual LOT behaviour, and presented three example cases where each was believed to indicate a specific type of channel; the characteristic pressure response of channels that are large and open, small and open, and a plugged channel. Postler highlighted the importance of multiple pressurizations to be able to distinguish between a channel and formation effects.

Raaen et al. [13] further illustrated utilizing field data and analytical equations, that even under favorable assumptions for well geometry, fluid and formation elastic properties, a stabilized fracture initiation cannot result in a gradual slope change as in Fig. C.3, due to its insignificant volume contribution. It is well known that the pressure needed to propagate a hydraulic fracture decreases with length of the fracture [8, 13], assuming that the fracture height is not limited by layers of higher stress magnitudes [5]. Thus, for the pressure to continue to increase after the leak-off point, i.e. assumed fracture initiation point, fracture growth has to be stabilized by stress concentrations induced by the borehole [13]. Other criteria are that the formation is linearly elastic, meaning a linear relationship between stress and strain, and that the horizontal stresses are anisotropic. A key point here is that all of the gradual slope change portion must be within fracture lengths where hoop stresses can influence and limit fracture growth, i.e. the volume is limited to a few borehole radii (see Fig. C.4 w/description), which is simply a too small volume as compared to what must be accounted for during the gradual slope change [13].

By the same argument, one cannot assign an increase in system compliance[2] responsibility for the gradual slope change: While the opening of a fracture in principle could add enough to the system compliance to be consistent with such gradual slope change, it is not possible to reflect the *initiation* of a new fracture. Recall that the volume injected during the gradual slope portion necessitates a fracture large enough to surely extend beyond the region of hoop stress influence, which again necessitates fracture breakdown/unstable fracture growth somewhere early in the gradual slope change portion (see Fig. C.3). The arguments collide, and thus cannot explain the slope change. Recognize that this applies for initiation of a fracture, while it is not the case for fracture re-opening, where unstable fracture growth is not a necessity and such a slope often is present [11]. By that, the work is in conjunction with the conclusion Addis et al. [1] had on the lower bound

Raaen et al. [13] concluded that for the LOP to reflect hydraulic fracture initiation, the slope change must be significant rather than subtle, which would mean no stable fracture growth de-

[2]System compliance [dV/dP] (inverse stiffness), with its different contributions and application for interpretation, is discussed in Chapter C.2.2.2.

scribed by the pressure/volume response in this early portion of the test (until unstable fracture propagation starts at point FBP shown in Fig. C.3). Stable fracture growth simply denotes a fracture volume that grows the same rate as the fluid injection rate, keeping the pressure in correspondence. Raaen et al. [13] emphasized strongly that pressure test data should be densely sampled to avoid misinterpreting a continuous slope change from start to FBP for linearity followed by a gradual slope change. Such a misinterpretation has been seen to trigger unnecessary remedial cement treatments with the objective to increase cement shoe integrity [9].

Note that Raaen et al. [13] do not exclude or argue against that a fracture is initiated or propagated at or around the LOP at a small scale, but rather argue that such an event in any case is not reflected by the gradual slope change portion often seen between LOP and FBP on a plot of pressure versus volume. Fracture propagation away from hoop stress influence is explained further in Chapter C.2.2.

On a general basis the LOP is not suitable for in-situ stress determination as it depends on a number of uncontrollable factors that are difficult to interpret. It cannot be assigned a clear physical explanation, and thus should not be used for stress determination. Consequently, the same goes for the use of individual LOTs [1, 8, 13].

C.2.2 The Extended Leak-Off Test

The extended leak-off test (XLOT/ELOT) is considered the most reliable method for estimating the minimum horizontal stress without the use of downhole packers [1]. It is a continuation and a refinement of the leak-off test by that it achieves the same objective as the LOT, but at the same time allows accurate stress estimations. By pressurizing the formation repeatedly, two or more cycles, it overcomes many of the limitations of a single leak-off test without taking significantly more time [1]. The test optimally approximates results from a hydraulic fracturing stress test, which is the ISRM recommended method for in-situ stress determination. The XLOT's advantage over the latter is simplicity and reduced cost, especially in deep wells [13]. By comparison it does not necessitate use of packers or a straddle arrangement to isolate the cement shoe and open hole section, and it comprises pumping the same fluid as used for drilling. Compared to water or brine used in hydraulic fracturing tests, non-Newtonian drilling fluids used in LOTS and XLOTS are more viscous and compressible and thus less ideal for robust stress estimation; a volume of 30-200 m^3 ([13]) of compressible fluid is typically pressurized in the well during an XLOT and has to be accounted for. In addition, the open hole length is

larger in such a test (≥3m) compared to around 1 meter in micro fracturing tests with packers [1], which increases the chance of encountering pre-existing weaknesses in the interval. Although, as will be discussed, these factors complicate the interpretation of XLOTS as compared to the ISRM recommended method, the test has shown to provide consistent and reliable in-situ stress estimates [1], and has been used in the industry for in-situ stress determination for over 20 years.

The fracture closure pressure (FCP), is the best-known indicator of minimum in-situ stress magnitude [1, 12, 8, 6]. In the exact moment the fracture closes mechanically, i.e. at the first touch of the fracture asperities, the fluid pressure will be in a state of equilibrium with the forces acting normal to the fracture surfaces to close the space. An accurate estimate of this magnitude requires that the fracture extends beyond the region of circumferential stress influence, also referred to as the "hoop" stress region in the literature. This is ensured in an

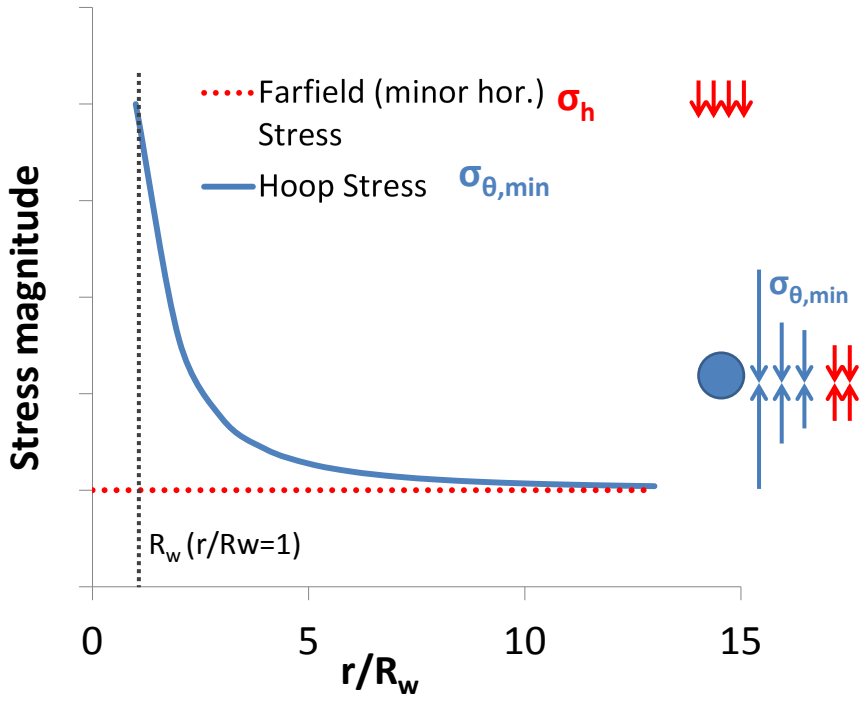

Figure C.4: Plot of hoop stress distribution as function of distance to borehole measured in number of borehole radiuses from its center, r/R_w.

XLOT by steadily pumping in fluid well beyond FBP until stable fracture growth is seen. Stable growth is identified by a stabilized pressure versus time response as shown in Fig. C.1, and is commonly achieved in the 1st or 2nd cycle, but subsequent cycles are often required to confirm consistency. This is illustrated in Fig. C.5, where four cycles were needed to prove stable

growth [5].

Fig. C.4 shows minimum hoop stress (circumferential stress) as function of increasing distance from the borehole wall of a vertical well in a formation following linear elasticity. It is a plot of the elastic hoop stress equation presented and explained in Chapter C.2.3, with anisotropy of $\sigma_h/\sigma_H = 3/4$. Recognize how the minimum hoop stress at the borehole wall converges towards the far field stress magnitude with increasing distance from the borehole, and how a significant part of the deviation is within only a few borehole radius lengths from the wall. When past this distance, only far field stresses add to threshold for further propagation.

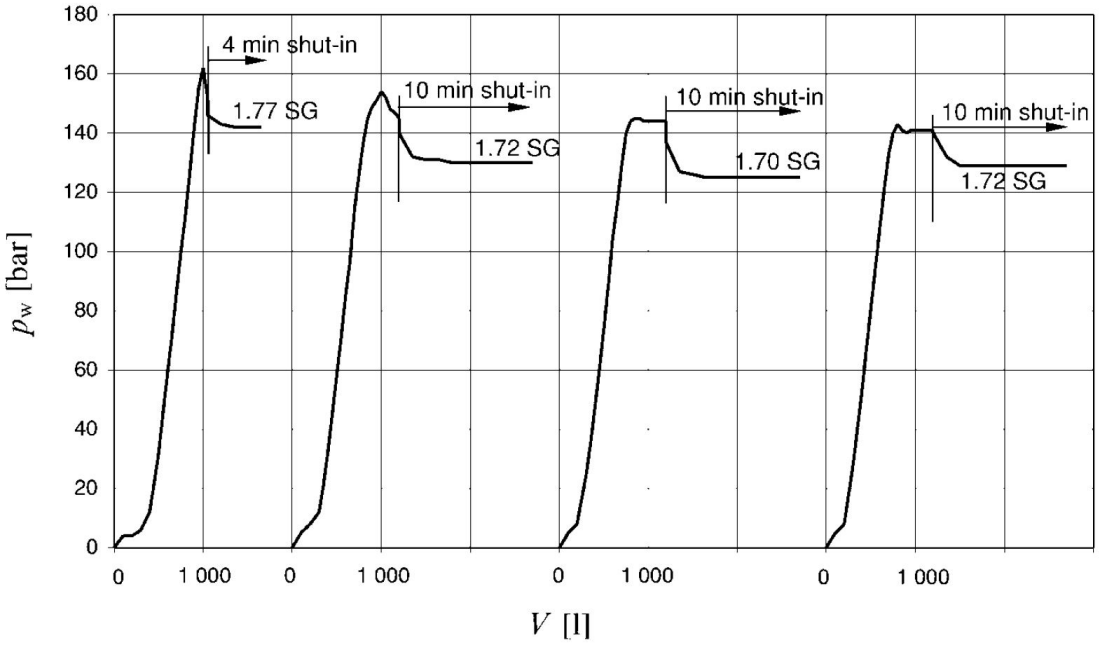

Figure C.5: Pump in phases of a four cycle XLOT from the field. Illustrating how stable fracture propagation can be observed by a stabilized pressure versus time response, here in the third and fourth cycle (Fjær et al. [5]).

After hoop stresses and (residual) tensile strength are overcome by ensuring stable fracture propagation in repeated cycles, an estimate of the minimum in-situ stress can be determined from the shut-in portion on a plot of pressure versus time. The approach requires that the pressure keeping the fracture open at the time of pump shut-off is allowed to decline by leak-off to the formation until the fracture is completely closed. The procedure and interpretation principles are based on those of minifracturing (minifrac) tests which have a rather standardized methodology natural to borrow. Minifrac tests are regularly performed as part of hydraulic fracturing jobs in reservoirs while isolated by downhole packers, where they yield accurate minimum in-situ stress estimates needed to optimize operational parameters for the treatment.

A problem emerges from the fact that such treatments are commonly performed in more permeable media and with newtonian fluids such as water and alcohol as pump-in fluid, whereas XLOTs commonly are performed in low permeability shales while drilling, and thus with fluids containing additivies to promote wellbore stability and cutting transport: The leak-off rate through the fracture surfaces may be insufficient for fracture closure, and the fracture may remain open throughout the test. The problem has manifested itself in field tests on the Norwegian continental shelf, where conventional XLOTs overestimated the minor horizontal stress by up to 20 bar ([10]). In some cases the data do not at all allow any interpretation to ascertain stresses. In both such cases a more recent and unconventional method can be applied, which allows the fracture to close by flowing fluid back to the surface instead of by percolation through the fracture surfaces. More specifically it comprises replacing the shut in phase of the second and subsequent cycles with a flow-back phase, which in addition reduces the total time of the test. A review of the approach, and how it differs from the conventional shut-in decline method with regards to principles and theoretical framework is explained in Chapter C.2.2.2 below. First it is constructive to go through the basic principles of shut-in test interpretation, and identify when and why its use is more limited in XLOT tests.

C.2.2.1 Determine σ_h from Shut-in Decline Analysis

As briefly mentioned in the introductory of different pressure integrity tests, the first deviation from a straight line after pumps are shut, denoted by the term "Instantaneous Shut-In Pressure" (ISIP), has been assumed to reflect the pressure at or near that of fracture closure. The undersigned recognizes how the abbreviations ISIP and FCP easily can be mixed, mostly due to the fact that the interpretation techniques and constituent nomenclature were developed for hydraulic fracturing tests. The fact is that ISIP loses much of its significance for stress determination when determined in XLOTs, whereas the FCP retains it. As such it is seen beneficial to explain their physical meaning, as well as to clarify the differences. Logically, both pressures can reflect fracture closure if near equal, but they are so only under certain ideal conditions; conditions more often seen in hydraulic fracturing tests than in XLOTs.

The word "instantaneous" in ISIP most likely describes the instant drop in pressure after pumps are shut, and to understand what happens physically it is helpful to first identify the governing pressure contributions in the fracture as it propagates. In conventional models (based on PKN or GDK), there are two governing contributions to the fracture propagation pressure:

- The pressure needed to overcome what acts to close the fracture: The minimum in-situ stress (i.e. the fracture closure pressure) and an excess pressure to maintain aperture.
- The pressure loss during pumping due to leak off and to the fluid's resistance to flow in the fracture (viscosity) [14].

In addition, as will be discussed more in Chapter C.2.3.3, there is a local net resistance needed to be overcome at the tip of the fracture. It consists of the resistance to open new fracture area at the tip (the fracture toughness), as well as a fluid lag effect and sometimes a local filter cake that isolates the tip and thus adds to the toughness. These have been observed in the field [14].

Of the contributions mentioned, only the pressure needed to keep the fracture open will ideally remain after pumps are shut. The others, being induced by pumping, immediately goes to zero, which is manifested by the characteristic drop at pump shut off. The excess pressure that allows the fracture to propagate, also called the net propagation pressure [12], can then be expressed as

$$P_{\text{net}} = P_{\text{fracture}} - \sigma_3 \tag{C.1}$$

It can be inferred that if assuming that P_{net} in Eq. C.1 is removed instantaneously after pump

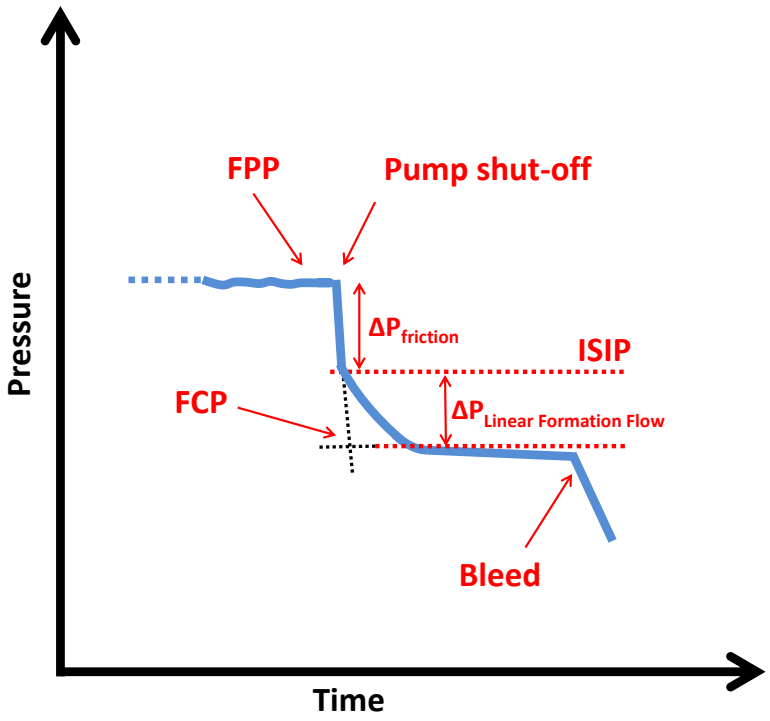

Figure C.6: Schematic plot of characteristic pressure versus time response for shut-in decline. ISIP, FPP, FCP, point of bleed and pump shut off are shown.

shut-off, then ISIP is a direct measure of the minimum in-situ stress. Note that this implies that ISIP and FCP are equal, and consequently that any additional pressure than what keeps the fracture surfaces apart (σ_h) is allowed to escape instantly. Although this is not seen in reality as it violates physical laws of mass, approximations are possible under certain conditions. Ideal parameters for small excess pressure are a small fracture volume and low viscosity pump-in fluid, i.e. parameters are not often seen in XLOTs. Conversely, one of the main goals of repeated cycles in XLOTs is to stably propagate a long fracture, and hence there will be a significant fluid volume in the fracture at ISIP which needs to be leaked off to the formation to get an accurate FCP. Fig. C.6 shows a plot of pressure versus time schematically for the shut-in decline portion of an XLOT, and the pressure needed to reach FCP is here indicated $\Delta P_{\text{Linear Formation Flow}}$. Another phenomena speculated is that of whether or not the excess pressure sometimes may be reduced by further fracture propagation post pump shut-off ([14]).

Although hydraulic fracturing tests are inherent of some of the ideal properties such as a low viscous fluid, a situation where the pressure stabilizes at ISIP would not be yearned because that would normally imply a too low formation permeability to allow flow regimes to properly describe the fracture closure process, and even more importantly to allow after closure radial flow analysis. The more detailed fracture behaviour analysis by characteristic flow regimes is facilitated by the use of low viscosity fluids and zonal isolation by packers. In conventional

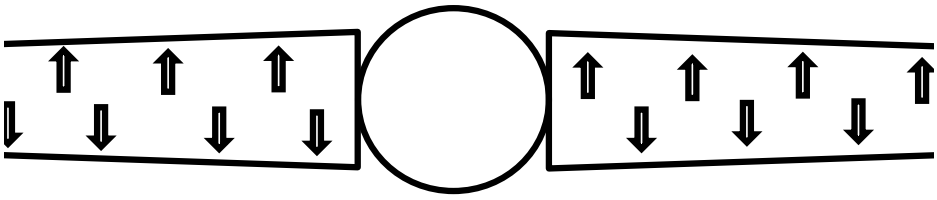

Figure C.7: Illustration of formation linear flow from a fracture.

fracture diagnostic testing based on transient analysis, four successive flow regimes are searched during shut in: Early fracture linear flow (storage effects), bilinear flow (simultaneous formation linear and fracture linear flow), formation linear flow (see Fig. C.7) and pseudo radial flow (formation radial flow after closure). Early fracture linear flow describes an *instantaneous* flow in the fracture due to decompression of fluid, i.e. fracture "unloading", and stabilized at ISIP. The transitional bilinear period will normally for a shut in test be too short to yield any data. Formation linear flow then follows, i.e the leak off part as the fracture closes, as illustrated in

Fig C.7. After closure, if the pressure transient is transmitted fast enough, a pseudo-radial flow regime will govern, which can yield transmissibility and pore pressure information [3].

Every regime has its own fingerprint described by pressure transient analysis. In high permeability formations, hydraulic closure is thus confirmed by radial flow analysis and determined with high accuracy from the intersection between formation linear and radial flow extrapolations, whereas in low permeability formations, it cannot. This is where ISIP has found its meaning for stress determination: When a sharp pressure drop was seen followed by stabilization it was anticipated that the fracture would not close due to poor permeability, and consequently that the FCP and the more important data for post closure analysis could not be determined and the test was stopped. As a remedial action, ISIP was derived from the two linear slopes, (mark that the transition between linear flow regimes then roughly is the first deviation from the instantaneous drop on a Cartesian plot, and not the intersection shown in Fig. C.6), knowing that it was an overestimate of the minimum in-situ stress. A point to be noted is that the over-estimate is likely to be even higher when viscous fluids are used.

For XLOTs it is implicit that the permeability is of magnitudes classified as low in the above context, either because of a mud cake, or the formation itself. The rate of leak-off will then decrease, while the pressure needed leaked off, i.e. $\Delta P_{\text{Linear Formation Flow}}$ in Fig. C.6 remains. Given that it is reliably ascertained from pressure time data, the ISIP can act as an upper limit approximation to the minimum in-situ stress, but the FCP is always a better indicator. As shown on Fig. C.6, the FCP can be approximated by intersecting the tangent lines of the instantaneous drop with that of the stabilized pressures as fracture is believed closed. Other plotting techniques such as logarithmic plots, g-function plots, and the mentioned square root of time plots are used to ease interpretation [6].

Flow regime analysis as described in the previous paragraphs has thus partly been transferred to XLOT interpretation of FCP, but as may be inferred, the post closure transient analysis is not utilized and there is uncertainty in when and if the fracture is actually closed. The latter is a result of that fracture closure is not an instant event, but rather a gradual process not easily described by conventional well testing methods [12]. On a Cartesian plot of pressure versus square root of time, the phase of linear flow (percolation) through the fracture surfaces after pump shut off will yield a straight line, and FCP is generally interpreted at a first deviation from this slope. As closure does not happen instantly, and as no other flow regime follows, the first deviation is merely the start of a fracture closure process, and not a measure of the equilibrium

pressure at closure. This is evident from the lack of a sharp drop in pressure which would be expected if the fracture saw instantaneous mechanical and hydraulic closure at the point where linear flow ends. Instead, typical behavior at this point is either an increase or a decrease in slope ([12]), as illustrated in Fig. C.8.

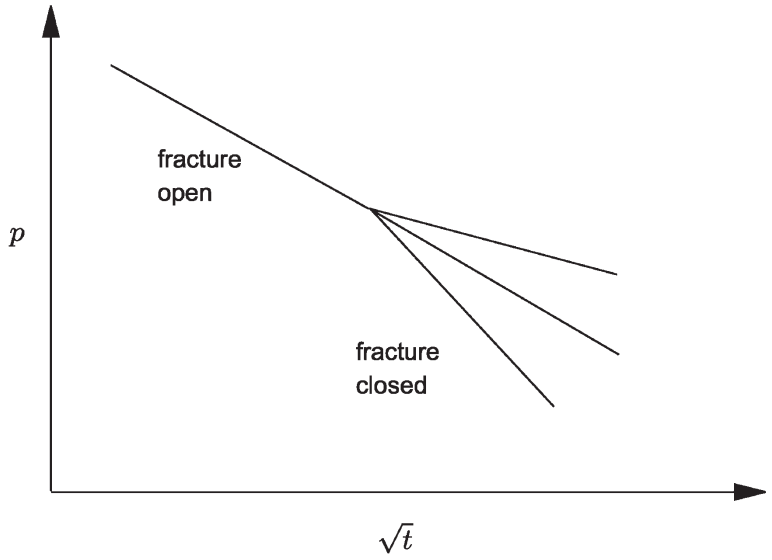

Figure C.8: Schematic plot of pressure response versus square root of time, and how the deviation can either increase or decrease depending on which mechanisms govern decline response at closure, - change in system stiffness or leak-off rate (from Raaen et al. [12]).

Raaen et al. [12] proposed that the pressure response at closure can be described as function of two mechanisms:

- an increase in system stiffness, corresponding to slope increase (towards well fluid stiffness), as shown in Fig. C.8
- a decrease in fracture leak-off rate, corresponding to slope decrease as shown in Fig. C.8

The concept of system stiffness is thereby introduced, which will be discussed more in the following subchapter. The approach, as it relates to shut-in decline interpretation, is based on the theory that closure ideally is a two stage process, where in the first stage the fracture length and height is constant while width decreases, followed by a stage where the fracture starts to close at the tip and then gradually closes in towards the wellbore wall [12]. The decrease in leak-off rate thus relates to stage two, where the conductive fracture length closes in. The stiffness of the system is assumed constant when length and height is constant during the first stage, and as stage two is starting the stiffness will increase. The two mechanisms can as such be said to compete to change the slope on pressure versus square root of time when describing

final closure, and as a result it is difficult to predict or interpret its exact point [12]. A question is also raised whether final closure is ever actually achieved during shut-in decline in impermeable formations.

Consequently, as only an accurate fracture closure pressure equals the minimum in-situ stress, the conventional shut-in decline analysis provides limited possibilities for accurate minimum in-situ stress estimates when performed in low permeability formations. Note that this statement applies when low viscosity fluids are used as well, however to a lower extent as the leak-off is more likely to dominate the pressure response. In permeable formations the fracture will close, but shut-in decline analysis may still prove inefficient if a filter cake[3] forms on the fracture surface as fluid linearly percolates through it [6, 12]. Upon it stops growing, the filter cake then may prevent the pressure front to diffuse into the formation, and the pressure will slowly increase behind the cake. Fluid still percolates through the cake, and the fracture may close, but flow is now dominated by the cake and not the formation, thus the pressure versus square root of time response is invalid [12]. Raaen et al. [12] utilized the system stiffness concept to describe this process analytically, and were able to derive an interpretation method that corrects for mud cake effects and thereby re-validates otherwise disregarded data from conventional methods. Raaen et al. [13] stated that an increasing fracture closure time by leak-off from cycle to cycle is typically explained by high formation permeability and the forming of a filter cake.

The applicability of conventional shut-in decline analysis to determine σ_h with *reasonable* accuracy from XLOTs, can be summarized to be limited to cases where

- the major part of the fracture length is outside the influence of hoop stresses at the time of closure, i.e. that closure is governed by far field stress and not hoop stress.
- the shut-in decline corresponds to a linear flow regime as described by transient pressure propagation analysis, which requires that
    - the rock has sufficient permeability to allow fracture closure by fluid percolation through its surfaces.
    - the rate of percolation is not altered or limited by the creating of a mud filter cake built on the fracture surfaces.

[3] A filter cake refers to the layer of particles left in the entry of a permeable path when a mud have filtered through it, decreasing the path's ability to conduct fluid.

For tighter rocks and cases where mud cake issues invalidates interpretation, evaluation of system stiffness with time is recommended by flowing back volume after fracture propagation. Thereby the fracture is allowed to close, and the interpretation does not require any high leak-off to the formation, rather the opposite. The concept of system stiffness and monitoring flow-back volume is not new to hydraulic fracturing tests where low viscosity fluids are used. Most flow-back interpretation schemes are however derived to monitor pressure versus time, where flow back rate is kept constant. The following subchapter reviews an approach dedicated to XLOT conditions.

C.2.2.2 Determine σ_h from Flow-Back Tests: The System Stiffness Approach

Raaen et al. [12] (Statoil ASA) presented the System Stiffness Approach in 2001, which is a unified model of pump-in/shut-in and pump-in flowback tests that is equally useful when high viscous drilling fluids are used, as with water. The method comprises evaluation of how system stiffness changes with time as the injected volume is flowed back to the surface and the fracture closes. The procedure is basically a simplification of the conventional shut-in decline analysis, as it replaces the shut-in decline in cycle two and subsequent cycles with flow back through a fixed surface choke. Shut-in decline in the first cycle provides an upper estimate of fluid-leak off volume, to which the approach is very sensitive. It will furthermore promote creation of filter cakes, which again may allow use of the approach in formations of initially too high permeability. Note how this differs from the conventional methods, where transient analysis requires high leak-off to facilitate interpretation.

Recently it was recommended that a three minute shut-in period should be included after each flow-back period to check for pressure rebound [6]. Rebounds are common to be observed in low permeability formations ([1, 11]), and is indicative of that fracture closure has not followed a two stage process as described above, but rather a cutting near wellbore closure during stage one, leaving trapped fluid in the fracture. For the system stiffness approach it is, as will be explained, a necessity that the assumption of a two stage closure process is somewhat correct.

Flow-back through a fixed choke, as compared to tests with a fixed rate, is an advantage especially for small flow-back volumes where rate can be hard to maintain [12]. In addition, because there is a simple relation between the flow rate through a choke and its pressure drop, new plotting techniques can be derived to yield a more accurate FCP. Given that it is known how the total system stiffness changes with time, and how volume changes with time, then the

pressure development with time can be predicted with Eq. C.2.

Statoil ASA, a Norwegian operator company, has had the approach implemented as part of their XLOT standard since 1999 [6]. They propose that it should be an industry standard, both in impermeable formations as well as in permeable formations. Several papers have been presented over the years, where they share their experience with the approach for minimum in-situ stress estimation, e.g [6, 8, 10, 11, 12, 13]. Raaen et al. [12] presented positive results for permeable formations with mud, and Raaen and Brudy [10] showed that the approach should be preferred in tight formations, where conventional methods overestimate in-situ stress by 20 bar [10]. In the following, some experiences from the papers will be reviewed, preceded by the main elements of the theory behind the approach.

The System Stiffness Approach

☞ System stiffness, S, can be defined as the change in pressure per change in volume content in the system ([12]), expressed

$$S = \frac{\mathrm{d}p}{\mathrm{d}V} \tag{C.2}$$

The system compliance, which is the inverse off stiffness, has two contributions:

- the borehole compliance
  - dominated by fluid compressibility
  - negligible contributions from borehole and casing expansion
- the fracture compliance when a fracture is open and hydraulically connected to the system

While the borehole compliance is dominated by fluid compressibility and is near independent of well pressure level, the fracture compressibility is strongly dependent on fracture length. It is therefore extra important in this approach to create a long enough fracture to obtain a significant difference between system compliance with an open and a closed fracture, i.e. that the fracture stiffness is low enough at closure. Other criteria for stress determination by direct measurement of system stiffness include that the surface controlled flowback rate is dominating the leak-off rate, to maintain volume control, and of course that pressure and volume are recorded [12]. The fracture stiffness, S_f for a non-propagating fracture of half length R, is

$$S_f = \frac{\mathrm{d}p}{\mathrm{d}V} = \frac{3E}{16R^3(1-\nu^2)} \tag{C.3}$$

where E is Young's modulus, v the Poisson's ratio. The fracture stiffness is, as clear from Equation C.3, constant at stage one of a fracture closure process if a two stage closure process is assumed (see previous subchapter). An illustration of a typical pump-in/flow-back cycle is shown in Fig. C.9, and is useful to help understand the principles of recording volume vs pressure. The early straight line during pump-in is due to (well) stiffness from fluid compressibility

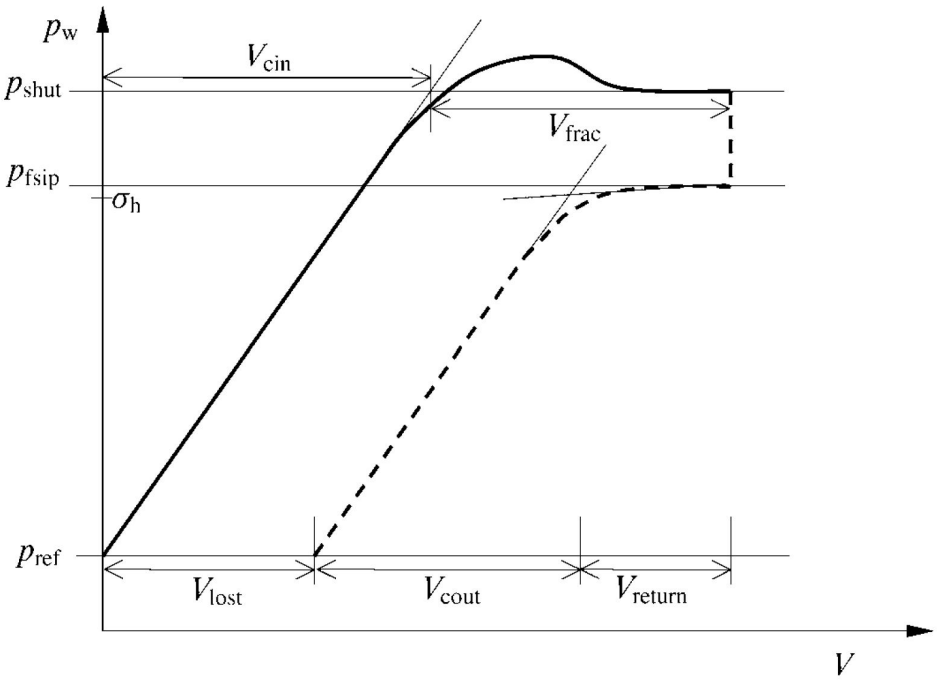

Figure C.9: Illustration of a typical pump-in/flow-back cycle with different volume recordings (from Fjær et al. [5]).

and wellbore effects, thus V_{cin} is a measure of the total compression. This is an important quality control of the test: The predicted slope can be compared to the observed slope, and thereby confirm assumptions or estimates of the system stiffness without an open fracture. Additionally, it can help reveal leaks in the casing shoe, where a smaller observed stiffness as compared to predicted would be expected [6]. The next volume point is V_{frac}, which is the change in volume since V_{cin}, i.e. it is the volume spent to create the fracture. Similar to in conventional methods, this volume can indicate whether the major part of the fracture extends away from hoop stress influence (Ch. C.2.2), but the length is as mentioned furthermore important here to induce a contrast in system stiffness at closure. At pump shut off, a sharp pressure drop is seen just as in conventional methods, and p_{fsip} is recorded. Recall that in the previous subchapter, it was stated that the ISIP loses much of its meaning for stress determination in XLOTs. Økland et al. [8] proposed that it instead can provide data to be derived for fracture geometry estimates, given that the minimum stress already is obtained. Please be referred to the paper for the derivations.

Following this is the flow-back phase, where the volum is subtracted from the total pumped volume. The change in system stiffness is used to derive the minimum horizontal stress as indicated by the intersecting tangents in Fig. C.9. This denotes the first plotting technique of the approach.

After closure, a straight line corresponding to the decompression of well fluid is seen until all the volume is flowed back. The corresponding slope and change in volume, V_{cout}, should thus be equal to the well loading line, given that the assumption of constant mud compressibility applies. The total leak-off volume V_{lost}, and the return volume, V_{return} is then measured directly. [12] found it useful for the interpretation to distinguish between mechanical and hydraulic fracture closure, where point of mechanical closure denotes the first touch of the asperities on the fracture surfaces, and the hydraulic closure correspond to when the fracture is no longer conductive. This implies that the mechanical closure pressure never can be lower than the hydraulic closure pressure. Mechanical closure best represents the minimum in-situ stress [12], because it is at this equilibrium the in-situ stress is transferred to the well pressure. In a conventional interpretation plot of pressure versus square root of time, the slope at the start of the closure process may, as discussed in the previous subchapter, either decrease or increase, where an increase in slope is due to increase in system stiffness due to mechanical closure. This is why it is difficult to find the exact point of mechanical closure with this method, and also where the system stiffness approach finds its edge:

The essence and advantage of the system stiffness approach is that the point of mechanical closure can be isolated in a different plot of system stiffness during closure. The plotting technique is facilitated by how the flow rate through a fixed choke relates to its pressure drop [12],

$$\frac{\mathrm{d}V_{\text{flow-back}}}{\mathrm{d}t} = c_1\sqrt{p(t)_{(\text{upstream pressure})} - p_{(0)}} \tag{C.4}$$

where c_1 is dependent on fluid properties and choke setting and can be assumed constant given that fluid density is constant. The upstream pressure is the pressure at time t during flowback, and the downstream pressure, p_0, is the pressure to which the choke is fixed. When multiplying with S (Eq. C.2) on both sides, and integrate with respect to time and then solve for upstream pressure, Eq. C.5 can be formulated,

$$p(t)_{(\text{upstream pressure})} = (\sqrt{p(0) - p_0} - \frac{Sc_1}{2}t)^2 + p_0 \tag{C.5}$$

Then Eq. C.5 is rearranged and solved for the square root of pressure recording at the choke, also referred to as topside pressure, to yield

$$\sqrt{\text{topside pressure}} = \sqrt{p(t) - p_0} = c_2 - \frac{Sc_1}{2}t \tag{C.6}$$

From Eq. C.6 it is clear that when system stiffness (S) is constant, a straight line will be observed on a plot of square root of topside pressure plotted versus time, as well as when when dp/dt is plotted versus time. The system stiffness will be straight during stage one of the closure stage process, as well as from the point in time where the fracture is hydraulically closed. According to the system stiffness approach, the point of mechanical closure can then accurately determined as the intercept of these two lines.

A field example, reproduced from a recent paper by Gederaas and Raaen [6], is helpful to show the simplicity and advantage of the approach. An XLOT was performed in a tight formation at 3500 m depth in a vertical well. 1.5 meter fresh formation was drilled below a 10 m long shoe track. The pump-in fluid was oil based mud (OBM). There was no sign of leak-off in

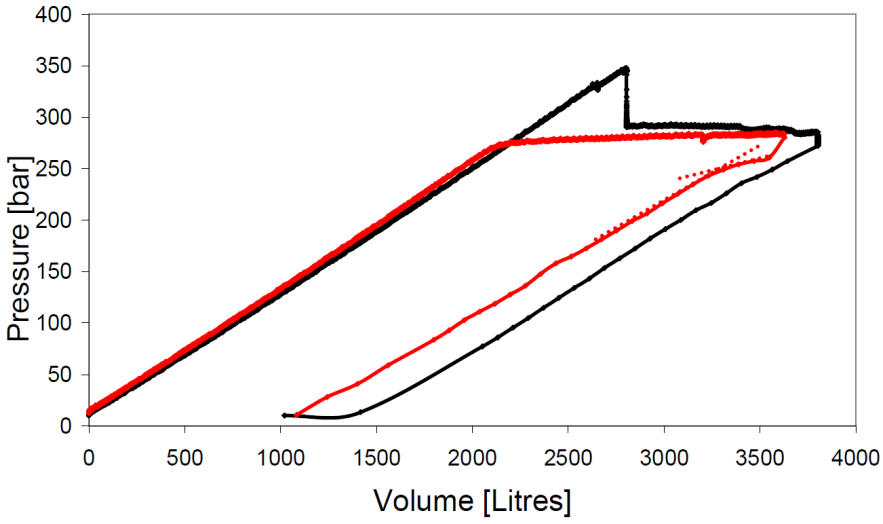

Figure C.10: Plot of surface pressure versus system volume from a field test example. The black line is recordings at cycle one, and red line cycle two. (from Gederaas and Raaen [6]).

until FBP at 345 bar, and stable fracture growth was established right after. No pressure drop was seen at fracture reopening, and the stable fracture propagation pressure, FPP, was consistent with that of the first cycle. The test consisted of only two cycles. Fig. C.10 shows surface pressure plotted versus system volume of the two cycles, the first cycle in black and the second in red color. In cycle two clear change in system stiffness was observed, and tangents marked

by dashed lines indicated (mechanical) FCP of 250 bar. Conventional shut-in decline analy-

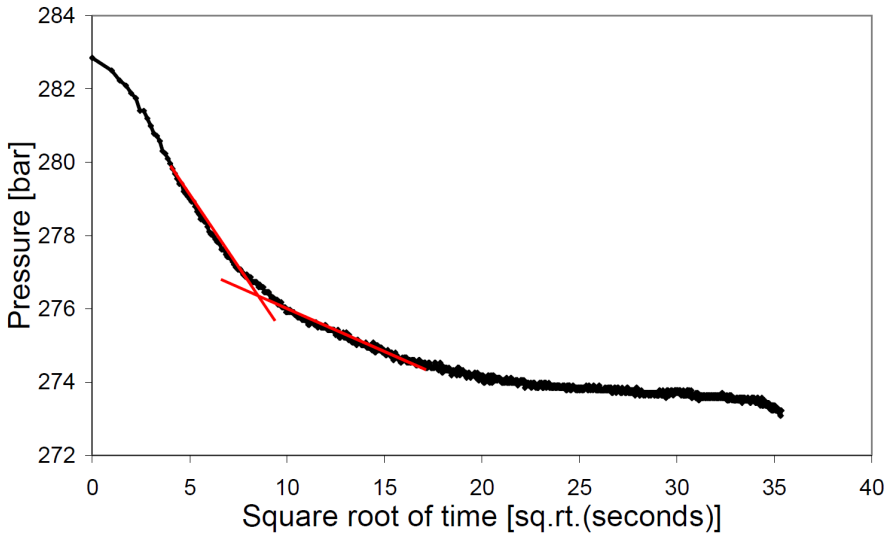

Figure C.11: Plot of pressure versus square root of time of shut-in decline period in cycle one (from Gederaas and Raaen [6]).

sis of pressure versus square root of time of cycle one data is shown in Fig. C.11, where the intercept of tangents was concluded to indicate FCP of 275-280 bar. A plot of square root of pressure versus time during flow-back of cycle two is shown in Fig. C.12. It showed two clear straight lines corresponding to constant system stiffness, which indicated agreement with the assumption the approach is based on, - that closure is a two stage process. The tangents were extrapolated and the intercept interpreted to 250 bar, i.e. it confirmed the estimate ascertained from the plot of surface pressure versus system volume. Gederaas and Raaen [6] concluded that the system stiffness approach placed the minimum in-situ stress magnitude at least 25 bar below the estimate from the conventional technique.

Challenges of the system stiffness approach relate, as with all other techniques, to when the assumptions on which it is derived is not sufficiently fulfilled. The most essential condition is that the flow-back rate is much larger than the fluid loss to the formation. As evident from experience presented in the papers by StatoilHydro, the condition is often fulfilled by either a tight formation, or the forming of a filter cake in permeable formations. The latter is not always achievable and in such cases, where also the shut-in response has been made ambiguous by the filter cake, an alternative use of the stiffness concept may be applied [12].

Situations may as previously discussed occur where the fracture is cut off near the well during in the first stage in the assumed two stage closure process. This leads to that the fracture

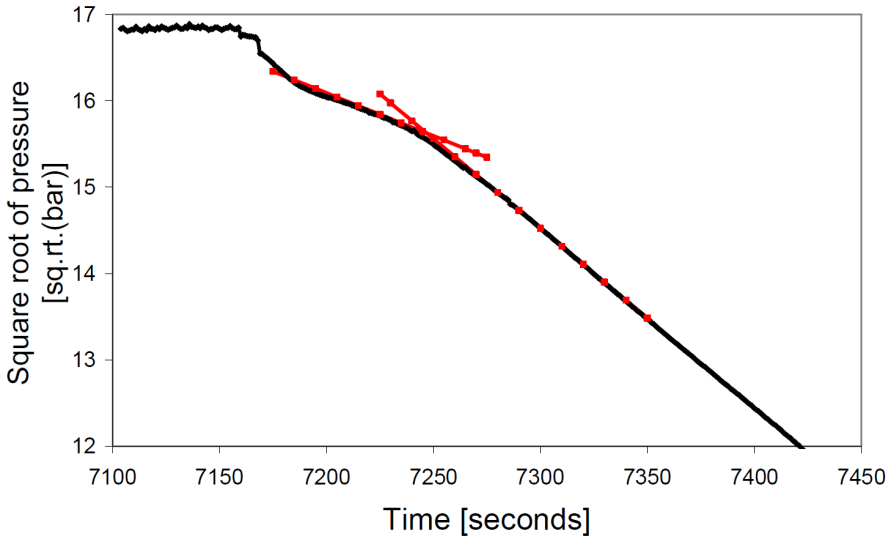

Figure C.12: Plot of square root of pressure versus time of during flow-back of cycle two. (from Gederaas and Raaen [6]).

stiffness face a sudden and sharp increase. Fracture closure is then not observed at the expected level, and the estimate is invalid [13]. It is clear from Equation C.3, that the fracture stiffness is highly dependent on the length. Cut off of the conductive path is promoted by if the fracture had to turn as it propagated outside hoop stress influence, as a result of unfavorable well inclination and azimuth (and how these relate to hoop stresses) [6]. Fracture rotation may also be an issue, which is possible at high pump rates [1].

If the integrity of the casing shoe is poor, the system stiffness approach may be ineffective for stress determination. A conduit in the cement can allow a fracture to initiate somewhere above the shoe, and make flow-back interpretation difficult. Gederaas and Raaen [6] presented a clear indication of this, where a 4 cycle pump in/flow back test in an impermeable formation showed some curious variations in minimum in-situ stress as compared to from a near by well. Clear indication of fracture growth was seen in all four cycles. The interesting thing was that while the nearby well estimated σ_h to be 1.55 sg, the lowest estimate of this well was 1.9. Gederaas and Raaen [6] do not reveal the test's conditions, such as if there were any time delay between drilling and pump-in and change in pump rate etc., but state that the test conditions were similar. The explanation served was that it had to be due to poor coupling between well and fracture. Such a small conduit will add a high frictional pressure drop, and thus the bottom hole pressure can be significantly higher than the pressure in the fracture situated somewhere above the conduit. When pumps are shut and flow back initiated the conduit may be resistant to allow flowing back volume leaving the pressure volume response dominated by wellbore

storage effects, i.e. a lower stiffness than what was inferred. This reveals how the pump-in/flow-back stiffness can be used as a tool to reveal poor cement integrity.

The use of the system stiffness approach to determine σ_h accurately from XLOTs, can be summarized to be optimal when

- the formation permeability is low, e.g. in shale, tight sand
  - Although possible to bullhead a high viscous pill, it involves risk of not achieving any interpretable test data: A partial mud cake may allow neither the shut-in nor flow-back technique to be utilized. Should be considered if shut-in is invalidated by filter cake forming
- the well is vertical, or horizontal with favorable azimuth
  - To minimize risk of near wellbore fracture cut off during closure.
- the fracture created is large (long) and extends far from the well
- the depth investigated is not closely confined in height
  - A long fracture with limited height infers high stiffness, and closure may be hidden due to lack of contrast [6].
- where cement shoe integrity is good [6]
  - May assist diagnostically by that it recognizes cement channel in the quality control of pump-in compliance/flow back compliance.
- there is no gas in the system

C.2.3 Theoretical Framework: Fracture Mechanics as it Relates to XLOT Interpretation

For better understanding the discussion of procedures and interpretation, as well as for the sensitivity study, it is beneficial to go through some basic theory of the mechanics in hydraulic fracturing.

C.2.3.1 Stress Distribution Around a Borehole

Consider a vertical borehole penetrating a tectonically relaxed saturated formation with anisotropy in the horizontal plane, i.e. $\sigma_v > \sigma_H > \sigma_h$. The borehole wall is assumed impermeable, either

due to a perfect mud cake formed during drilling or an ideal impermeable rock, resulting in a near well pore pressure unaffected by well pressure *during* pressurization towards fracture initiation.

The elastic stress distribution around the borehole is described by the "Kirsch equations"[4].These stresses are generally higher in magnitude than the far field horizontal stresses as they quantify the effect of the load that was previously carried by the drilled out rock. Equations evaluated in this report are limited to those relevant for stress determination tests by fracturing in a vertical well aligned with the maximum principal stress direction. The following equations are summarized from Fjær et al. [5] (2008). For the full set of general elastic equations, please be referred to the fourth chapter of the book.

Under the mentioned assumptions and expressed in polar coordinates, the stresses in the horizontal plane at a distance r from the center of a bore hole with radius R_w are

$$\sigma_r = \frac{\sigma_H + \sigma_h}{2}\left(1 - \frac{R_w^2}{r^2}\right) + \frac{\sigma_H - \sigma_h}{2}\left(1 + 3\frac{R_w^4}{r^4} - 4\frac{R_w^2}{r^2}\right)\cos 2\theta + P_w\frac{R_w^2}{r^2} \tag{C.7a}$$

$$\sigma_\theta = \frac{\sigma_H + \sigma_h}{2}\left(1 + \frac{R_w^2}{r^2}\right) - \frac{\sigma_H - \sigma_h}{2}\left(1 + 3\frac{R_w^4}{r^4}\right)\cos 2\theta - P_w\frac{R_w^2}{r^2} \tag{C.7b}$$

$$\sigma_{r\theta} = -\frac{\sigma_H - \sigma_h}{2}\left(1 - 3\frac{R_w^4}{r^4} + 2\frac{R_w^2}{r^2}\right)\sin 2\theta \tag{C.7c}$$

where σ_θ is borehole circumferential stress, σ_r radial stress, $\sigma_{r\theta}$ tangential shear stress and P_w the well pressure. θ is measured relative to the major horizontal stress, σ_H. The different variables in Eqs. C.7 are illustrated relative to each other and the borehole in Fig. C.13. At the borehole wall, where fracture initiation will take place, $r = R_w$, and Eqs. C.7 reduce to

$$\sigma_r = P_w \tag{C.8a}$$

$$\sigma_\theta = \sigma_H + \sigma_h - 2(\sigma_H - \sigma_h)\cos 2\theta - P_w \tag{C.8b}$$

$$\sigma_{r\theta} = 0 \tag{C.8c}$$

[4]E. G. Kirsch (1898, Die Theorie der Elastizität und die Bedürfnisse der Festigkeitslehre) first derived formulas describing the distribution of elastic stress around a circular opening in an infinite plate due to one-directional tension. The formulas were later generalized to describe stresses near a borehole in an anisotropic stress field, also known as the Kirsch equations [5].

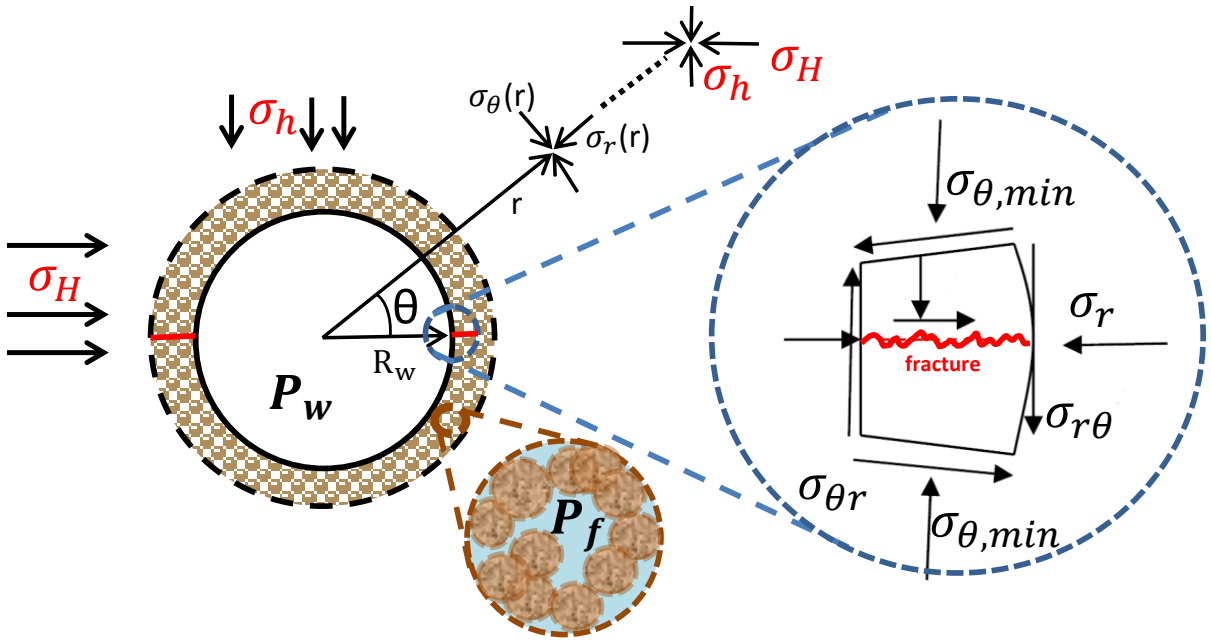

Figure C.13: Schematic overview of a borehole cross section as a fracture initiates in its wall. The borehole is vertical, aligned with major principal stress σ_v. Un-equal far field stresses.

C.2.3.2 Fracture Initiation Criteria

A fracture will initiate when the circumferential Terzaghi[5] effective stress, σ_θ', at the borehole wall equals the rock tensile strength, T_0, constituting the criteria for tensile failure

$$\sigma_\theta - P_f \leq -T_0 \tag{C.9}$$

The fracture will naturally initiate in the direction of least resistance, which is where the circumferential stress has its minimum value. With anisotropic stresses, σ_θ ranges from maximum to minimum value in the direction of σ_h at $\theta = 90^o$ and direction of σ_H at $\theta = 0^o$, respectively. The fracture will have two wings in symmetry across the borehole, both perpendicular to the least minimum stress. Please be referred to Fig. C.4 for a plot of minimum hoop stress, i.e. Eq. C.7b with $\theta = 0$, as function of distance to the borehole. With $\theta = 0^o$, Eq. C.8b reduces to

$$\sigma_{\theta min} = 3\sigma_h - \sigma_H - P_w \tag{C.10}$$

[5]Dr. Karl Terzaghi, introduced the effective stress concept in 1923. "All the measurable effects of a change in stress, such as compression, distortion, and a change in shearing resistance, are exclusively due to changes in effective stress σ_1', σ_2' and σ_3' (1936)". Effective stress, $\sigma' = \sigma - Pf$, replaces total stress in tensile and shear failure criteria [5].

Following the assumption of unaltered formation pressure, P_f, the failure criterion in Eq. C.9 necessitates Eq. C.7b to be negative to be fulfilled, which is it at sufficiently large well pressures, P_w:

$$P_{w_{frac.initiation}} = 3\sigma_h - \sigma_H - P_f + T_0 \tag{C.11}$$

Note that these equations assume a perfectly impermeable borehole wall, but can also apply for high pump rates in slightly permeable formations where fluid diffusion during loading is too slow to influence the hoop stress. On the other hand, if the wall is slightly permeable such as can be seen in tight formations absent a mud cake, poroelastic[6] effects must be accounted for. At pump rates (loading rates) low enough to allow fluid diffusion between the well and the formation, fracture initiation pressure can be reduced due to alteration of near wellbore pore pressure (P_f) and total stresses. If there is no forming of a filter cake on the wall, then the pore pressure here will equilibrate fast to the imposed well pressure and thus the Terzaghi effective stress in the failure criteria is lowered. The other effect, that on total stress, is included by adding a poroelastic constant η, ranging from 0 to 0.5, which describes magnitude of total stress induced by the fluid diffusion [4]. The constant is multiplied with the difference in pressure by which the fluid diffuses through the wall, $P_w - P_{f,farfield}$. The following modification of Eq. C.11 then quantifies the effect that fluid diffusion has had at the moment of initiation. Following this, fracture initiation pressure is expressed (from Detournay and Carbonell [4])

$$P_{w_{frac.initiation}} = \frac{3\sigma_h - \sigma_H - 2\eta P_{f.farfield} + T_0}{2(1-\eta)} \tag{C.12}$$

Another time dependent poroelastic effect is that due to volumetric strains from drill out. Situating a wellbore in the formation of unequal far field stresses changes the mean stress around it, which results in a volumetric strain. The strain will lead to pore pressure increase in the direction if the maximum horisontal stress (at $\Theta = 0^o$ on Fig. C.13). In relation to fracturing theory, the important point is that the pore pressure increase is drained quickly at the wall, leading to a shielding effect from the fact that drained moduli are smaller than undrained. With time a pore pressure decreases outside the wall, the shielding will steadily reduce and the hoop stress at the wall increase. This effect does, in contrast to the above, not require lack of filter cake to occur. In an XLOT, often performed in shale and with high injection rates, the effect is likely to be

[6]The presence of free moving fluid in a porous and permeable rock modifies its mechanical behavior. Fluid diffusion can make loading a time dependent problem, where the elastic response of rock can be delayed in time [4].

dominated by pore pressure increase due to invasion.

For fracture re-opening in the second and third cycle there is in principle no tensile strength to be overcome, which entails reducing Eq. C.11 to

$$P_r = 3\sigma_h - \sigma_H - P_f \tag{C.13}$$

when a fracture has been created. The re-opening pressure, P_r, is thus expected to be lower than the initiation pressure. If assuming that a fracture initiates at FBP, this suggests that the formation tensile strength can be determined from the difference between the first and the second peak, as illustrated by red dotted lines in Fig. C.14.

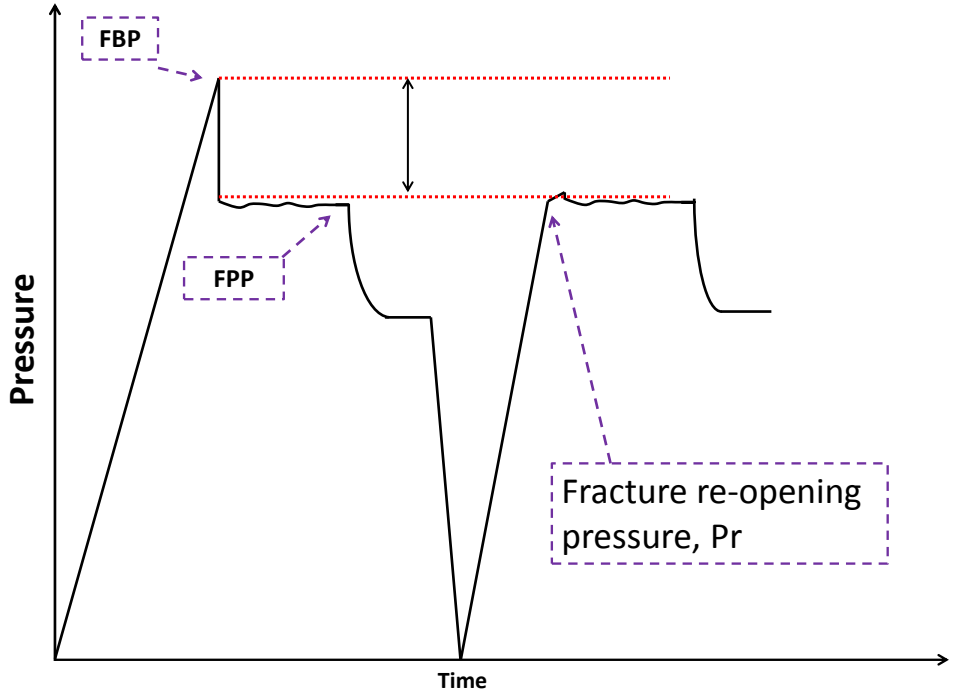

Figure C.14: Schematic plot of pressure versus time of a two cycle XLOT, illustrating how formation tensile strength ideally can be approximated given that the break down and reopening defined by linear elasticity.

While this is done in hydraulic fracture tests, it is not commonly done in XLOTs [1]. The difference between the peaks is in practice not only due to removal of tensile strength. The magnitude of the first peak is as discussed in Chapter C.2.1 influenced by a number of different factors, and as is the second peak. The creation of a fracture may redistribute stresses at the borehole wall, and as a result the effective hoop stresses may reduce [5]. Temperature effects, osmosis, and the effect of poroelastic behavior as described by Eq. C.12, can all add to the uncertainty. Another effect is what is referred to as fracture healing, where experience has

shown that particularly the use of water based muds (WBM) as compared to oil based muds (OBM), can restore fracture opening threshold over time [8].

C.2.3.3 Fracture Propagation Pressure

The pressures present inside a fracture to further propagate it were described in Chapter C.2.2.1. The sum of contributions can be equated with the following expression

$$P_{\text{open new length}} = P_{\text{maintain aperture}} + P_{\text{friction}} + P_{\text{tip}} \tag{C.14}$$

where the first contribution denotes the pressure to overcome σ_3 plus the excess pressure needed to maintain aperture in which the pump-in fluid will flow. The excess pressure is a function the elastic moduli Young's modulus and Poisson's ratio as well as fracture width and size [14]. The second contribution, the frictional pressure loss due to flow in the fracture, is dependent on the fracture surface area and roughness, in addition to pump-in rate and fluid properties such as viscosity and density. The third contribution is the pressure needed to be overcome at the fracture tip, which can be seen as the additional pressure needed to initiate failure inside the fracture and keep it growing [14]. Eq. C.1 express a the net propagation pressure to be the sum of the above contributions minus the minimum in-situ stress.

Elastic fracture mechanics define the tip propagation pressure as

$$P_{\text{tip}} = K_{\text{lc}}\sqrt{\frac{\pi}{48L}} \tag{C.15}$$

where K_{lc} is a critical stress intensity factor also known as the fracture toughness, and L is the length of the fracture. K_{lc} has to contributions: A material specific toughness and an apparent toughness. Fracture toughness as a material property can be defined as the strength of a material in the presence of a pre-existing flaw [14]. It can further be explained by considering a crack in car wind shield in glass: The shield has high tensile strength and is thus not easily broken, but the moment a crack is present the strength is severely reduced, which is manifested by a quickly and effortlessly propagating crack.

In relation to a propagating fracture, the effect of fracture toughness can be observed in a characteristic pressure versus time response referred to as "saw-tooth" behavior. It can be explained by considering a field test example conducted offshore Norway (from Raaen et al. [13]). The well was vertical with sea water as pump-in fluid. Due to the formation being a

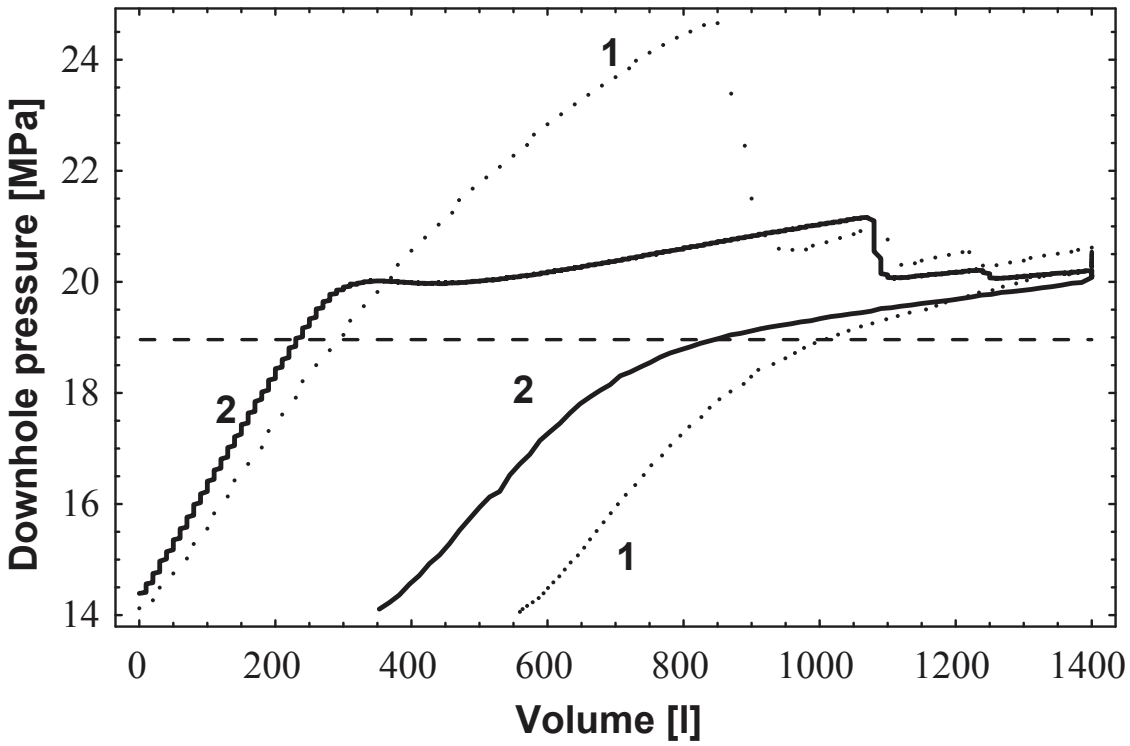

Figure C.15: Pressure versus time for a two cycle test with shut-in and flow-back in the first cycle, and only flow-back in the second cycle. The characteristic saw-tooth behaviour is clearly observed. (from Raaen et al. [13])

sandy shale inherent some permeability, a highly viscous bentonite mud pill of 10000 litres was bullheaded in the well, with the objective to decrease leak-off in the fracture and thereby increase chances of high quality use of the system stiffness approach to ascertain FCP. Fig. C.15 shows a plot of pressure versus time for the test, where the "saw-tooth" response is clearly observed after formation breakdown as well as after fracture reopening in the second cycle. The sharp decline on each "saw-tooth" can be interpreted as rapid growth incidents, where the fracture toughness, - both apparent and as a material property, are overcome. Then the pressure builds to once again overcome the fracture toughness. Recognize first how the rate of pressure increase after each rapid growth incident decreases from cycle to cycle. This is explained by that the fracture stiffness is highly dependent on fracture length, in accordance with Eq. C.3: The longer fracture, the less excess pressure is needed to expand width, while length and height are constant. The peak pressure at which rapid growth happens, decreases with time, not only due to the decrease in required excess pressure to keep the fracture open, but possibly from a decrease in fracture toughness, as is clear from Eq. C.15.

The magnitude of fracture toughness, K_{Ic} with its effect on the peak pressure on each growth incident, is dependent on more than only the material property toughness. The apparent fracture

toughness adds to K_{lc} and may consist of several phenomena not described by elastic fracture mechanics:

- a fluid lag effect, isolating the tip
- fracture healing, where the tip is further isolated due to a filter cake bridging on the fracture surface (in permeable formations), and/or due to plugging the tip area with fines
- a zone of plastic deformation around the tip

The fluid lag effect is a long-recognized phenomena, and is simply due to that fluids do not move instantaneously, especially viscous pump-in muds, and will lag behind as new area cracks open. Some other fluid fills the space, and as the mud reaches the front as shown on Fig. C.16, it cannot enter (e.g. due to mud additives in combination with surface tension effects). The tip is then isolated from the well pressure acting to open up new area, and the apparent toughness increases.

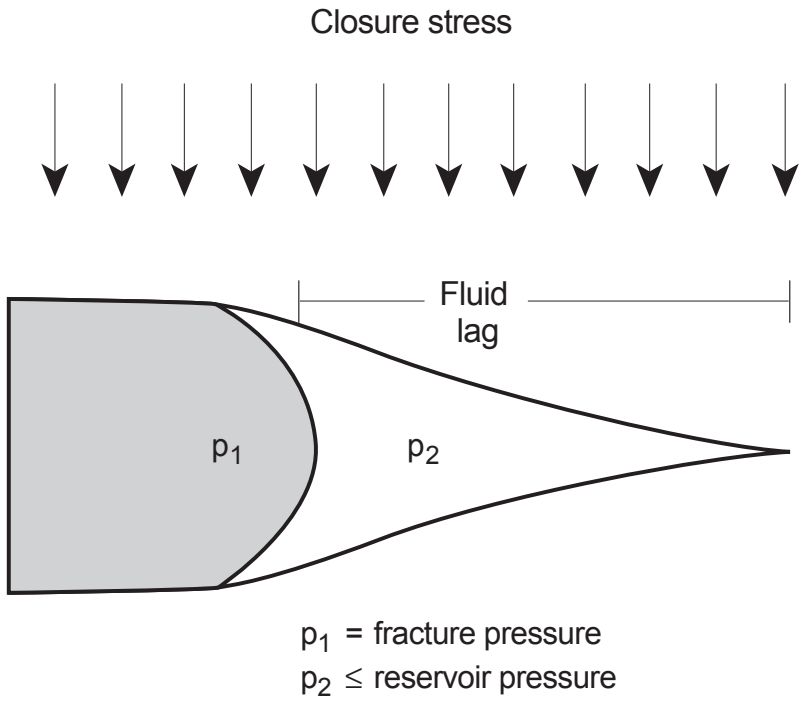

Figure C.16: Illustration of a schematic fracture cross section, showing the fluid lag effect that isolates the tip and adds apparent fracture toughness to its resistance to open new area (from Smith and Shlyapobersky [14])

Fracture healing denotes the forming of a filter cake on the fracture surfaces and bridges at the tip, which adds additional space between the tip and the well pressure. This effect is naturally more often seen in permeable formations, where it can add greatly to the propagation

pressure as well as the reopening pressure [8] in repeated cycles. In addition, WBMs are known for their high filtrate loss and ability to build filter cake, as compared to OBMs and water. Therefore it is possible that tip effects can be reduced by changing the pump-in fluid.

A zone of plasticity, the last point, describes a situation where non-elastic rock deformation around the tip stabilizes the fracture and adds to its strength. The yield stress in the zone has then been exceeded during loading, i.e. as fracture width increases. Energy has been consumed and stresses redistributed, with the result that a yielded and stronger plastic zone remains.

It is clear from the above paragraphs that the conventional understanding of K_{lc} in Eq. C.15 as a constant, and the P_{tip} derived by elastic fracture mechanics, are not accurately describing the propagation process. Field experience agree with this, where data have indicated fracture extension pressures above 20 bar higher than what expected [14]. This has led to search for explanations and lab/field experiments, with the above phenomena as findings. P_{tip}, being a function of these case specific non-material properties, should be obtained by calibration of pressure data, if needed [14].

C.2.4 Stress Determination in Active Thrust Belts

Couzens-Schultz and Chan [2] recently addressed one of the points that have been used to argue the unreliability of the XLOT; that the test sometimes shows an unrealistically low leak off pressure when performed in compressional stress settings. Traditionally, such situations have either led to data being thrown away as poor, or in some cases used to derive a stress state not in agreement with geologic and geophysical understanding of the formation: In tectonically active thrust belts with horizontal compressive stresses, the minimum stress is the vertical in-situ stress. Too low leak-off pressure magnitudes have then been derived to minimum stresses 30-60% below the actual overburden stress [2].

The explanation proposed by Couzens-Schultz and Chan [2] is that the leak-off test, instead of to induce a fracture by tensile failure, causes shear failure on pre-existing discontinuities. Fracture surfaces are not perfectly smooth, and will dilate when sheared, creating a hydraulically conductive path between them (illustrated in Fig. C.17 C). Flow through these critically stressed fractures happens at pressures lower than the vertical stress, and may thus be misinterpreted as a LOP due to fracture initiation by tensile failure or fracture reopening.

With this interpretation and hypothesis in mind, the authors presented a new way to constrain the stress state. The presented method of interpretation allows not only to constrain the minor

horizontal stress, but in some cases the major horizontal stress as well.

C.2.4.1 Interpretation Technique

Couzens-Schultz and Chan [2] observed that LOTS conducted at different locations in thrust belts indicated large variations in the minimum in-situ stress. Both leak-off pressures near σ_v were observed, as well as much lower pressures, implying that the vertical stress significantly varied within the same field. The behaviour could in some cases be explained by that principal stresses are rotated near active faults, where the difference between vertical stress and minimum principal stress can be up to 10% [2]. The variations have however been observed much more

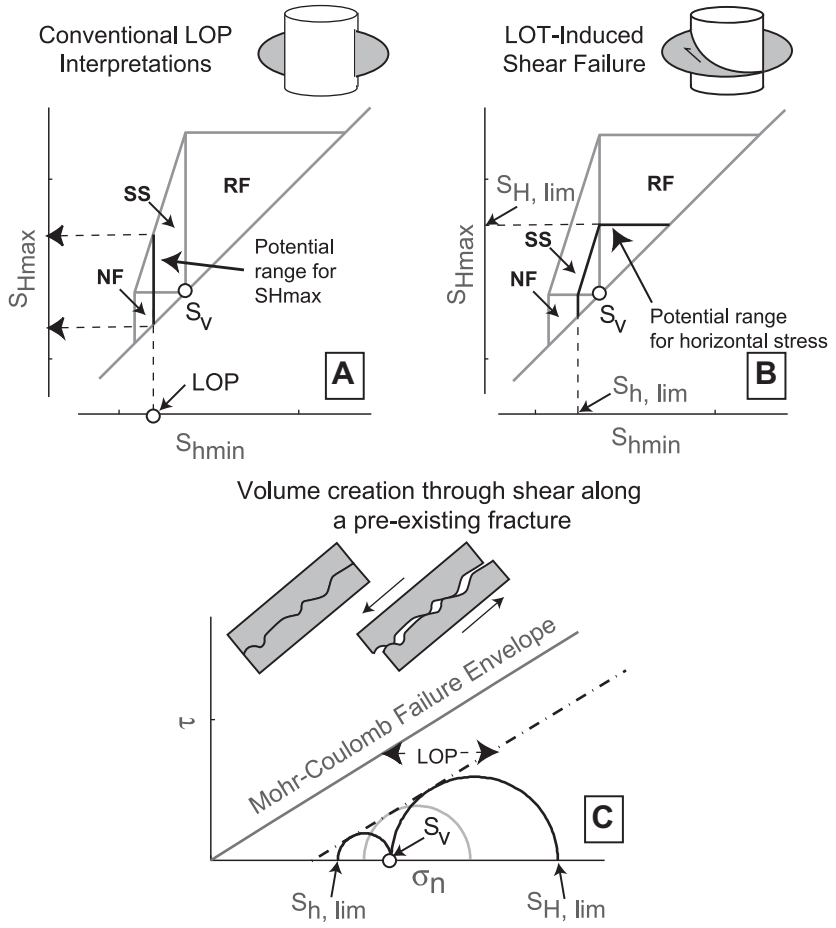

Figure C.17: Illustration of how to constrain stress state for A, the conventional method of interpretation where LOP reflects fracture reopening and B, the new method of interpreting the LOP as shear induced dilatency. In A, the range of stresses is merely the thick black line, and in B the stress state is constrained by the thick-lined polygon. In C, the different possible failure regimes are sketched with Mohr circles, using constraints from B. SS = "strike slip", RF = "reverse fault" and NF = "normal fault" regime. (from Couzens-Schultz and Chan [2])

significant, and for such cases the authors state that the low LOP should be evaluated to be a

result of shear induced dilation in pre-existing fractures. Other possible explanations should preferably be ruled out first, such as leakage up the annulus. For a normal stress regime, it was concluded in Chapter C.2.1.1 that the LOP and subsequent gradual slope change can only be due to reopening of a pre-existing fracture, if cement shoe imperfections and formation leak off are ruled out. In compressive settings, this additional explanation should be considered.

Fig. C.17 A and B show stress constraints for the conventional fracture reopening interpretation and for new method of interpretation, respectively. The lower bound of the constraint polygon in B is the case where horizontal stresses are equal, and the left and upper bound are determined by frictional equilibrium for a given and assumed coefficient of internal friction, allowing the failure to be assigned to the indicated stress states [2]. The overburden stress, indicated by a white circle, is assumed known, and divides the polygon into different governing stress states. Fig. C.17 C shows how the stress state in B can be constrained in a Mohr diagram with use of σ_v and the recorded LOP magnitude, along with knowledge of different possible stress regimes and corresponding fault types: Normal fault case ($\sigma_{\mathrm{v}} > \sigma_{\mathrm{Hmax}} > \sigma_{\mathrm{hmin}}$) in the smallest circle to the left, strike slip fault case ($\sigma_{\mathrm{Hmax}} > \sigma_{\mathrm{v}} > \sigma_{\mathrm{hmin}}$) in the gray mid circle, and reverse fault case ($\sigma_{\mathrm{Hmax}} > \sigma_{\mathrm{hmin}} > \sigma_{\mathrm{v}}$) in the large right-bound circle.

In a low permeable formation without forming of a filter cake during pressurization, it can be assumed that fluid enters the hydraulically conductive path opened by shear dilatency instead of by overcome hoop stresses. The LOP is recorded from the test, and is used as illustrated in Fig. C.17 B and C, to divide the ranges of possible in-situ stress states with Mohr circles that are in contact with the shear failure line. Then depending, on the stress governing stress regime, either the lower limit $\sigma_{\mathrm{h,lim}}$ normal fault case, or the upper limit $\sigma_{\mathrm{H,lim}}$ reverse fault case, can be ascertained:

$$\sigma_{\mathrm{h,\,lim}} = \sigma_{\mathrm{v}} - \frac{2(\sigma_{\mathrm{v}} - (LOP - \frac{C_0}{\tan\phi}))\sin\theta}{1+\sin\phi} \tag{C.16}$$

$$\sigma_{\mathrm{H,\,lim}} = \sigma_{\mathrm{v}} + \frac{2(\sigma_{\mathrm{v}} - (LOP - \frac{C_0}{\tan\phi}))\sin\theta}{1-\sin\phi} \tag{C.17}$$

where ϕ is the friction factor, C_0 the cohesion and σ_{v} the vertical stress, which is assumed to be a principal stress. Between these limits, there is a range of strike slip Mohr circles dependent on stress magnitudes and degree of anisotropy in the horizontal plane.

The full in-situ stress state can be inferred if the interpretation approach is used in combination with independent stress estimates from breakouts or drilling induced breakdown occur-

rences [2]. The advantage of the approach where its assumptions are correct is obvious: Instead of obtaining underestimates of σ_v from data otherwise considered as poor, the approach may allow to characterize the maximum horizontal stresses.

C.2.4.2 Field Example From an Active Thrust Fold Belt

Couzens-Schultz and Chan [2] presented field examples where the use of their method of interpretation was illustrated. Five LOTs were conducted in an offshore deepwater fold belt, and at larger depths there were great variations in the recorded leak-off pressure data. Several indications of a compressional setting at these depths were observed, such as: Core samples taken while drilling showed compressional mesostructures and indications of compaction incongruous with the present vertical stress. In addition, there was evidence of an elliptical borehole shape from caliper logs, and indication of shear velocity anisotropy.

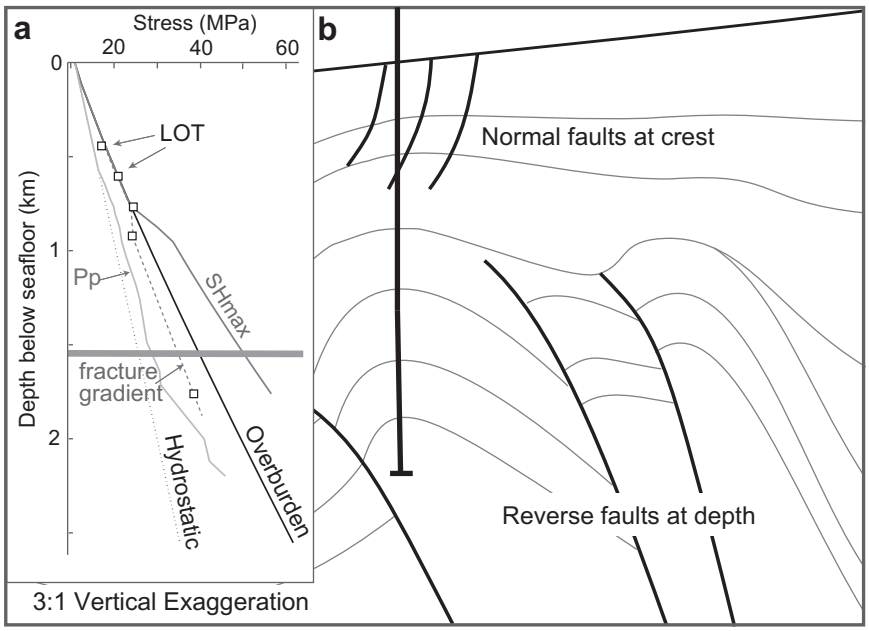

Figure C.18: Schematic cross-section and stress profile versus depth of a well located in a deep water fold belt. Five LOTs were conducted, - three at depths of normal stress regime, and two at depths of an anticipated reverse fault regime. Pp is the formation pressure at depth. (from Couzens-Schultz and Chan [2])

Three LOTs were conducted at shallow depths of the well, as indicated by white squares in Fig. C.18. The LOP pressures were of magnitudes close to the expected vertical stress, which would imply either a nearly isotropic stress state, or a reverse-fault stress state. This did however not agree with other (geological) information such as the observed shallow normal faults and lack of compaction. Two LOTs were conducted in the same well, at depths of the anticline

fold, which presented LOP data significantly lower than the shallower data. The conventional interpretation would here infer a horizontal minimum stress and an either strike slip or normal fault stress regime, which disagreed with all other information at hand. The above points suggested that the alternate method of interpretation could be applied. Friction factors were

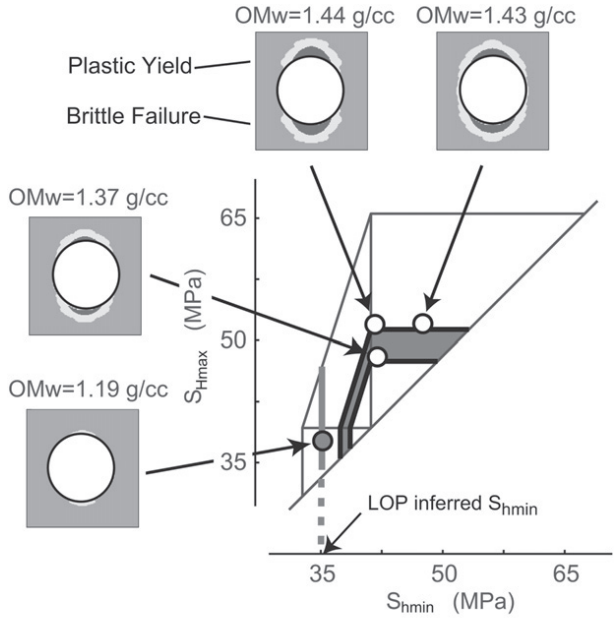

Figure C.19: Field example stress polygon. Maximum horizontal stress constrained between magnitudes of 45.8 MPa and 50.5 MPa by use of Eq. C.17. (from Couzens-Schultz and Chan [2])

assumed and based on laboratory measurements, and assuming a reverse fault regime, the range of maximum horizontal stress magnitude could be estimated with Eq. C.17, to be between 45.8 and 50.5 MPa. The observed wellbore deformation was as a quality and credibility control simulated in a number of numerical simulations, were the objective was to confirm the concluded stress state; a reverse fault regime. The simulations for a reverse fault regime were successfully in agreement with the caliper log, whereas what inferred from conventional method, - a normal fault or strike slip regime, indicated strain within linear elasticity. The argument of a compressional stress setting with shear induced dilatency as the reason for low leak-off pressures was furthermore supported by the fact that it explained not only low LOP data, but the plastically flowed borehole shape, shear velocity anisotropy and reservoir porosity distribution as well.

The significance and benefits of the methods presented are easily recognized; data that previously would have been dismissed as poor or false can instead be evaluated with new understanding that may yield information not possible up to this publication. The method require

good geological and geophysical understanding of the formation, and may then explain cases of significantly lower leak-off pressures than what expected. The authors emphasize, however, that the presented method of interpretation does not replace traditional methods for subsurface stress determination, but rather is an approach to be considered when such tests present results in disagreement with other information.

C.2.5 The Maximum Horizontal Stress

While the minimum horizontal stress, σ_h, can be determined directly from the pressure response at which fracture closes with an error of less than 5 % ([13]), the procedure to estimate the maximum horizontal stress, σ_H, is more complicated. To estimate σ_H from an extended leak-off tests requires direct use of either Eq. C.11 for fracture initiation or Eq. C.13 for fracture reopening to be solved for σ_H. Assuming that the LOP reflects fracture initiation, the former can be applied:

$$\sigma_H = 3\sigma_h - LOP - P_f + T_0 \tag{C.18}$$

Recall that the above assumption requires linear elasticity and an impermeable and perfectly in-gauge borehole wall, which is as discussed is not the case in reality. An imperfect borehole will as illustrated in Chapter C.2.1.1 give a too low LOP, as compared to the ideal linear elastic case where LOP reflects fulfillment of the tensile failure criteria. In turn, this will lead to an over estimate of the maximum horizontal stress from Eq. C.18. In Chapter C.2.1 it was concluded that the LOP is not suitable for stress determination as its magnitude depends on an unknown number of phenomena effecting the pressure versus time response in varying and uninterpretable degree. With the LOP once again disqualified for accurate stress estimation, the criteria for fracture reopening is evaluated.

$$\sigma_H = 3\sigma_h - P_r - P_f \tag{C.19}$$

Also here there are major shortcomings leaving little confidence in the estimates. The reopening pressure can be flawed by

- redistribution of stresses $\Rightarrow$ lower effective hoop stresses, $P_r \downarrow$
- poroelastic effects (timedelayed) $\Rightarrow P_r \downarrow$
- fracture tip effects and fracture healing $\Rightarrow P_r \uparrow$

- rate induced effects (field experience, Postler [9]), where higher rate $\Rightarrow P_r \uparrow$
- non-perfect borehole $\Rightarrow P_r \downarrow$
- imperfectly closed fractures $\Rightarrow P_r \downarrow$

To apply Eq. C.19 or Eq. C.18 the first criteria is that the parameters are readily available. From the above arguments, it follows that the tensile strength cannot be accurately determined from the difference between LOP and reopening pressure.
Now, given that

- all of the above effects on reopening pressure evens out to zero
- the tensile strength is determined with reasonable accuracy from either borehole breakouts or core tests such as the hollow cylinder test
- the minimum horizontal stress has been estimated with the highest accuracy available, i.e. 5%

then the maximum horizontal stress can be estimated with an accuracy of 15%, at a very best.

Information about the maximum horizontal stress can be important for modeling and understanding of fluid flow, compaction, wellbore stability, reservoir simulation. In formations with a compressive stress regime, where $\sigma_{\mathrm{Hmax}} > \sigma_{\mathrm{hmin}} > \sigma_{\mathrm{v}}$, information of the maximum horizontal stress magnitude may be additionally important as it allows more accurate evaluation of a reservoirs ability to sequestrate/store CO_2. In such settings, an alternate way of interpretation may show valuable, specifically in cases where the estimated minimal in-situ stress (vertical stress) is significantly lower than what inferred from other information. The method, which allows estimating a range constraint to the horizontal stresses, is explained and discussed in Chapter C.2.4.

References Appendix C

[1] M.A. Addis, T.H. Hanssen, Yassir N., Willoughby D.R., and J Enever. A comparison of leak-off test and extended leak-off test data for stress estimation. *SPE/ISRM*, 1:1–2, 1998.

[2] Brent A. Couzens-Schultz and Alvin W. Chan. Stress determination in active thrust belts: An alternative leak-off pressure interpretation. *Journal of Structural Geology*, 32:1061–1069, 2010.

[3] D.D. Cramer and D.H. Nguyen. Diagnostic fracture injection testing tactics in unconventional reservoirs. *SPE-163863*, 2013.

[4] E. Detournay and R. Carbonell. Fracture-mechanics analysis of the breakdown process in minifracture or leakoff test. *SPE Production and Facilities*, 12:195–199, 1997.

[5] E. Fjær, R.M. Holt, P. Horsrud, A.M. Raaen, and R. Risnes. *Petroleum Related Rock Mechanics*. Developments in Petroleum Science, 53. Elsevier, Chapters 4 8, 2 edition, 2008.

[6] T.B. Gederaas and A.M. Raaen. Precise minimum horizontal stress determination from pump-in/flowback tests with drilling mud. *American Rock Mechanics Association (ARMA)*, 88, 2009.

[7] L. Jing and J.A. Hudson. Numerical methods in rock mechanics. *International Journal of Rock Mechanics & Mining Sciences*, 39:409–427, 2002.

[8] D. Økland, G. K. Gabrielsen, J. Gjerde, K. Sinke, and E. L. Williams. The importance of extended leak-off test data for combatting lost circulation. *SPE/ISRM*, 2002.

[9] D.P Postler. Pressure integrity test interpretation. *SPE/IADC*, 1997.

[10] A. M. Raaen and M. Brudy. Pump-in flowback tests reduce the estimate of horizontal in-situ stress significantly. *SPE 71367*, 2001.

[11] A.M. Raaen. The pump-in/flowback test improves routine minimum horizontal stress magnitude determination in deep wells. In *International Symposium on In-Situ Rock Stress*. Statoil ASA, 2006.

[12] A.M. Raaen, E. Skomedal, H. Kjørholt, P. Markestad, and D. Økland. Stress determination from hydraulic fracturing tests: the system stiffness approach. *International Journal of Rock Mechanics and Mining Sciences*, 38:529–541, 2001.

[13] A.M. Raaen, P. Horsrud, H. Kjørholt, and D. Økland. Improved routine estimation of the minimum horizontal stress component from extended leak-off tests. *International Journal of Rock Mechanics and Mining Sciences*, 43:37–48, 2006.

[14] M.B. Smith and J.W. Shlyapobersky. Basics of hydraulic fracturing. *Chapter 5.5, Reservoir Stimulation*, 2000.